

SENSORS & TRANSDUCERS

ISSN 1726-5479

vol. 215

8 / 17



Sensors and Signal Processing

International Frequency Sensor Association Publishing



Sensors & Transducers

**International Official Open Access Journal of the
International Frequency Sensor Association (IFSA)
Devoted to Research and Development
of Sensors and Transducers**

Volume 215, Issue 8, August 2017

Editor-in-Chief

Prof., Dr. Sergey Y. YURISH



IFSA Publishing: Barcelona • Toronto

Sensors & Transducers is an open access journal which means that all content (article by article) is freely available without charge to the user or his/her institution. Users are allowed to read, download, copy, distribute, print, search, or link to the full texts of the articles, or use them for any other lawful purpose, without asking prior permission from the publisher or the author. This is in accordance with the BOAI definition of open access. Authors who publish articles in *Sensors & Transducers* journal retain the copyrights of their articles. The *Sensors & Transducers* journal operates under the Creative Commons License CC-BY.

Notice: No responsibility is assumed by the Publisher for any injury and/or damage to persons or property as a matter of products liability, negligence or otherwise, or from any use or operation of any methods, products, instructions or ideas contained in the material herein.

Published by International Frequency Sensor Association (IFSA) Publishing. Printed in the USA.





Editors-in-Chief: Professor, Dr. Sergey Y. Yurish, tel.: +34 696067716, e-mail: editor@sensorsportal.com

Editors for Western Europe

Meijer, Gerard C.M., Delft Univ. of Technology, The Netherlands
Ferrari, Vittorio, Università di Brescia, Italy
Mescheder, Ulrich, Univ. of Applied Sciences, Furtwangen, Germany

Editor for Eastern Europe

Sachenko, Anatoly, Ternopil National Economic University, Ukraine

Editors for North America

Katz, Evgeny, Clarkson University, USA
Datskos, Panos G., Oak Ridge National Laboratory, USA
Fabien, J. Josse, Marquette University, USA

Editor for Africa

Maki K., Habib, American University in Cairo, Egypt

Editors South America

Costa-Felix, Rodrigo, Inmetro, Brazil
Walsoe de Reça, Noemi Elisabeth, CINSO-CITEDEF
UNIDEF (MINDEF-CONICET), Argentina

Editors for Asia

Ohyama, Shinji, Tokyo Institute of Technology, Japan
Zhengbing, Hu, Huazhong Univ. of Science and Technol., China
Li, Gongfa, Wuhan Univ. of Science and Technology, China

Editor for Asia-Pacific

Mukhopadhyay, Subhas, Massey University, New Zealand

Editorial Board

Abdul Rahim, Ruzairi, Universiti Teknologi, Malaysia
Abramchuk, George, Measur. Tech. & Advanced Applications, Canada
Aluri, Geetha S., Globalfoundries, USA
Ascoli, Giorgio, George Mason University, USA
Atalay, Selcuk, Inonu University, Turkey
Atghiaee, Ahmad, University of Tehran, Iran
Augutis, Vygantas, Kaunas University of Technology, Lithuania
Ayeshe, Aladdin, De Montfort University, UK
Baliga, Shankar, B., General Monitors, USA
Barlingay, Ravindra, Larsen & Toubro - Technology Services, India
Basu, Sukumar, Jadavpur University, India
Booranawong, Apidet, Prince of Songkla University, Thailand
Bousbia-Salah, Mounir, University of Annaba, Algeria
Bouvet, Marcel, University of Burgundy, France
Campanella, Luigi, University La Sapienza, Italy
Carvalho, Vitor, Minho University, Portugal
Changhai, Ru, Harbin Engineering University, China
Chen, Wei, Hefei University of Technology, China
Cheng-Ta, Chiang, National Chia-Yi University, Taiwan
Cherstvy, Andrey, University of Potsdam, Germany
Chung, Wen-Yaw, Chung Yuan Christian University, Taiwan
Cortes, Camilo A., Universidad Nacional de Colombia, Colombia
D'Amico, Arnaldo, Università di Tor Vergata, Italy
De Stefano, Luca, Institute for Microelectronics and Microsystem, Italy
Ding, Jianning, Changzhou University, China
Djordjevic, Alexander, City University of Hong Kong, Hong Kong
Donato, Nicola, University of Messina, Italy
Dong, Feng, Tianjin University, China
Erkmen, Aydan M., Middle East Technical University, Turkey
Fezari, Mohamed, Badji Mokhtar Annaba University, Algeria
Gaura, Elena, Coventry University, UK
Gole, James, Georgia Institute of Technology, USA
Gong, Hao, National University of Singapore, Singapore
Gonzalez de la Rosa, Juan Jose, University of Cadiz, Spain
Goswami, Amarjyoti, Kaziranga University, India
Guillet, Bruno, University of Caen, France
Hadjiloucas, Sillas, The University of Reading, UK
Hao, Shiyong, Michigan State University, USA
Hui, David, University of New Orleans, USA
Jaffrezic-Renault, Nicole, Claude Bernard University Lyon 1, France
Jamil, Mohammad, Qatar University, Qatar
Kaniusas, Eugenijus, Vienna University of Technology, Austria
Kim, Min Young, Kyungpook National University, Korea
Kumar, Arun, University of Delaware, USA
Lay-Ekuakille, Aime, University of Lecce, Italy
Li, Fengyuan, HARMAN International, USA
Li, Jingsong, Anhui University, China
Li, Si, GE Global Research Center, USA
Lin, Paul, Cleveland State University, USA
Liu, Aihua, Chinese Academy of Sciences, China
Liu, Chenglian, Long Yan University, China
Liu, Fei, City College of New York, USA
Mahadi, Muhammad, University Tun Hussein Onn Malaysia, Malaysia

Mansor, Muhammad Naufal, University Malaysia Perlis, Malaysia
Marquez, Alfredo, Centro de Investigacion en Materiales Avanzados, Mexico
Mishra, Vivekanand, National Institute of Technology, India
Moghavvemi, Mahmoud, University of Malaya, Malaysia
Morello, Rosario, University "Mediterranea" of Reggio Calabria, Italy
Mulla, Intiaz Sirajuddin, National Chemical Laboratory, Pune, India
Nabok, Aleksey, Sheffield Hallam University, UK
Neshkova, Milka, Bulgarian Academy of Sciences, Bulgaria
Passaro, Vittorio M. N., Politecnico di Bari, Italy
Patil, Devidas Ramrao, R. L. College, Parola, India
Penza, Michele, ENEA, Italy
Pereira, Jose Miguel, Instituto Politecnico de Seteabal, Portugal
Pillarsetti, Anand, Sensata Technologies Inc, USA
Pogacnik, Lea, University of Ljubljana, Slovenia
Pullini, Daniele, Centro Ricerche FIAT, Italy
Qiu, Liang, Avago Technologies, USA
Reig, Candid, University of Valencia, Spain
Restivo, Maria Teresa, University of Porto, Portugal
Rodríguez Martínez, Angel, Universidad Politécnica de Cataluña, Spain
Sadana, Ajit, University of Mississippi, USA
Sadeghian Marnani, Hamed, TU Delft, The Netherlands
Sapozhnikova, Ksenia, D. I. Mendeleev Institute for Metrology, Russia
Singhal, Subodh Kumar, National Physical Laboratory, India
Shah, Kriyang, La Trobe University, Australia
Shi, Wendian, California Institute of Technology, USA
Shmaliy, Yuriy, Guanajuato University, Mexico
Song, Xu, An Yang Normal University, China
Srivastava, Arvind K., Systron Donner Inertial, USA
Stefanescu, Dan Mihai, Romanian Measurement Society, Romania
Sumridetchkajorn, Sarun, Nat. Electr. & Comp. Tech. Center, Thailand
Sun, Zhiqiang, Central South University, China
Sysoev, Victor, Saratov State Technical University, Russia
Thirunavukkarasu, I., Manipal University Karnataka, India
Thomas, Sadiq, Heriot Watt University, Edinburgh, UK
Tian, Lei, Xidian University, China
Tianxing, Chu, Research Center for Surveying & Mapping, Beijing, China
Vanga, Kumar L., ePack, Inc., USA
Vazquez, Carmen, Universidad Carlos III Madrid, Spain
Wang, Jiangping, Xian Shiyong University, China
Wang, Peng, Qualcomm Technologies, USA
Wang, Zongbo, University of Kansas, USA
Xu, Han, Measurement Specialties, Inc., USA
Xu, Weihe, Brookhaven National Lab, USA
Xue, Ning, Agiltron, Inc., USA
Yang, Dongfang, National Research Council, Canada
Yang, Shuang-Hua, Loughborough University, UK
Yaping Dan, Harvard University, USA
Yue, Xiao-Guang, Shanxi University of Chinese Traditional Medicine, China
Xiao-Guang, Yue, Wuhan University of Technology, China
Zakaria, Zulkarnay, University Malaysia Perlis, Malaysia
Zhang, Weiping, Shanghai Jiao Tong University, China
Zhang, Wenming, Shanghai Jiao Tong University, China
Zhang, Yudong, Nanjing Normal University China

Contents

Volume 215
Issue 8
August 2017

www.sensorsportal.com

ISSN 2306-8515
e-ISSN 1726-5479

Research Articles

Review on Ultra-Sensitive QCM Mass Sensor and Microfluidic for Diagnostic Point of Care <i>Selemani Seif, Thomas Thundert and Kenneth Cadien</i>	1
Capacitive Measurer of Linear Displacement <i>Boris Mamikonyan and Lusine Abrahamyan</i>	8
Cadmium Sulfide Quantum Dot Particles (CdSQD) Dispersed in Poly Methyl Methacrylate as an Effective Gamma Counter for the Scintillation Detector <i>Askari Mohammad Bagher, Beheshti - Marnani Amir Khosro, Mirzaei Mahmoud Abadi Vahid, Seifi Majid, Tavakoli Banizi Zoha, Hosseini Ranjbar Abbas and Batool Tahamipour</i>	13
Cardio-metabolic Diseases Prevention by Self-monitoring the Breath <i>Danila Germanese, Mario D'Acunto, Massimo Magrini, Marco Righi and Ovidio Salvetti</i>	19
Automated Indexing and Search of Video Data in Large Collections with inVideo <i>Shuangbao Paul Wang, Xialong Cheng, Carolyn Maher, William Kelly</i>	27
Semi-Implicit Additive Operator Splitting Scheme for Image Segmentation Using the Chan-Vese Model <i>Messaoudi Zahir, Berki Hemza and Younsi Arezki</i>	35
Color Space Axioms and Fiber Bundles <i>Edoardo Provenzi</i>	43

Authors are encouraged to submit article in MS Word (doc) and Acrobat (pdf) formats
by e-mail: editor@sensorsportal.com. Please visit journal's webpage with preparation instructions:
<http://www.sensorsportal.com/HTML/DIGEST/Submission.htm>

Review on Ultra-Sensitive QCM Mass Sensor and Microfluidic for Diagnostic Point of Care

Selemani SEIF, Thomas THUNDERT and * Kenneth CADIEN

University of Alberta, Department of Chemical & Materials Engineering
9211-116 Street NW, Edmonton, Alberta, Canada T6G 1H9

*Tel.: (780) 492 7380

*E-mail: kcadien@ualberta.ca

Received: 14 July 2017 /Accepted: 15 August 2017 /Published: 31 August 2017

Abstract: This review discusses on Quartz Crystal Microbalance (QCM) and microfluidic driven by ultrasonic acoustic forces, as possible alternative technologies to develop compact and portable diagnostic point of care (POC). Extension of QCM to measure 10^{-15} g/cm² is possible and development of this technology will open up new business opportunities in public health, life sciences, and material sciences. The experimental results showed that QCM technology can be 1000 times more sensitive, than the currently available mass sensor systems in the market. The target market is on diagnostic POC, focussing on home care, public health, and agriculture and food industry sectors. Some of the challenges discussed are: 1) A centrifuge for blood plasma separation (BPS), and 2) Microfluidic driven by ultrasonic acoustic forces, for separation of suspended particles in the whole blood. We also present an overview of the expected global market growth from 2011 to 2020 and the benefits to the end users.

Keywords: Femtogram, QCM, Microfluidic, Ultrasonic blood plasma separation (BPS), Free-BPS, Whole blood.

1. Introduction

The CANARY/PANTHER technology is currently used as diagnostic POC for detection of virus and bacteria in site buildings, emergency response, and rapid screening of other disease outbreak in public areas, but encounters a lot of problems. These problems are primarily sample preparation [1-2], involving micro-centrifuges, and micro-air handling devices, burdened by the long-term storage of refrigerated B-cells, which are ineffective in other applications. Mass Spectroscopy (MS) and electron microscopy are very effective in conducting scientific research and can be used for identification of diseases in several hours or weeks, but face challenges such as miniaturization, preprocessing samples, introducing

samples to the MS chamber, and interpreting spectral signals. Therefore, there is a need to develop cost-effective portable diagnostic POC equipment for detection of diseases in real time.

The nanoscale mass sensor devices which can be used to develop cost-effective and modern diagnostic POC systems do exist and the patents have been reported elsewhere [3-14]. The existing inventions are sensitive enough to measure the mass of bacteria, virus, cells, molecules, and troponins. These devices are based on Carbon Nanotube (CBN), QCM, Micro-Electromechanical Systems (MEMS), and Microcantilevers, with the capability to measure mass from picogram (pg/cm² or 10^{-12} g/cm²) to zeptograms (zg/cm² or 10^{-21} g/cm²). Among these devices, the only one which is cost-effective, cheap, easy to fabricate

and manufacture, and commercially available in the market, is QCM mass sensors [15-18].

Sauerbrey [19] was the first to recognize the potential usefulness of the QCM technology and demonstrated the mass sensitivity nature towards frequency changes at the surface of QCM electrodes. He derived the equation which relates the mass change per unit area at the QCM electrode surface to the observed change in oscillation frequency of the crystal as shown in the expression: $K = 2f^2/\sqrt{\rho\mu} = 2.26 \times 10^{-6} f^2 \text{Hz}^{-1} \text{cm}^2/\text{g}$, where K is the mass sensitivity coefficient, $\rho = 2.648 \text{g/cm}^3$, is the density of quartz crystal, and $\mu = 2.947 \times 10^{11} \text{g/cm}^2 \cdot \text{s}^2$, is the shear modulus of quartz crystal. If the mass sensitivity coefficient (K) and the detection limit $\Delta f(\tau)$ parameters are known, it is possible to estimate mass resolution; using Allan deviation $\sigma(\tau)$ which represents noise instability in the time domain less than 10 seconds [20-21]. The $\sigma(\tau)$ is calculated using the equation; $\sigma = (1 \times 10^{-7})/Q$, where Q is the Q-factor of an AT-cut quartz disk. The $\Delta f(\tau)$ is calculated using the equation; $\sigma(\tau) \times f(\tau) = \Delta f(\tau)$, while the mass resolution [22] is calculated by taking the ratio of $\Delta f(\tau)$ to K .

To verify that the mass resolution depends not only on the frequency shift but also the diameter of the central active electrode, we have designed, fabricated, and characterized 5 disks. The diagrams which show the designs and the experimental set-up for measurement of the Q-factors and the frequencies are shown in Sections 3 and 4. Section 5 discusses on calculated $\sigma(\tau)$, K , $\Delta f(\tau)$, and mass resolution in g/cm^2 . Sections 6 and 7 discuss on challenges for developing diagnostic POC using QCM mass sensor interfaced with microfluidic driven by ultrasonic acoustic forces. Section 8 discusses on market overview and benefits to end users while the last section summarizes what has been discussed in this review.

2. Design, Fabrication and Characterization of the Disks

The disks were designed and fabricated using sputter deposited Gold electrode layers (~300 nm) on Chromium adhesion layer (~50 nm). The diagram which shows the fabricated disks is depicted in Fig. 1.

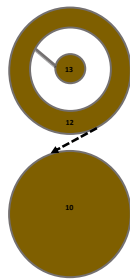


Fig. 1. The top views show the gap with numeral 11, the ring electrode with numeral 12, and the center electrode with numeral 13. The bottom side is a full coated electrode with numeral 10.

Referring to Fig. 1, the top side of the disk is described using three numerals; 11, 13 and 12. Numeral 11 is the gap between the center electrode and the outer ring electrode. Numeral 13 is the center electrode as viewed from the top of the Quartz disk. Numeral 12 is the ring electrode, at the bottom side of the Quartz disk, is the full electrode marked with numeral 10. The center dot with numeral 13 has different diameters (1 mm, 2 mm, 3 mm, 4 mm and 5 mm) for disks 1 to 5 respectively.

3. Experimental Set-up

The experimental set up for Q-factor measurements using 4294A Precision Impedance Analyzer which is connected to Signatone (S-1160 model) Probe Station is shown in Fig. 2 (a).

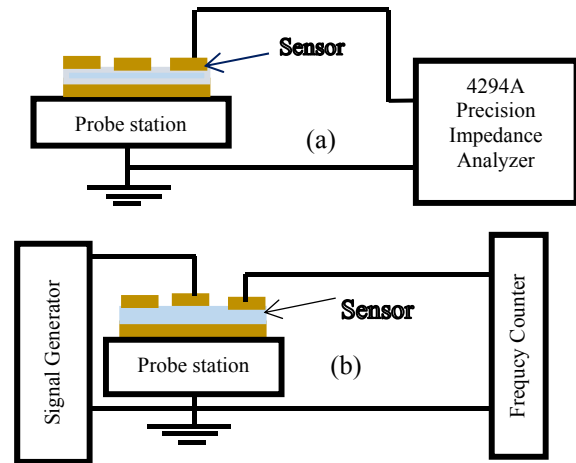


Fig. 2. (a) Set-up for measurements of Q-factors versus frequencies; (b) Set-up for measurement of frequency stability.

These disks were mounted on a Signatone (S-1160 model) Probe Station and connected using a coaxial cable to the 4294A Precision Impedance Analyzer in the series configuration. The electrical signal (150 mV) is applied at a resonant frequency on the top layer labeled with numeral 12 while the ground terminal is connected to a full bottom electrode labeled as numeral 10. The measured parameters were Q-factors, in the frequency range between 1 MHz and 1.10 MHz. The set-up for frequency shift measurements using Frequency Counter, Signal Generator, and Signatone (S-1160 model) Probe Station is shown in Fig. 2 (b). The disks were mounted on the top of the probe stations and the sinusoidal electrical signals (10 V) were applied from the signal generator to the ring electrode while the full bottom electrode grounded. The Frequency Counter was then used to measure frequencies using lab view program installed in the computer.

4. Results and Discussion

In this section we present results based on:

- 1) Q-factors and Allan deviation calculation;
- 2) Calculation of mass sensitivity coefficients;
- 3) Calculation of detection limit;
- 4) Calculation of mass resolution.

4.1. Q-factors and Allan Deviation Measurements

The curve which shows the measured Q-factors versus frequencies is in Fig. 3(a), the obtained results show the maximum Q-factor to be 50000 at resonance (1.067 MHz) for the disk with 3 mm diameter. For the disks with 1 mm, 2 mm, 4 mm and 5 mm, diameters, the measured Q-factors were 40000, 46000, 42000 and 38000 respectively.

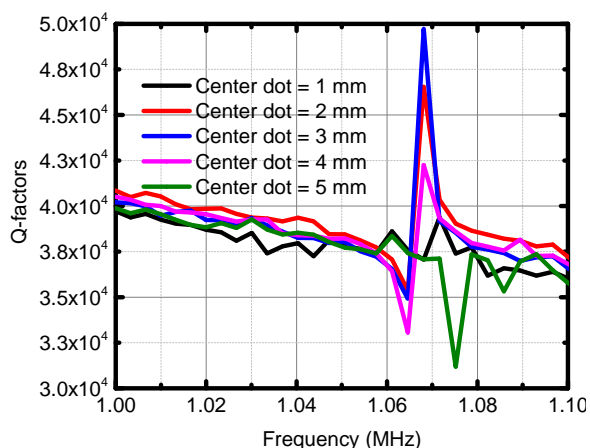


Fig. 3 (a). The curve which shows the measured Q-factors of five disks as a function of frequencies and the diameters of the central electrodes.

The curve which shows the calculated Allan deviation is in Fig. 3 (b). The highest Allan deviations were calculated from the disks with 5 mm and 4 mm diameters; the $\sigma(\tau)$ of the disk with 5 mm as a central diameter was 3.2×10^{-12} , while the $\sigma(\tau)$ of the disk with 4 mm as a central diameter was 3.05×10^{-12} . The disk with the smallest Allan deviation was that with 1 mm diameter, where $\sigma(\tau)$ is equal to 2.7×10^{-12} . By comparing the results obtained in Fig. 3 (a) and (b) we noted that as Q-factors increases the value of calculated $\sigma(\tau)$ decreases.

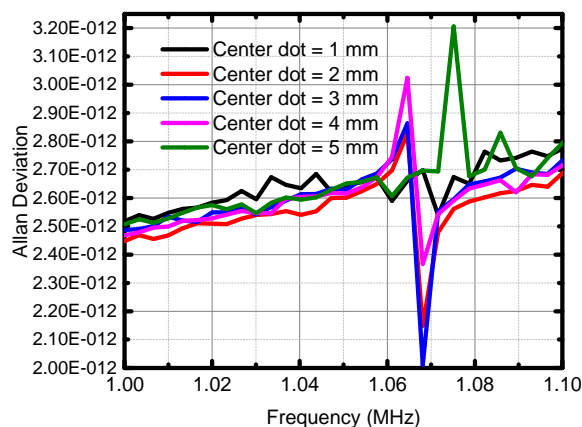


Fig. 3 (b). The curve which shows the calculated Allan deviation versus frequencies of five disks with different center dot electrodes.

4.2. Mass Sensitivity Coefficient and Detection Limit

The obtained $\sigma(\tau)$ as a function of frequencies was then used to calculate the detection limit; $\Delta f(\tau)$, as shown in Fig. 3(c). The disk with 3 mm as central diameter was found to be more sensitive and the maximum detection limit was approximately $2.15 \mu\text{Hz}$.

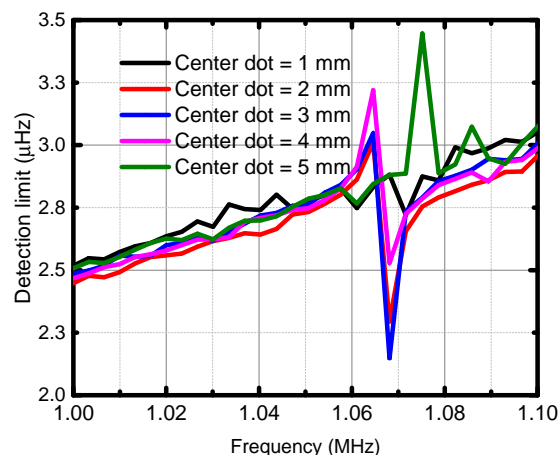


Fig. 3 (c). The curve which shows the calculated detection limit versus frequencies of five disks with different central diameters.

In Fig. 3 (d), are results showing the calculated mass sensitivity coefficients as a function of the measured frequencies, showing the specific mass sensitivity of approximately $2.6 \text{ MHz} \cdot \text{g}^{-1} \cdot \text{cm}^2$ when the resonant frequency is 1.07 MHz.

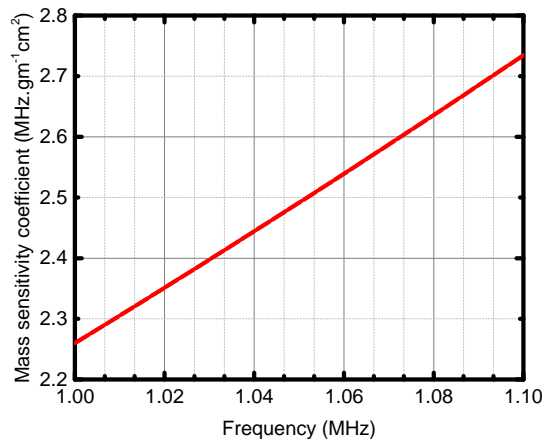


Fig. 3(d). The curve which shows the calculated mass sensitivity coefficients using Sauerbrey mass sensitivity coefficient equation.

4.3. Calculated Mass Resolution

The mass which can be detected on the surface of active center electrode area of each disk were calculated by taking the ratio of detection limit Δf (τ) in Fig. 3 (c) to mass sensitivity coefficient (K) in Fig. 3 (d). The curve which shows mass resolution per unit area of each disk is in Fig. 3 (e). The minimum mass resolution is 825 femtograms at 1.067 MHz for the disk with a diameter of 3 mm.

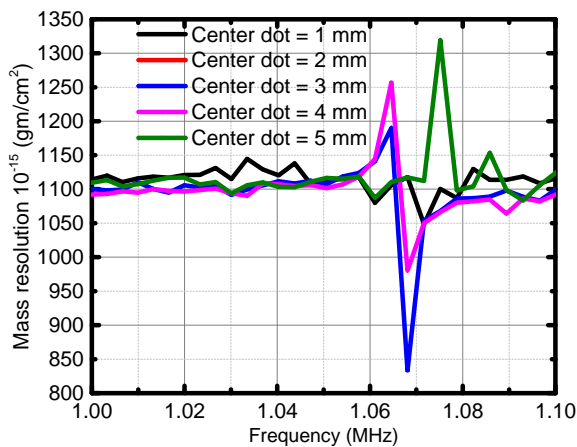


Fig. 3 (e). The curve which shows the calculated mass resolution as a function of frequencies and electrode diameters of five disks.

4.4. Measured Mass Using Frequency Shift

In order to convert the frequency shift to mass added on the surface of the active gold electrode, the Volume (V) of the Gold layer was calculated using the equation $\pi r^2 t$ where the thickness (t) is 3×10^{-5} cm and the radius (r) is 0.15 cm. The mass (m) of the Gold layer is calculated by multiplying the density of gold to the volume it occupies. Therefore the mass is given

by multiplying $\pi r^2 t \times \rho = (3.14 \times 0.15 \text{ cm} \times 0.15 \text{ cm} \times 3 \times 10^{-5} \text{ cm}) \times (19.3 \text{ g/cm}^3) = 4.09 \times 10^{-5} \text{ g}$, where ρ is the density of Gold which is equal to 19.3 g/cm^3 . The measured frequency shift (Δf) was 2×10^{-8} MHz when the resonant frequency (f) was 1.067 MHz. The frequency ratio ($\Delta f/f$) at resonance was found to be 1.9×10^{-8} . The mass change (Δm) is given by the expression: $\Delta f/f \times m = 1.9 \times 10^{-8} \times 4.09 \times 10^{-5} \text{ g} = 7.77 \times 10^{-13} \text{ g}$. This mass is approximately $8.25 \times 10^{-13} \text{ g/cm}^2$ calculated by taking the ratio of mass sensitivity coefficient to the detection limit, as seen in Fig. 3 (e). These results are almost the same as those reported by Mecea [23] with a frequency stability of $(\Delta f/f) = 1.5 \times 10^{-9}$, showing mass which is equivalent to $1 \text{ pg} \times \text{cm}^{-2}$.

5. Challenges for Developing Diagnostic POC Based on QCM Mass Sensor

One of the challenges facing the development of femtogram mass sensors is particle selectivity and separation from the blood. Recently, biomarkers have shown good results for selectivity of certain virus, bacteria, cells, and molecules [24-28]. Moreover; the technological advances in microfluidic driven by ultrasonic acoustic forces which separate suspended particles in the fluid medium [29-32], have shown that it possible to combine QCM mass sensor technology with microfluidic to develop portable diagnostic POC. This review has shown that the separation technique based on microfluidic driven by ultrasonic acoustic forces is better than other conventional particle preparation and separation; using electro-spin [33], centrifuge [34], and BPS [35].

The conventional microfluidic techniques faces tremendous challenges such as:

1) Inconsistencies with diluting blood samples which causes inaccuracies into the measurements and reduced concentration of target analyses, leading to reduced assay sensitivity,

2) Complex designs that are cost-ineffective to integrate into microfluidic platforms,

3) Time consuming workflow systems with low extraction rates [36].

By using the new development of simplified microfluidic systems controlled with ultrasound standing waves, now it is possible to build a miniaturized microfluidic system for particles separation from whole blood [37-39]. This technology is currently used for separation of lipid particles in blood during major surgery, significantly reducing the embolic load to the brain after cardiac surgery [40]. Also, through this review, we noted that the low power ultrasonic acoustic forces can be used to separate suspended particles in the fluid in microscale to the nanoscale regime, while the high-power ultrasonic acoustic forces can be used to enhance industrial fluid/solid particle separation processes in macro scale [41].

6. Integration of Microfluidic to QCM Mass Sensor

In the flowchart shown in Fig. 4, the blood is injected into the microfluidic driven by ultrasonic acoustic forces which separate blood into cells, antigens, electrolytes, bacteria, and troponins. The components of the microfluidic delivery system are not discussed in this flowchart but include; micro pumps, micro valves, micro volumes, ultrasonic acoustic forces and a reflector, while the sensing components consist of biomarkers and special assay formats with gold nanoparticles on QCM. Successfully interfacing the microfluidic delivery system with QCM mass sensor will make it possible to develop cost-effective diagnostic POC system.

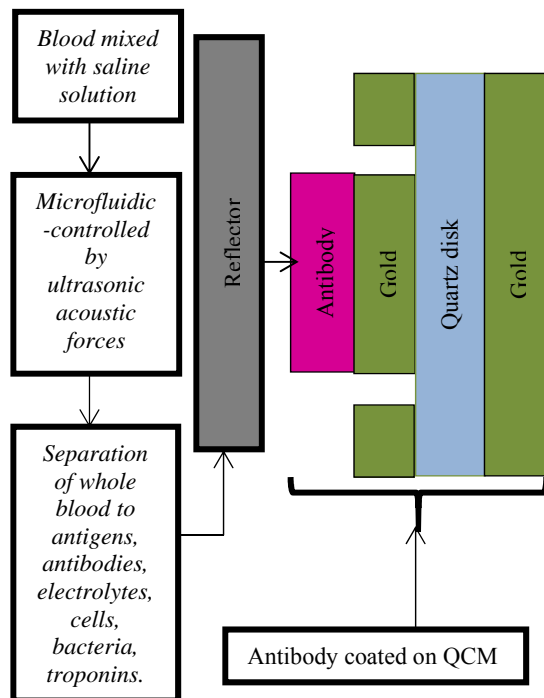


Fig. 4. The flow chart which shows blood flow into the microfluidic driven by ultrasonic acoustic standing wave attached to a sensor with antibody and gold, functionalized on QCM mass sensor.

7. Market Overview

The emerging market is expected to be in the home care, public health, agriculture, and food industry sectors. In the home care, there is a need to develop cost-effective diagnostic POC portable systems based on QCM mass sensor functionalized with anti-troponin [42-45]. Anti-troponin is gold standard sensitive biomarkers used to detect Myocardial Infraction (MI) by attracting troponin molecule from the blood. It is expected that troponin biomarkers could grow to encompass much of the diagnostic point of care (POC) market with a more sensitive and less expensive option [46]. The benefits of using POC tests can drastically increase patients' chances of survival

as they can be administered much more quickly than lab tests in the hospitals [47]. A report [48] prepared by the Canadian Agency for Drugs and Technologies in Health (CADTH) estimated an annual cost of C\$1,652,433,246 to do troponin (cTn) laboratory testing for suspected Acute Coronary Syndrome (ACS) patients, admitted through the emergency department in the hospital. This report showed that replacement of laboratory testing of cTn with POC devices could save billions of Canadian dollars and save the lives of many people by detecting the ACS before it happens in homes.

In the public health, agriculture and food industry sectors, the global cost to prevent and cure SARS outbreak was estimated to be 40 billion dollars [49] in 2003 while an outbreak of foot and mouth disease in the UK (2001) was about 5.8 billion dollars in reduced livestock production earnings [50]. Therefore, there is a need to use the existing inventions based on QCM mass sensor or any Bulk Acoustic Wave (BAW) biosensor which can detect a mass in femtogram regime, to build diagnostic POC equipment, for detecting SARS and foot and mouth diseases before infection. The global market for BAW biosensors was predicted to be 2000 to 17000 million US dollars from 2000 to 2018 and, valued to reach \$22.68 billion [51] by 2020. Among these BAW biosensors, two-thirds is expected to be based on QCM mass sensor which is equivalent to \$15.12 billion.

8. Conclusions

The QCM is limited to nanogram (10^{-9} g) but we have shown that it is possible to extend this technology to measure (10^{-13} g to 10^{-15} g) in the air. Also, we have shown that many inventions are reported to measure femtograms (10^{-15} g) but this technology does not exist due to the complexity of reproducing the claimed patents. Among these inventions, QCM disks are cost effective, currently available in the market, and can be reproduced easily. One of the future challenges is to integrate the sensor component with sample holders such as microfluidic, micro air, and microcentrifuge. The new development of novel ultrasonic acoustic standing wave devices for particle separation and nanoparticle/composite materials bioassays may provide suitable free-BPS POC solutions, which can overcome the matrix effects of whole blood.

The advances in bioassays have also led to increasing number of sensitive, smart and simplified POC based on whole blood, bypassing BPS, hence creating a rationale for its exclusion in use with "An Ultrasensitive High Q-factor QCM Mass Sensors" [52]. Also, we envision that a diagnostic POC with femtogram sensitivity will reduce the patient severity, death, false-positive hospital admittance, unnecessary costs to the hospital, and will have a potential to impact many scientific research fields; including medicine, nanotechnology, semiconductor manufacturing, and pharmaceutical research. This technology will create new business

opportunities; therefore, creating new jobs in research institutions, hospitals, homeland security, pharmaceutical industries, and agriculture and food industry sectors.

Acknowledgments

I thank Prof. Thomas Thundat and Kenneth Cadien for their financial support, feedbacks, and for allowing me to use their laboratories. I also thank Dr. Prashanthi Kovur for helping me with Impedance measurements of my samples.

References

- [1]. A. Sharma, E. Clark, J. D. McGlothlin, S. K. Mitta, Efficiency of airborne sample analysis platform (ASAP) bioaerosol sampler for pathogen detection, *Journal of Front. Microbiol.*, Vol. 6, 2015, pp. 1-7.
- [2]. M. S. Petrovick, J. D. Harper, F. E. Nargi, E. D. Schwoebel, M. C. Hennessy, T. H. Rider, M. A. Hollis, Rapid sensors for biological-agent identification, *Lincoln Laboratory Journal*, Vol. 17, No. 1, 2007, pp. 63-84.
- [3]. S. Faegh, N. Jalili, S. Sridhar, A self-sensing piezoelectric microcantilever biosensor for detection of ultra-small adsorbed masses: Theory and Experiments, *Sensors*, Vol. 13, No. 5, 2013, pp. 6089-6108.
- [4]. M. L. Routes, K. L. Ekinici, Apparatus and method for ultrasensitive nanoelectromechanical mass detection, US Patent No. 6 722 200, 2004.
- [5]. K. L. Ekinici, X. M. H. Huang, M. L. Roukesb, Ultrasensitive nanoelectromechanical mass detection, *Journal of Applied Physics Letters*, Vol. 84, No. 22, 2004, pp. 4469-4471.
- [6]. N. V. Lavrik, P. G. Datskos, Femtogram mass detection using photo thermally actuated nanomechanical resonators, *Journal of Applied Physics*, Vol. 82, No. 16, 2003, pp. 2697-2699.
- [7]. S. Dohn, W. Svendsen, A. Boisen, Mass and position determination of attached particles on cantilever based mass sensors, *Review of Scientific Instruments*, Vol. 78, No. 10, 2007, pp. 1033031-1033033.
- [8]. M. Villarroya, *et al.*, System on chip mass sensor based on polysilicon cantilevers arrays for multiple detections, *Sensors and Actuators A: Physical*, Vol. 132, No. 1, 2006, pp. 154-164.
- [9]. Y. T. Yang, C. Callegari, X. L. Feng, K. L. Ekinici, M. L. Routes, Zeptogram-scale nanomechanical mass sensing, *NANO Letters*, Vol. 6, No. 4, 2006, pp. 583-586.
- [10]. B. Ilic, H. G. Craighead, S. Krylov, W. Senaratne, C. Ober, Atograms detection using nanoelectromechanical oscillators, *Journal of Applied Physics*, Vol. 95, No. 7, 2004, pp. 3694-3703.
- [11]. S. Akita, T. Erie, Carbon nanotube mechanical resonators for mass sensing, *Sensors and Materials*, Vol. 21, No. 7, 2009, pp. 339-349.
- [12]. Y. Dayagi, L. Dayan, M. Shalom, Sensitive and selective method and device for the detection of trace amounts of a substance, US Patent No. 7 159 463 B2, January 9, 2007.
- [13]. V. Smith. R. Bhethanabotla, A. J. Richardson, Uniform mass sensitivity thickness shear mode quartz resonator, US Patent No. 8 215 171 B, July 2012.
- [14]. W. Hin, Quartz crystal microbalance (QCM) mass sensor, Patent No. CN 102967521 B, April 2015.
- [15]. C. K. O'Sullivan, G. G. Guilbault, Commercial quartz crystal microbalances – theory and applications, *Biosensors and Bioelectronics*, Vol. 14, No. 8-9, 1999, pp. 663-670.
- [16]. R. E. Speight, M. A. Cooper, A survey of the 2010 quartz crystal microbalance literature, *Journal of Molecular Recognition*, Vol. 25, No. 9, 2012, pp. 451-473.
- [17]. M. A. Cooper, V. T. Singleton, A survey of the 2001 to 2005 quartz crystal microbalance biosensor literature: applications of acoustic physics to the analysis of biomolecular interactions, *Journal of Molecular Recognition*, Vol. 20, No. 3, 2007, pp. 154-184.
- [18]. B. Becker, M. A. Cooper, A survey of the 2006-2009 quartz crystal microbalance biosensor literature, *Journal of Molecular Recognition*, Vol. 24, No. 5, 2011, pp. 754-787.
- [19]. M. Sauerbrey, Verwendung von schwingquarzen zur wägung dünner schichten und zur mikrowägung, *J. Zeitschrift Für Physik*, Vol. 155, No. 2, 1956, pp. 206-222.
- [20]. G. O. Garcia-Martinez, *et al.*, Development of a mass sensitive quartz crystal microbalance (QCM)-based DNA biosensor using a 50 MHz electronic oscillator circuit, *Sensors*, Vol. 11, No. 8, 2011, pp. 7656-7664.
- [21]. M. J. Moure, P. Rodiz, D. Valdes, L. F. Rodriguez-Padro, J. Farina, An FPGA-based system for the measurement of frequency noise and resolution of QCM sensors, *Latin American Applied Research*, Vol. 37, No. 1, 2007, pp. 25-30.
- [22]. L. Rodriguez-Pardo, J. F. Rodriguez, C. Gabrielli, H. Perrot, Sensitivity, noise, and resolution in QCM sensors in liquid media, *IEEE Sensors Journal*, Vol. 5, No. 6, 2005, pp. 1251-1257.
- [23]. V. M. Mecea, Is quartz crystal microbalance really a mass sensor? *Sensors and Actuators A: Physical*, Vol. 128, No. 2, 2006, pp. 270-277.
- [24]. S. P. Martin, R. J. Townsend, L. A. Kuznetsova, K. A. J. Borthwick, M. Hill, M. B. McDonnell, W. T. Coakley, Spore and micro-particle capture on an immunosensor surface in an ultrasound standing wave system, *Biosensors and Bioelectronics*, Vol. 21, No. 5, 2005, pp. 758-767.
- [25]. O. Manneberg, B. Vanherberghen, J. Svennebring, H. M. Hertz, B. Onfelt, M. Wiklund, A three-dimensional ultrasonic cage for characterization of individual cells, *Journal of Applied Physics Letters*, Vol. 93, No. 6, 2008, p. 063901.
- [26]. F. L. Dickert, P. Lieberzeit, O. Hayden, Sensor strategies for microorganism detection – from physical principles to imprinting procedures, *Analytical and Bioanalytical Chemistry*, Vol. 377, No. 3, 2003, pp. 540-549.
- [27]. M. R. Gaso, C. M. Iborra, Á. M. Baidés, A. A. Vives, Surface generated acoustic wave biosensors for the detection of pathogens: A Review, *Sensors*, Vol. 9, No. 12, 2009, pp. 5740-5769.
- [28]. D. Klenerman, V. P. Ostanin, F. N. Dultsev, Measurement and use of molecular interactions, *United States Patent*, Patent No. US 6,589,727 B1, July 8, 2003.
- [29]. F. Petersson, A. Nilsson, C. Holm, H. Jonsson, T. Laurell, Separation of lipids from blood utilizing

- ultrasonic standing waves in microfluidic channels, *Analyst*, Vol. 129, No. 10, 2004, pp. 938–943.
- [30]. M. Gröschl, Ultrasonic separation of suspended particles - part I: fundamentals, *ACUSTICA- Acta Acustica*, Vol. 84, 1998, pp. 432-447.
- [31]. N. Oyama, S. Yamaguchi, T. Shimomura, K. Miki, A method for detecting target sequences by oscillation frequency, *United States Patent*, Patent No. 5,552,274, Sep. 3, 1996.
- [32]. J. J. Hawkes, W. T. Coakley, Force field particle filter, combining ultrasound standing waves and laminar flow, *Sensors and Actuators B: Chemical*, Vol. 75, 2001, pp. 213-222.
- [33]. Y. S. Park, V. Sunkara, Y. Kim, W. S. Lee, J. R. Han, Y. K. Cho, Fully automated centrifugal microfluidic device for ultrasensitive protein detection from whole blood, *Journal of Visualized Experiments*, Issue 110, 2016, pp. 1-7.
- [34]. D. R. Gossett, W. M. Weaver, A. J. Mach, S. C. Hur, H. T. Tse, W. Lee, H. Amini, D. D. Carlo, Label-free cell separation and sorting in microfluidic systems, *Analytical and Bioanalytical Chemistry*, Vol. 397, No. 8, 2010, pp. 3249-3267.
- [35]. S. Tripathi, Y. V. Bala, V. Kumar, A. Prabhakar, S. S. Joshi, A. Agrawal, Passive blood plasma separation at the microscale: a review of design principles and microdevices, *Journal of Micromechanics and Microengineering*, Vol. 25, No. 8, 2015, pp. 1-24.
- [36]. W. S. Mielczarek, E. A. Obaje, T. T. Bachman, M. Kersaudy-Kerhoas, Microfluidic blood plasma separation for medical diagnostics: is it worth it?, *Lab on a Chip*, Vol. 16, No. 18, 2016, pp. 3441-3448.
- [37]. D. G. Sadikova, T. N. Pashovkin, Cell concentration and separation in the field of a standing ultrasonic wave for medicine and biotechnology, *Open Journal of Biophysics*, Vol. 3, No. 1A, 2013, pp. 70-75.
- [38]. A. Wloch, H. Czy, T. Jasiski, Ultrasonic methods of the cells separation in human blood, *Acta Physica Polonica A*, Vol. 128, No. 2, 2015, pp. 234-236.
- [39]. H. Jonsson, A. Nilsson, F. Petersson, M. Allers, T. Laurell, Particle separation using ultrasound can be used with human shed mediastinal blood, *Perfusion*, Vol. 20, No. 1, 2005, pp. 39-43.
- [40]. D. Bergman, I. M. Hartvig, S. Uhrberg, Assay device and method, WO 2005089082 A2, Application No. PCT/SE2005/000429, Sep 29, 2005.
- [41]. E. R. Sarabia, J. A. Gallego-Juarez, G. R. Corral, L. E. Segura, Application of high-power ultrasound to enhance fluid/solid particle separation processes, *Ultrasonic*, Vol. 38, No. 1-8, 2000, pp. 642–646.
- [42]. T. Keller, *et al.*, Sensitive troponin I assay in early diagnosis of acute myocardial infarction, *The New England Journal of Medicine (NEJM)*, Vol. 361, No. 9, 2009, pp. 868-877.
- [43]. D. B. Diercks, *et al.*, Diagnostic accuracy of a point-of-care troponin I assay for acute myocardial infarction within 3 hours after presentation in early presenters to the emergency department with chest pain, *American Heart Journal*, Vol. 163, No. 1, 2012, pp. 74-80.
- [44]. T. Reichlin, *et al.*, One-hour rule-out and rule-in of acute myocardial infarction using high-sensitivity cardiac troponin T, *Arch. Intern. Med*, Vol. 172, No. 16, 2012, pp. 1211-1218.
- [45]. B. Cummins, *et al.*, Cardiac-specific troponin-I radioimmunoassay in the diagnosis of acute myocardial infarction, *American Heart Journal*, Vol. 113, No. 6, 1987, pp. 1333-1344.
- [46]. P. B. Lippa, Carolin Muller, Alice Schlichtiger, Harald Schlebusch, Point-of-care testing (POCT): Current techniques and future perspectives, *Trends in Analytical Chemistry*, Vol. 30, No. 6, 2011, pp. 887-898.
- [47]. P. von Lode, Point-of-care immune testing: Approaching the analytical performance of central laboratory methods, *Clinical Biochemistry*, Vol. 38, Issue 7, 2005, pp. 591-606.
- [48]. Canadian Agency for Drugs and Technologies in Health (CADTH), Point-of-care cardiac troponin testing in patients with symptoms suggestive of acute coronary syndrome, *CADTH Optimal Use Report*, No. 5.1a, 2015, pp. 1-3.
- [49]. J. W. Lee, W. J. McKibbin, Estimating the global economic costs of SARS, website at <http://www.ncbi.nlm.nih.gov/books/NBK92473/>
- [50]. D. L. P. J. Leatherman, T. C. Schroeder, G. S. Alward, The economic impact of foot –and- mouth disease outbreak region analysis, website at <http://ageconsearch.umn.edu/bitstream/10252/1/sp07pe01.pdf>
- [51]. Biosensors Market worth \$22.68 Billion by 2020, website at <http://www.marketsandmarkets.com/Market-Reports/biosensors-market-798.html>
- [52]. S. Seif, T. Thundat, K. Cadien, An Ultrasensitive AT-Cut quartz crystal microbalance femtogram mass sensor, US-Provision Patent No. 2016010-072-82-25, filed November 2016.



Capacitive Measurer of Linear Displacement

¹ Boris MAMIKONYAN and ² Lusine ABRAHAMYAN

¹ National Polytechnical University of Armenia, Gyumri Branch
2, Mher Mkrtychyan, 3103, Gyumri, Armenia

² National Polytechnical University of Armenia, Yerevan Educational Complex
105, Teryan, 0009, Yerevan, Armenia

¹ Tel.: +374312-46832, fax: +374312-43528

¹ E-mail: b_mamikonyan@seua.am

Received: 30 July 2017 /Accepted: 30 August 2017 /Published: 31 August 2017

Abstract: The features of constructing of a linear displacement measurer with differential capacitive transducer are considered. The measuring circuit is analyzed, which makes possible to implement a linear algorithm for determining the measured displacement. With an appropriate choice of the base element, in the production conditions the device can provide measurement of linear displacements with a limit of the permissible basic comparative error not exceeding 0.12 %.

Keywords: Measurement, Measuring circuit, Capacitive transducer, Phase signal, Microcontroller, Computer.

1. Introduction

Capacitive measuring transducer (CMT) are widely used for conversion of various physical and mechanical values into an electrical signal. The advantages of the CMT are simplicity of design, low weight and dimensions, low inertia, high mechanical and electrical overload capacity, low cost, great functional flexibility, high temperature stability over a wide range of temperature changes [1, 2]. Preference is given to the differential design of the CMT: the presence of two identical halves of the CMT in one body allows to implement comparative transformation of the working capacity, to protect from the influence of external symmetrical handicaps, reduces the influence of electrostatic forces acting on the CMT plates, maintain high metrological characteristics in the temperature range up to 200 °C [3].

2. Research Object

For the measurement of small displacements, it is advisable to use a CMT with a variable gap [1]. For

such a CMT with a plane-parallel electrode system, the static conversion characteristic is determined by the known formula

$$C_x = \epsilon_0 \epsilon S / d, \quad (1)$$

where $\epsilon_0 = 8,854 \cdot 10^{-12}$ F/m is the dielectric permeability of the vacuum (air) which is the physical constant, ϵ is the comparative dielectric permeability of environment between the electrodes, S and d are the overlap area and the distance between the electrodes.

It follows from (1) that the sensitivity of the CMT to the air gap

$$K = \frac{\partial C_x}{\partial d} = -\frac{\epsilon_0 \epsilon S}{d^2}$$

That's why the increase of sensitivity is achieved by reducing the initial gap between the electrodes and increasing the size of the CMT. The resolution of the CMT with variable gap can reach 10-6 μm [4].

The measured movement x affects on the parameter d , increasing or decreasing it, and the capacitance C_x is inversely proportional to this distance. The electronic secondary converter can be constructed in such a way that its output voltage (or current) will be proportional to capacitance C_x rather than capacitance $X_C = 1/\omega C_x$ [1]. The output signal will be directly proportional to the measured displacement.

However, it is necessary to take into account peculiarities of the application of the CMT in control and monitoring systems: the CMT have a small initial capacity, which in most cases lies in the range from 10 to 10^3 pF. This circumstance leads to the need to use high frequency voltage from $1 \cdot 10^3$ to $(1 \div 2) \cdot 10^8$ Hz for the operation of sensors. Using low frequencies, for example, an industrial frequency of 50 Hz, the CMTs have a large reactive resistance, which limits their use in measuring circuits.

The use of a high-frequency signal leads to the need for additional analog and digital conversion in order to obtain unified signals (current, frequency or voltage) convenient for remote transmission over distances and subsequent use in control and monitoring systems [5].

Modern CMTs have sufficiently high metrological characteristics, their error of primary conversion does not exceed $\pm 0.1\%$ [5]. Therefore, the main direction of improving the accuracy of modern information and measurement systems based on the capacitive method is the improvement of known or the design of new methods for processing measuring signals (methods of converting electrical capacitance into an electrical signal) of the CMT, as well as methods for recording and compensating external disturbances.

The differential CMT displacement, based on the change of the distance d between the plates, is a flat condenser with electrodes 1, 2 and 3 (Fig. 1). Electrodes 1 and 2 are fixed immovably, and electrode 3 is the reproducing part of CMT. The function of transforming differential CMT displacements is the dependence $\Delta C = C_1 - C_2 = f(x)$.

In the initial position of the movable electrode, when the measured movement $x = 0$, we do have

$$d_1 = d_2 = d_0, C_1 = C_2 = C_0 = \frac{\epsilon_0 \epsilon S}{d_0} = \frac{A}{d_0},$$

$$\Delta C = C_1 - C_2 = 0.$$

Under the action of displacement x the capacity of the CMT is changing as follows

$$C_1 = \frac{A}{d_0 - x}, C_2 = \frac{A}{d_0 + x}, \quad (2)$$

and we obtain a nonlinear function of displacement transformation x :

$$\Delta C = \frac{2A \cdot x}{d_0^2 - x^2} = \frac{2A \cdot x}{d_0^2 (1 - x^2/d_0^2)}$$

In this regard, to limit the error of non-linearity, the measuring range is limited by the value $x \leq 0,1d_0$.

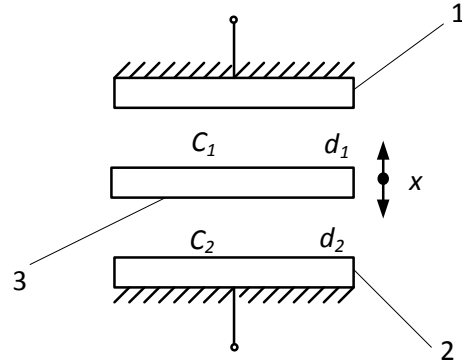


Fig. 1. Differential CMT with variable gap.

Then the maximum nonlinearity obtained at the end of the measurement range and determined by a deviation from unity of the value is $1 - x^2/d_0^2$, equal to $1 - x_m^2/d_0^2 = 1 - 0,01$ which does not exceed 1.0%.

With accurate measurements, this error value is also unacceptable, besides, such a limitation of the measuring range is not always desirable. Thus, in the measuring circuit (MC), in which the passive information parameter ΔC is converted into the active value - into an electrical signal, the task of ensuring the linearity of the functional dependence between the output signal and the measured motion must be solved.

3. Research Methods

In this research, this problem is solved by selecting the appropriate MC scheme, in which the phase angle of displacement between u_s and u_x is used as the output signal (Fig. 2). In this scheme, CMT is series connected with supporting exemplary resistor R_0 via an electronic switch, which forms a voltage divider with an CMT - powered by the current of the generator of sinusoidal oscillations (G).

In the initial position of the switch, the angle of phase φ_1 of displacement between the output voltages u_s and u_x is determined by the expression

$$\operatorname{ctg} \varphi_1 = \frac{U_x}{U_0} = \frac{IX_{C1}}{IR_0} = \frac{X_{C1}}{R_0}$$

$$\operatorname{ctg} \varphi_2 = \frac{X_{C2}}{R_0}$$

In the second position of the switch the difference

$$F = ctg\varphi_2 - ctg\varphi_1 = \frac{X_{C2} - X_{C1}}{R_0} \quad (3)$$

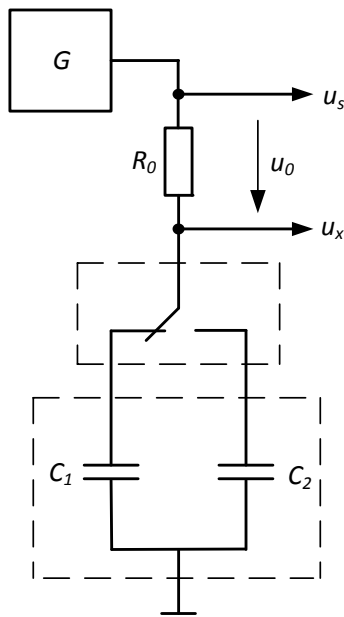


Fig. 2. The scheme of measuring circuit of CMT.

Taking into account the values $X_{C1} = 1/\omega C_1$, $X_{C2} = 1/\omega C_2$, where ω - the angular frequency of the generator, we obtain from (3)

$$F = \frac{1}{\omega R_0} \cdot \frac{C_1 - C_2}{C_1 C_2} \quad (4)$$

Taking into account the dependences (2), expression (4) get the form

$$F = \frac{2}{\omega R_0 \varepsilon_0 \varepsilon S} \cdot x \quad (5)$$

Consequently, the MC in Fig. 2 provides a linear dependence between the measuring displacement and value F . Thus, from (5) we obtain an algorithm for determining the displacement x

$$x = \frac{\omega R_0 \varepsilon_0 \varepsilon S}{2} \cdot (ctg\varphi_2 - ctg\varphi_1) \quad (6)$$

From (6) it can be seen that the measurement result is not affected by the voltage and current of the generator and the measuring circuit, which indicates a high noise immunity of the measurement method. It is necessary to measure only the angle of phase displacement between two voltages, which is the most accurately measured value in the digital electrical measuring technique.

4. Electrical Circuit

In the developed device (Fig. 3), the voltages u_s and u_x are applied to the inputs of a programmable microcontroller (MCR) 4, which controls the operation of the switch and measures the φ angle values. In the MCR the φ angle is converted into a time interval τ . The time intervals τ and T (the period of voltages u_s and u_x) are measured by the discrete counting method by filling them with impulses of the exemplary frequency f_0 of the MCR generator using its integrated timer-counter. Further, the angle is calculated by the formula $\varphi = \tau \cdot 360^\circ / T$.

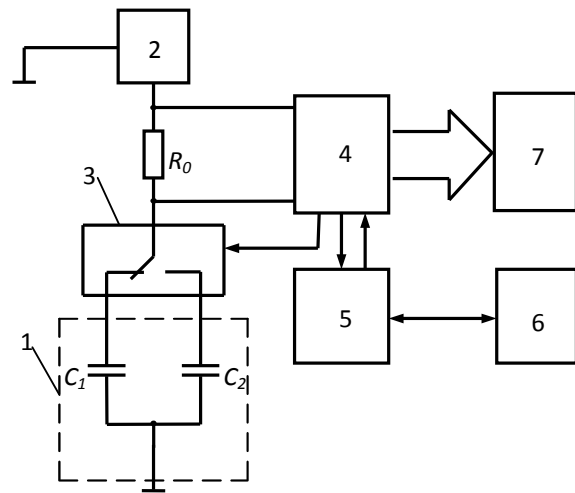


Fig. 3. Simplified scheme of connections of a linear displacement with a differential CMT.

Then, from the measured values φ , the MCR calculates the value x according to Formula (6). To increase the accuracy of the measurements, each measurement MCR repeats 10 times and determines the average value of the results. From the MCR, the digitized signals of angles φ_1 and φ_2 via the AVR309 interface converter 5 are sent to the computer 6, where they are processed and the measurement results are output to the computer monitor. The MCR displays the results of the measurement also on the digital readout device 7.

When selecting a power supply for the measuring circuit, it should be taken into account that the stability of its voltage is not significant, but the measurement result depends on the frequency of the generator. The presence of MCR dictates the appropriateness of using integrated circuits for the programmable generators of sinusoidal signals (for example, type AD9833). At each measurement, the MCR sets the frequency of the generator and uses this frequency value when calculating the measured value, so that possible changes in the generator frequency do not affect the accuracy of the measurement. The frequency of the

measuring current is preferably at least 50 kHz. In this case, it should be taken into account that with increasing frequency of power supply MC accuracy in measuring the phase angle is reduced.

The resistance of the supporting resistor must be selected in such a way that the maximum sensitivity of the conversion of the CMT parameter to the angle φ is ensured. This is the case, where at the initial point of the conversion $C_1 = C_2 = C_0$, when the condition $\varphi_1 = \varphi_2 \approx 45^\circ$ is valid. Hence, from the condition $\text{ctg } \varphi = 1$

$$X_{C_0} = R_0 \text{ or } R_0 = \frac{1}{\omega C_0}.$$

For example, with the use of CMT, these values are as follows: $C_0 = 50$ pF, $f = 50$ kHz, therefore, should be $R_0 = 127,4$ kOhm. The developed device uses a resistor type C2-29B with a tolerance of 0.1 %.

As a switch, it is advisable to select a sensitive electronic switch-multiplexer ADG859. The chip is intended for commutation of DC and AC circuits, has the following parameters: channel resistance in the closed state is $1,3 \Omega$, in open mode it is about $\sim 10^{11} \Omega$, channel impedance mismatch is $0,01 \Omega$, maximum current through the closed channel is 300 mA, The supply voltage is unipolar, 1,8...5,5 V, the on/off time is 8/4,5 ns, the frequency range is 125 MHz, the operating temperature range is -40°C to $+125^\circ\text{C}$. This chip best suits the operating conditions of this device.

When choosing the MCR, it should be taken into account that it must have the highest possible frequency f_0 of the clock generator and, more importantly, two internal comparators, whose inputs will receive voltages u_s and u_x (preferably through voltage-buffer repeaters, so as not to load the MC), to convert the angle φ into the duration τ of rectangular pulses. The use of an internal ADC of MCR for this purpose is inadvisable, because the value of the conversion period (sampling) of the ADC limits the minimum possible value τ , thereby substantially increasing the sensitivity threshold of the measurer.

5. Results

A method for theoretical investigation of the error in measuring the displacement by the phase method is developed. It is established that the use of time separation of the measurement channel ensures elimination of the methodical error due to the capacitance of the connector cable of the CMT and the imperfection of the element base of the measuring circuit. The expression for the comparative measurement error is obtained in the form

$$\delta(x) = \frac{f}{f_0} \cdot (\varphi_1 - \varphi_2) \cdot \text{ctg}(\varphi_1 - \varphi_2)$$

It can be seen that the measurement error can be reduced by increasing the frequency f_0 of the MCR clock generator and decreasing the frequency f of the power supply MC generator. At the same time, as the difference $(\varphi_1 - \varphi_2)$ increases, the error decreases. If, for technical reasons, a higher frequency of the supply voltage of the MC is required, then the MCR with a higher clock frequency generator should be selected.

The measurement error has been evaluated depending on all parameters influencing on the accuracy of the measurement and it is stated that with appropriately selected MC parameters and generator frequencies, the required measurement accuracy can be provided.

6. Conclusion

Analysis of the research results shows that the selected MC scheme and the used phase method of measurement, based on the time separation of the measuring channel, provide a digital invariant measurement of the informative parameter of the differential CMT. The developed device is simple in practical implementation and can provide high accuracy of measurement due to the use of phase signals instead of potential signals and current signals, which ensures high noise immunity of measurement results. With an appropriate choice of the base element, in the production conditions the device can provide measurement of linear displacements with a limit of the permissible basic comparative error not exceeding 0.12 %.

References

- [1]. Grinevich F. B., Novik A. I., Measuring compensation-bridge devices with capacitive sensors, *Naukova Dumka*, Ukraine, Kiev, 1987 (in Russian).
- [2]. Nebolyubov E. Yu., Novik A. I., Electronic converters for working with capacitive sensors (analog and digital), *Tech. Electrodinamika*, Issue 3, 2015, pp. 67-74.
- [3]. Arbuзов V. P., Mishina M. A., Belinceva P. N., Ananina I. Yu., Measuring circuits of high-temperature capacitive pressure sensors, *Izmerenie, Monitoring, Upravlenie, Kontrol*, Issue 1, 2015, pp. 81-88 (in Russian).
- [4]. Topilskii V. B., Microelectronic measuring transducers, *BINOM*, Moscow, 2013 (in Russian).
- [5]. Mastepanenko M. A., Vorotnikov I. N., Anikuev S. V., Sharipov I. K., Mathematical models and methods of processing measuring signals of capacitive DC converters: Monograph, *AGRUS Stavropol State Agrarian University*, Stavropol, 2015 (in Russian).

First International Conference on Optics, Photonics and Lasers OPAL' 2018

2018 OPAL

9-11 May 2018
Barcelona, Spain

<http://www.opal-conference.com>

OPAL 2018 will incorporate the following three symposiums covering a broader range in optics, photonics and lasers, and provide an excellent opportunity to exchange ideas and present latest advancements in these areas. The OPAL 2018 will be organized by IFSA. Media partner - journal *Photonics* (ISSN 2304-6732).

The conference is focusing any significant breakthrough and innovation in optics, photonics, lasers and its applications

- Optical and Fibre Optical Sensors and Instrumentation
- Micro-Opto-Electro-Mechanical Systems (MOEMS)
- Physical Optics
- Optoelectronic Devices, Photonics, Nanophotonics and Biophotonics
- Organic Optoelectronics and Integrated Photonics
- Optical Communications, Switching and Networks
- High-speed Opto-electronic Networking
- Optical Fiber Technology: Materials, Devices and Systems
- Optical Information Processing
- Holography
- Optical Metrology
- Optical Imaging Systems and Machine Vision
- Optical Computing
- Guided Wave Optics
- Optics in Condensed and Soft Matter
- Quantum Optics
- Lasers and Laser Applications
- Nonlinear Optics
- Nano and Micro Optics
- Matter Waves
- Quantum Information
- Bio and Medical Optics
- Optical Materials, Characterization Methods and Techniques
- Optical Methods for Process Control
- Microscopy and Adaptive Optics
- Lasers in Medicine and Biology
- Engineering Applications of Spectroscopy
- Optical Microscopy of Composites

Special Sessions:

Authors are welcome to organize and manage special sessions during the conference. Each session will contain 4-6 papers in a related field as specified above.

Deadlines:

Submission (2-page abstract):
Notification of acceptance:
Registration:
Camera ready (4-6 pages paper):

30 January 2018
28 February 2018
15 March 2018
30 March 2018

Contribution Types:

Keynote presentations
Invited presentations
Regular papers
Posters

One event - three publications !

1. All registered abstracts will be published in the conference proceedings.
2. Selected extended papers will be published in *Sensors & Transducers* journal.
3. The best full-page papers will be recommended to extend to book chapters for 'Advances in Optics: Reviews' Book Series.

Chairman:

Prof., Dr. Sergey Y. Yurish (IFSA, Spain)

Advisory Chairmen:

Dr. Qiang Wu (Northumbria University, Newcastle Upon Tyne, UK)
Prof., Dr. Mahmoud Daoudi (National Center for Nuclear Sciences and Technologies, Tunisia)

Conference Manager:

Mrs. Tetyana Zakharchenko
(IFSA Publishing, S.L., Spain)



Published by International Frequency Sensor Association (IFSA) Publishing, S. L., 2017
(<http://www.sensorsportal.com>).

Cadmium Sulfide Quantum Dot Particles (CdSQD) Dispersed in Poly Methyl Methacrylate as an Effective Gamma Counter for the Scintillation Detector

^{1,4} Askari Mohammad Bagher, ² Beheshti - Marnani Amir Khosro,
³ Mirzaei Mahmoud Abadi Vahid, ¹ Seifi Majid, ¹ Tavakoli Banizi Zoha,
³ Hosseini Ranjbar Abbas and ⁵ Batool Tahamipour

¹ Department of Physics, University of Guilan, Rasht 41335-1914, Iran

² Department of Chemistry, Payame Noor University, Tehran, Iran

³ Faculty of Physics, Shahid Bahonar University of Kerman, Kerman, Iran

⁴ Department of Physics, Payame Noor University, Tehran, Iran

⁵ Young Researchers and Elite Club, Sirjan Branch, Islamic Azad University, Sirjan, Iran

² Tel.: +989132985611

E-mail: Beheshti@pnu.ac.ir

Received: 29 June 2017 / Accepted: 7 August 2017 / Published: 31 August 2017

Abstract: The synthetic material, cadmium sulfide quantum dot particles (CdSQD), using a hydrothermal method was dispersed in poly methyl methacrylate (PMM) polymer. In order to study the synthesized quantum dot particles, X-ray diffraction (XRD) and Fourier transform infrared spectroscopy (FTIR) techniques were applied. Transmission electron microscopy (TEM) and *scanning electron microscopy* (SEM) images were also used to study the surface morphology of synthetic quantum dot particles. Energy-dispersive X-ray spectroscopy (EDX) test was done for identification of constituent percent of prepared material. Optical properties of CdSQD particles were evaluated by UV-visible and photoluminescence spectroscopy (PL). Finally the capability of CdSQD particles dispersed in poly methyl methacrylate (CdSQD@PMM) as a scintillator material was investigated by photomultiplier tube (PMT) test. The result of PMT test along with statistical studies showed that the CdSQD@PMM can be applied as a crystalline promising material in the field of inorganic scintillator detectors regarding to the efficiency and economic aspects.

Keywords: Scintillation detector, Gamma counter, CdS quantum dot particles, Poly methyl methacrylate, PMT test.

1. Introduction

Scintillator detectors are widely used in various sciences such as nuclear physics and analytical chemistry [1, 3]. They have three main parts [4]: the scintillator crystalline which absorbs the high energy

radiations (such as gamma and X-rays) and converts them to a the visible photons [5], the photo multiplier device that is responsible for conversion of the visible photons to electrons and for their multiplication, and the output electrons that are converted to an electronic signal and counted by an electronic circuit. The most

important feature of the detector is its rough proportionality of the number of produced photons to the energy of in-coming radiation. Typically, it has a high sensitivity to the wavelengths less than 2 Å [6-7].

The florescent materials can also absorb the energy of radiation and convert it to photons in a few microseconds [8-9]. These kinds of materials are widely used in the scintillation devices [10]. A most required feature of the material is their transparency to the out-coming photons [11]. Inorganic scintillators such as LiI(Tl) [12] and CsI(Tl) [13] are the most suitable transparent crystals. On the other hand, the organic scintillators in comparison to the inorganic ones have generally low transparency [14].

In the current work considering both critical features of the scintillator crystals, photoluminescence and transparency, poly methyl methacrylate (PMM) dispersed with fluorescent quantum dot particles of cadmium sulfide (CdSQD@PMM) [15-16] have been studied. The structure and photo properties of the quantum dot particles and capability of hybrid preparation as scintillation applications were investigated by XRD, FTIR, SEM, TEM, EDX and PMT test. In addition, it is expected that the synthetic hybrid, CdSQD@PMM, possesses the appropriate flexibility with anti humidity properties due to its organic nature of the polymer. The softness and flexibility of the hybrid can also help toleration against shocks and vibrations. Finally, the results of PMT test evaluated by meaningfulness statistical parameters (T and Chi-squared) proved the promising application of the synthetic hybrid as an economic and effective materials in comparison to the expensive trade devices.

2. Materials and Methods

The cadmium sulfate octa hydrate (CdS.8H₂O) and thioglycolic acid (TGA) were obtained from Merck. Poly methyl methacrylate and Dimethyl formamid (DMF) as the polymer solvent, were purchased from Sigma Aldrich.

3. Synthesis of CdS Quantum Dot Particles (CdSQD)

About 50 µl of TGA was added to 0.01 molar solution of cadmium sulfate. It was agitated for 10 minutes then after continuing with adding drop wise of sodium sulphid of 0.01 molar and stirred for another 10 minutes. The prepared solution was transferred to a stainless steel autoclave and exposed to 140 °C for 30 minutes through the hydrothermal condition. The obtained precipitate was centrifuged and washed with deionized water and ethanol for three times. Finally the product was dried in an oven at 60 °C for 6 hours.

4. Preparation of CdSQD@PMM

About 0.005 gr of poly methyl methacrylate powder was dissolved in 3 milliliters of DMF and then 0.001 g of the prepared CdSQD particles was added to the mixture. The prepared gel was sonicated for 15 minutes. The obtained hybrid was dried in an oven at 40 °C for 6 hours.

5. Characterization of Synthetic Hybrid

To study of structural features of the prepared material, X-ray diffraction (XRD) and FTIR spectra of prepared CdSQD were obtained. Field emission SEM (FESEM) and TEM images were also obtained for confirmation of synthesis of quantum dot CdS. EDX analysis also endorsed the composition of constituents of synthetic CdSQD. In order to study the energy level of the defects on the surface and interface of the materials, the photoluminescence properties of prepared CdSQD was observed.

6. Results and Discussion

6.1. XRD Characterization of CdSQD

The XRD spectrum of quantum dot CdS particles is shown in Fig. 1. As can be seen, the peak at $2\theta=25.8$, 43.2 and 51.3 appeared can be related to crystalline plates (111)_c, (220)_c and (311)_c of cubic phase of CdSQD particles. The average size of the crystalline particles was calculated with the Scherrer equation (Eq. (1)) [17].

$$D = \frac{0.9\lambda}{\beta \cos \theta} \quad (1)$$

where D is the size of particles; β is the full width at half maximum in radian wavelength of Cu-K α radiation. The value D for CdSQD was obtained to be 3.9 nm.

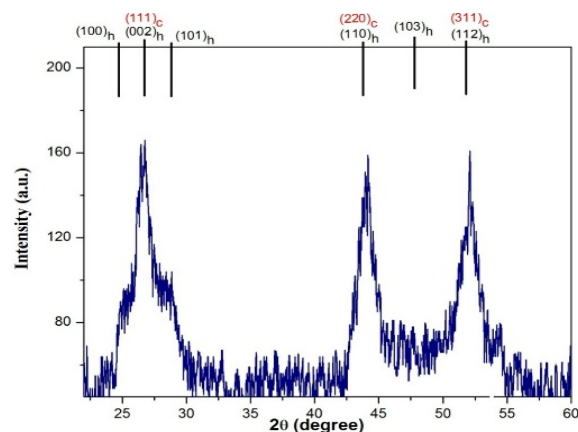


Fig. 1. XRD spectrum of CdSQD.

6.2. FTIR Characterization of CdSQD

The spectrum of CdSQD particles is shown in Fig. 2. The strong bands were seen in 1005, 1130, 1616 and 3412 cm^{-1} and weak bands at 606, 1377, 650 and 1565 cm^{-1} . The broad band at 3912 cm^{-1} represents the stretching vibration related to OH groups of water molecule. The very weak band at 2930 cm^{-1} also indicates the vibration stretching of CH bond which may be considered as the residual of organic reagents used in synthesis process. The small band seen at 541 cm^{-1} can be related to S-S bonds.

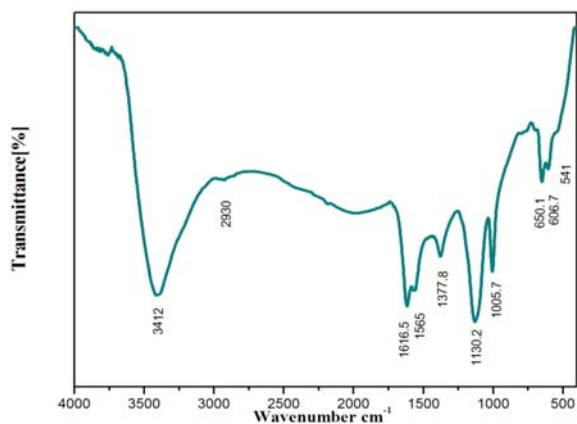


Fig. 2. FTIR spectrum of CdSQD.

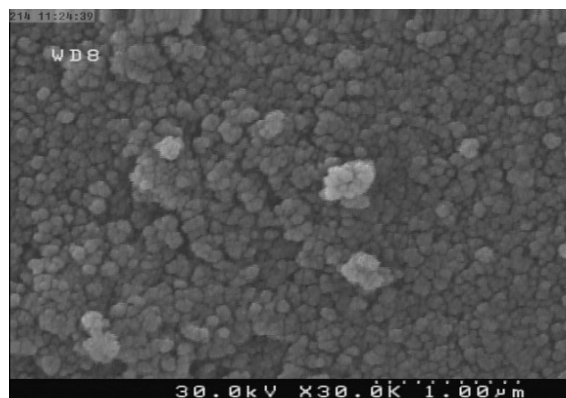


Fig. 4. FESEM image of CdSQD.

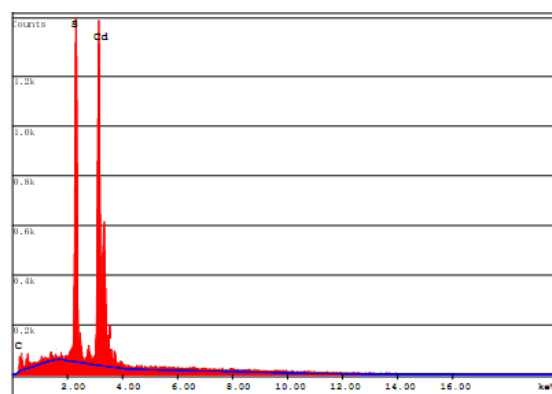


Fig. 5. EDX spectrum of elemental analysis of CdSQD.

6.3. Morphological and Elemental Analysis Studies

In order to study the morphological of CdSQD particles, FESEM and TEM images were obtained. Fig. 3 shows the TEM images of spherical shape of CdS quantum dot particles which obviously depends on the size of particles less than 10 nm. FESEM image of CdSQD is shown in Fig. 4. It suggests the homogeneity of synthetic particles with the lowest impurity and amorphous phases.

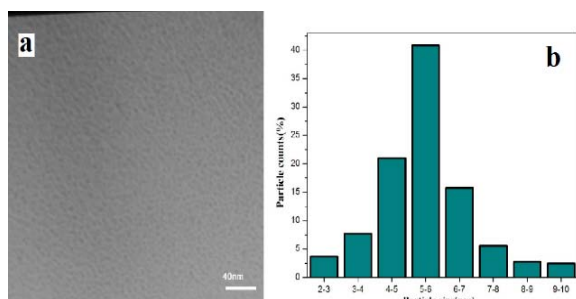


Fig. 3. (a) The TEM image of CdS nanoparticles, (b) Particle size distribution histogram.

Elemental analysis was also done using EDX. As it is shown in Fig. 5, the existence of cadmium and sulphur is being confirmed in the synthetic CdSQD.

6.4. Study of Photoluminescence (PL) Properties of Synthetic CdSQD

The photoluminescence properties of CdSQD particles was investigated by an exciting 380 nm radiation at room temperature. The prepared material showed a broad emission spectrum in the range of 450 to 620 nm. According to the spectrum (Fig. 6) three individual peaks are seen: the weak peaks are considered as the blue emission and the strong one is considered as the green–yellow emission at maximum of 556 nm.

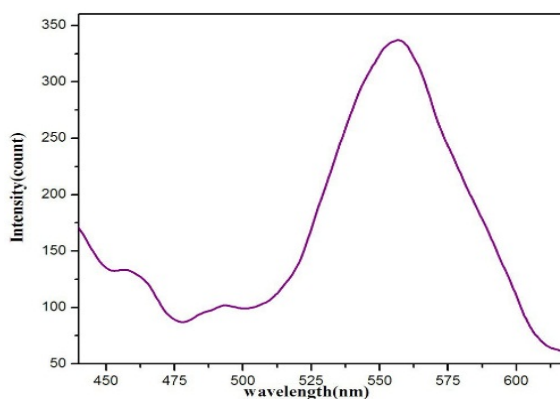


Fig. 6. Photoluminescence spectra of CdSQD particles.

As can be seen the PL spectrum of CdSQD particles consists of two parts: the first one is in the range of 420-500 nm which is referred to the band edge emission and the second part is range 530-620 nm which is referred to the surface defect emission.

7. Photomultiplier Tube (PMT) Experiments

All the tests were done in room temperature by ^{60}Co source in a few second ranges with the set up shown in Fig. 7. The CdSQD@PMM hybrid that was uniformly covered on a glass slide, placed exactly between the ^{60}Co source as the gamma emitter and the PMT input slit. The counts of released photons were recorded 8 times in absence of the hybrid CdSQD and in the presence of the hybrid where the counts reached to the constant value. Fig. 7 shows the diagram of PMT test.



Fig. 7. The setup of the PMT test.

As illustrated in curve Fig. 8(b) they obtained spectrum shows a peak at channel 793 with 28402 counts in absence of CdSQD@PMM. Regard to impermeability of the PMT chamber relative to external radiations, the existence of this peak could be related to electron generation resulted from gamma beam.

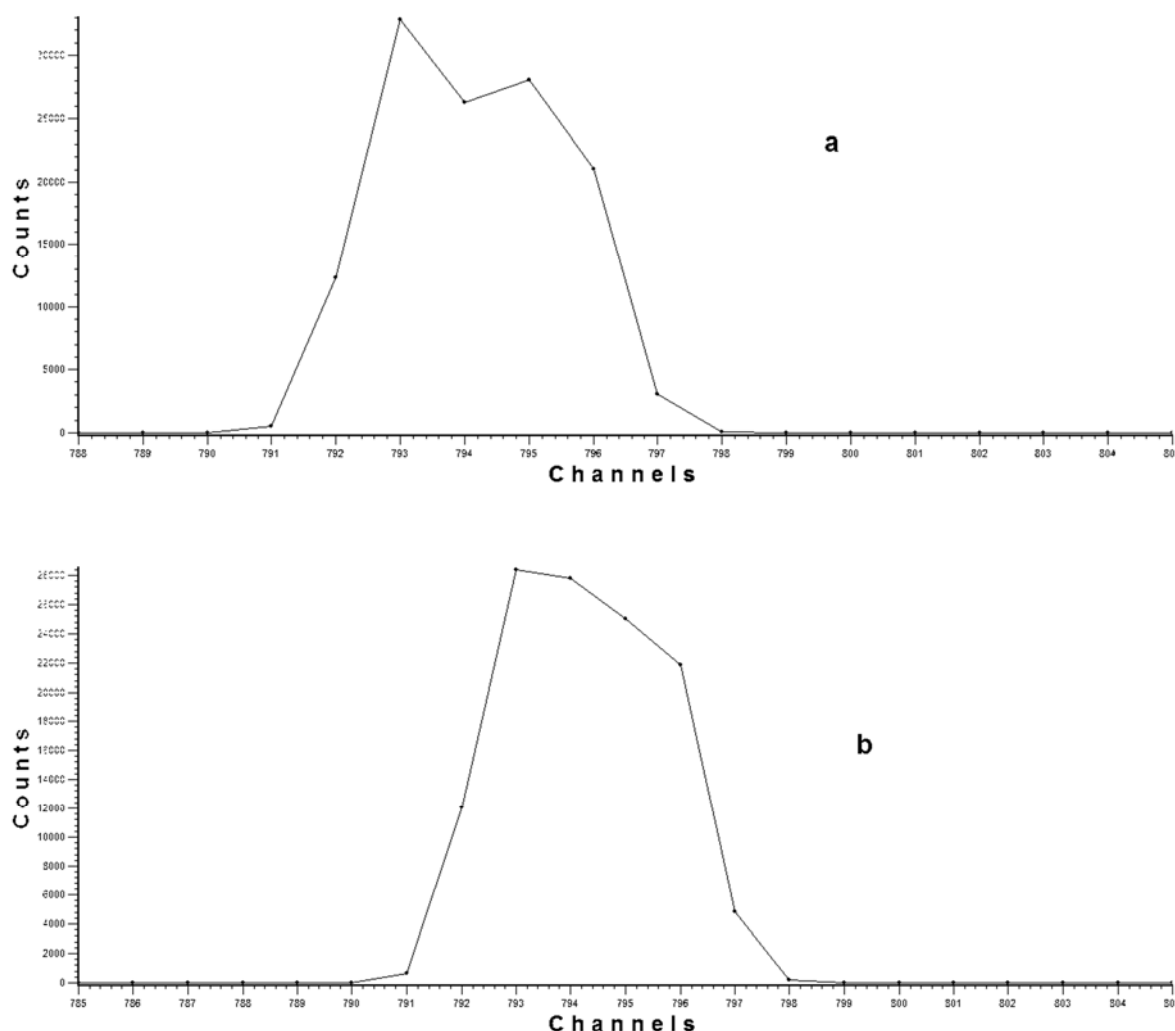


Fig. 8. The PMT spectrum of (a) in presence, (b) in absence of CdSQD@PMM.

In the Fig. 8 (a) in addition to similar peak observed in curve b, there is another peak at channel

795 with count 28048. The mentioned peak can be due to electron generation resulted from visible photons

that originated from gamma photon discharge in CdSQD@PMM structure.

8. The Meaningful Tests of T and Chi-squared

Considering the lack of systematic error (null hypothesis, H_0), the meaningful tests, T test and chi-squared test were used to compare the averages of data and the meaningfulness of frequency of data distribution, respectively [18-20]. As the source of the data presented in Table 1 are the same, the Eq. (2) was used for the T test.

$$t = \frac{(\bar{X}_1 - \bar{X}_2)}{S_{pooled} \sqrt{\frac{1}{N_1} + \frac{1}{N_2}}} \quad (2)$$

$$S_{pooled}^2 = \frac{(N_1 - 1)S_1^2 + (N_2 - 1)S_2^2}{N_1 + N_2 - 2}, \quad (3)$$

where the \bar{X}_1 and \bar{X}_2 are the averages of the column A and B of Table 1, respectively, N_1 and N_2 are the number of data of column A and B of Table 1, S_{pooled} represents the accumulated standard deviation which is calculated from Eq. (3) and S_1 and S_2 are the standard deviations of column A and B of Table 1, respectively.

Table 1. The data obtained from PMT test in 100 seconds at room temperature.

Number of tests	In the presence of the gamma source and in the absence of the hybrid	In the presence of the gamma source and the hybrid
1	120799	124147
2	119312	125272
3	121605	129704
4	121601	131838
5	121609	135236
6	121605	135686
7	121599	141664
8	121604	139785

The obtained T volume of 5.18 is obviously higher than the critical volume reported in 99 % confidence level (3.50) [18]. Thus, the difference between two averages due to the presence and absence of synthetic hybrid implies that the meaningfulness and orientating of scintillation process is beyond the random and unpredictable errors.

The Chi-square test was also applied to the data using Eq. (4). It was obtained to be 2133.36 which is much higher than the critical value of 14.07 in the references [18]. It shows the meaningfulness of the

difference between the data obtained from the hydride exposed with gamma beam.

$$\chi^2 = \sum \frac{|O-E|^2}{E}, \quad (4)$$

where O is the observed frequency and E is the desired frequency (roughly the same volume for average).

9. Conclusions

The dispersion of quantum dot CdS particles in poly methyl methacrylate could emit significant amount of visible photon when interacting with gamma rays. This would be a good characteristic of scintillation process. The composition of CdSQD and poly methyl methacrylate is highly transparent to visible light which in turn decreases the self-absorption of produced photons and efficiency enhancement.

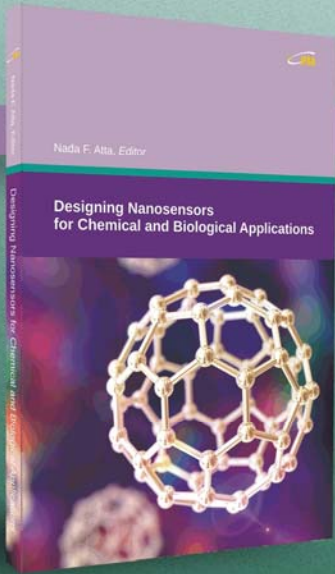
References

- [1]. Cicillini Simone Aparecida, Ana Maria Pires, Osvaldo Antonio Serra, Luminescent and morphological studies of Tm-doped Lu3Al5O12 and Y3Al5O12 fine powders for scintillator detector application, *Journal of Alloys and Compounds*, Vol. 374, Issue 1, 2004, pp. 169-172.
- [2]. Nikl Martin, Scintillation detectors for x-rays, *Measurement Science and Technology*, Vol. 17, Issue 4, 2006, pp. R37-R54.
- [3]. Carl Eugene Crouthamel, Freddy Adams, Richard Dams, Applied Gamma-ray Spectrometry, *Elsevier*, 2013.
- [4]. Antoni T., *et al.*, The cosmic-ray experiment KASCADE, Nuclear Instruments and Methods in Physics Research Section A: Accelerators, Spectrometers, *Detectors and Associated Equipment*, Vol. 513, Issue 3, 2003, pp. 490-510.
- [5]. E. V. D. Van Loef, *et al.*, High-energy-resolution scintillator: Ce 3+ activated LaBr3, *Applied Physics Letters*, Vol. 79, Issue 10, 2001, pp. 1573-1575.
- [6]. J. M. F. Dos Santos, *et al.*, Development of portable gas proportional scintillation counters for x-ray spectrometry, *XRS*, Vol. 30, 2001, pp. 373-381.
- [7]. Akazawa Y., *et al.*, Development of a cylindrical tracking detector with multichannel scintillation fibers and pixelated photon detector readout, *Nuclear Instruments and Methods in Physics Research Section A: Accelerators, Spectrometers, Detectors and Associated Equipment*, Vol. 787, 2015, pp. 193-196.
- [8]. Lin Liping, *et al.*, Luminescent graphene quantum dots as new fluorescent materials for environmental and biological applications, *TrAC Trends in Analytical Chemistry*, Vol. 54, 2014, pp. 83-102.
- [9]. Guo Lei, Man Shing Wong, Multiphoton excited fluorescent materials for frequency upconversion emission and fluorescent probes, *Advanced Materials*, Vol. 26, Issue 31, 2014, pp. 5400-5428.
- [10]. Kamada Kei, *et al.*, Cz grown 2-in. size Ce: Gd3 (Al, Ga) 5O12 single crystal; relationship between Al, Ga site occupancy and scintillation properties, *Optical Materials*, Vol. 36, Issue 12, 2014, pp. 1942-1945.

- [11]. Alekhin Mikhail S., *et al.*, Optical and scintillation properties of CsBa₂ I 5: Eu²⁺, *Journal of Luminescence*, Vol. 145, 2014, pp. 723-728.
- [12]. Khan Sajid, H. J. Kim, Y. D. Kim, Scintillation characterization of thallium-doped lithium iodide crystals, *Nuclear Instruments and Methods in Physics Research Section A: Accelerators, Spectrometers, Detectors and Associated Equipment*, Vol. 793, 2015, pp. 31-34.
- [13]. Tsuda Shuichi, Kimiaki Saito, Spectrum-dose conversion operator of NaI (Tl) and CsI (Tl) scintillation detectors for air dose rate measurement in contaminated environments, *Journal of Environmental Radioactivity*, Vol. 166, 2017, pp. 419-426.
- [14]. Comrie A. C., *et al.*, Digital neutron/gamma discrimination with an organic scintillator at energies between 1 MeV and 100 MeV, *Nuclear Instruments and Methods in Physics Research Section A: Accelerators, Spectrometers, Detectors and Associated Equipment*, Vol. 772, 2015, pp. 43-49.
- [15]. Zeng Jijun, *et al.*, Processing and properties of poly (methyl methacrylate)/carbon nano fiber composites, *Composites Part B: Engineering*, Vol. 35, Issue 2, 2004, pp. 173-178.
- [16]. Pedram Parisa, *et al.*, Cadmium sulfide quantum dots modified with the human transferrin protein siderophile for targeted imaging of breast cancer cells, *Microchimica Acta*, Vol. 183, Issue 1, 2016, pp. 67-71.
- [17]. Khosravani Shima, *et al.*, The effect of various oxidation temperatures on structure of Ag-TiO₂ thin film, *Microelectronic Engineering*, Vol. 163, 2016, pp. 67-77.
- [18]. Miller James N., Jane Charlotte Miller, Statistics and Chemometrics for Analytical Chemistry, *Pearson Education*, 2005.
- [19]. Schumacker Randall, Sara Tomek, Chi-square test, Understanding Statistics Using R., *Springer-Verlag*, New York, 2013, pp. 169-175.
- [20]. Lowry Richard, Concepts and applications of inferential statistics, 2014, <http://vassarstats.net/textbook/>



Published by International Frequency Sensor Association (IFSA) Publishing, S. L., 2017 (<http://www.sensorsportal.com>).



IFSA

Nada F. Atta, Editor

Designing Nanosensors for Chemical and Biological Applications

The present book aims at providing the readers with some of the most recent development of new and advanced materials and their applications as nanosensors. Examples of such materials are ferrocene and cyclodextrins as mediators, ionic liquid crystals, self-assembled monolayers on macro/nano-structures, perovskite nanomaterials and functionalized carbon materials. The emphasis of the book will be devoted to the difference in properties and its relation to the mechanism of detection and specificity. Miniaturization on the other hand, is of unique importance for sensors applications. The chapters of this book present the usage of robust, small, sensitive and reliable sensors that take advantage of the growing interest in nano-structures. Different chemical species are taken as good example of the determination of different chemical substances industrially, medically and environmentally.

The book will be useful for scientists and researchers, doctors and students working in medical research, engineers and students working in environmental research, professionals working in industrial field.

http://www.sensorsportal.com/HTML/BOOKSTORE/Designing_Nanosensors.htm

Cardio-metabolic Diseases Prevention by Self-monitoring the Breath

¹ Danila GERMANESE, ² Mario D'ACUNTO, ¹ Massimo MAGRINI,
¹ Marco RIGHI and ¹ Ovidio SALVETTI

¹ Institute of Science and Technology Information, ISTI-CNR, Via G. Moruzzi 1, 56127 Pisa, Italy

² Institute of Biophysics, IBF-CNR, Via G. Moruzzi 1, 56127 Pisa, Italy

¹E-mail: danila.germanese@isti.cnr.it

Received: 1 June 2017 /Accepted: 7 August 2017 /Published: 31 August 2017

Abstract: As new as very promising technique, breath analysis allows for monitoring the biochemical processes that occur in human body in a non-invasive way. Nevertheless, the high costs for standard analytical instrumentation (i.e., gas chromatograph, mass spectrometer), the need for specialized personnel able to read the results and the lack of protocols to collect breath samples, set limit to the exploitation of breath analysis in clinical practice.

Here, we describe the development of a device, named *Wize Sniffer*, which is portable and entirely based on low cost technology: it uses an array of commercial, semiconductor gas sensors and a widely employed open source controller, an Arduino Mega2560 with Ethernet module. In addition, it is very easy-to-use also for non-specialized personnel and able to analyze in real time the composition of the breath. The *Wize Sniffer* is composed of three modules: signal measurement module, signal conditioning module and signal processing module. The idea was born in the framework of European SEMEiotic Oriented Technology for Individual's CardiOmetabolic risk self-assessment and Self-monitoring (SEMEOTICONS) Project, in order to monitor individual's lifestyle by detecting in the breath those molecules related to the noxious habits for cardio-metabolic risk (alcohol intake, smoking, wrong diet). Nonetheless, the modular configuration of the device allows for changing the sensors according to the molecules to be detected, thus fully exploiting the potential of breath analysis.

Keywords: Bio-signals, Signal processing, Breath analysis, E-nose, Semiconductor gas sensors.

1. Introduction

Its un-obtrusiveness and its inherent safety make breath analysis a very promising technique in healthcare diagnostics. On one hand, it enables the monitoring of biochemical processes: the volatile organic compounds (VOCs) from the metabolic processes are generated within the body, travel via the blood, participate to the alveolar exchanges and appear in exhaled breath; on the other hand, breath is easily and non-invasively accessible [1-3]. In human breath, more than 200 volatile molecules have been identified

and assessed. Some of such molecules were correlated to various diseases such as diabetes, oxidative stress, lung cancer, gastrointestinal diseases, etc. [2], [4-5]. For instance, exhaled pentane and ethane were investigated as lipid per-oxygenation product in case of oxidative stress [6]; isoprene (the major hydrocarbon present in human breath) was suggested to be linked with cholesterol synthesis [7] and cardiac output [8]; breath ammonia may be a useful biomarkers both for the evaluation of clinical treatments in case of renal diseases [9-10] and for monitoring the level of severity in case of liver

diseases [11]. Nonetheless, despite its great potential, the use of breath analysis in clinical diagnostic is limited because of the costs of the specific, high accurate standard instrumentation (i.e., gas chromatograph, mass spectrometer) and the need of expert personnel to perform the analysis, which also are very time consuming [9].

Formerly designed for broader applications (environmental gases monitoring, for instance), in recent years the idea of exploiting e-noses also for clinical applications has been arisen [12]. Since they are able to perform breath gas analysis in real time, in many studies they have been employed in different fields of medicine: in oncology, for instance, to monitor volatile biomarkers related to cancer [13], in infectiology [14], in respiratory medicine to evaluate asthma [15]. Nevertheless, the majority of such e-noses exploit very expensive technology [16-17] or requires complex circuitry [18-19].

By developing the *Wize Sniffer* (WS) [20-22], here presented, we aimed to overcome all these limitations:

- it is a portable device for the real time monitoring of a set of breath molecules;
- it is based on low cost technology: the employed gas sensors are commercial, semiconductor-based and easily embeddable in the circuitry; a widely employed open source controller, an Arduino Mega2560, reads and processes raw data;
- the WS is very easy to use, also for non-specialized personnel. In addition, it is designed in order to send breath analysis results also to a remote care center.

The WS was conceived in the framework of SEMEOTICONS European Project [23]. It aimed to develop the *Wize Mirror*, an interactive platform having the appearance of a mirror, able to assess individual's well-being state by detecting in the human face all those signs related to cardio-metabolic risk [24-25]. The WS was designed to be a *Wize Mirror*'s tool for detecting in human breath the molecules related to those noxious habits for cardio-metabolic risk: alcohol intake, wrong diet and smoking. Nonetheless, we aimed to design a device which could work also in a stand-alone configuration. Not only: thanks to the modular architecture, the WS can detect other volatile compounds simply by changing the gas sensor array.

In the paper, Section 2 lists the VOCs detected by the WS and describes the device's general architecture; Section 3 reports the WS functionality tests and the different data analysis approaches.

2. The Wize Sniffer, How it Works

By developing the WS, we aimed to design a portable, easy to use device which could be useful for user's health self-monitoring and self-surveillance, also in home environment. In addition, we exploited low-cost technology in order to promote its purchase and use.

2.1. Harmful Molecules for Cardio-metabolic Risk

Within the WS, an array of semiconductor-based gas sensors is able to detect those breath VOCs considered as indices of noxious habits for cardio-metabolic risk:

- **Carbon monoxide** (CO). More than 5000 compounds in cigarette smoke are dangerous. CO , in particular, decreases the amount of oxygen that is carried in the red blood cells. It also increases the amount of cholesterol that is deposited into the arteries;
- **Ethanol** (C_2H_6O). Moderate ethanol consumption, in healthy subjects, reduces stress and increases feelings of happiness and well-being, and may reduce the risk of coronary heart disease. Heavy consumption of alcohol, instead, causes addiction and leads to an accumulation of free radicals into the cells, causing oxidative stress.

In addition, the device can also provide useful information about metabolism, carbohydrates adsorption and vascular status by detecting:

- **Oxygen and carbon dioxide** (O_2 and CO_2): the amount of O_2 which is retained in the body, and the one of CO_2 which is produced as a by-product, can be considered as a measure of the metabolism;
- **Hydrogen** (H_2): it is related to the carbohydrates breakdown in the intestine and in the oral cavity by anaerobic bacteria;
- **Hydrogen sulfide** (H_2S): it is a vascular relax agent; it has a therapeutic effect in hypertension.

2.2. Wize Sniffer, Hardware and Software

In Fig. 1, WS' hardware is shown. The user blows once into a disposable mouthpiece, placed at the beginning of a corrugated tube. A flowmeter allows for calculating the volume of the exhaled gases. A heat and moisture exchanger (HME) filter absorbs the water vapor present in exhaled breath, reducing the humidity which affects semiconductor gas sensors' behavior. The core of the WS is the signal measurement module that is the sensor array, composed of six semiconductor-based gas sensors, placed within the gas sampling box (made up of ABS and Delrin and whose capacity is 600 ml according to the tidal volume [26]). Other two gas sensors work in flowing regime by means of a sampling pump, which injects the gases from the sampling box at a fixed rate (120 ml/sec). Within the gas sampling box also a sensor for temperature and humidity (Sensirion SHT11) is placed. Sensors' outputs are pre-processed by a signal conditioning module: a series of voltage buffer amplifiers transfers sensors' signal from the measurement module to the micro-controller board, an Arduino Mega2560 with Ethernet module (which is low cost, widely employed and has an open source integrated development environment).

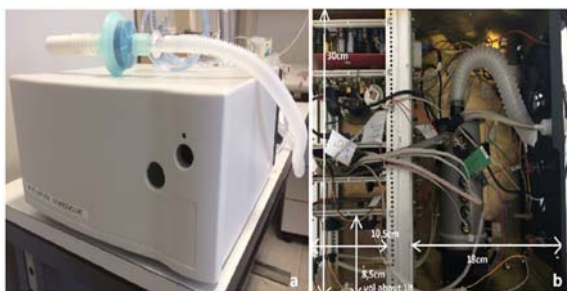


Fig. 1. Wize Sniffer's hardware: a) External configuration; b) Internal configuration.

At the end of a breath test, a flushing pump “purges” the sampling box to recovery the sensors’ steady state.

In Table 1, all the gas sensors are listed. Our choice was to employ metal oxide semiconductor (MOS)-based gas sensors, manufactured by Figaro Engineering. If, on one hand, humidity strongly affects their behavior, and cross-sensitivity makes these sensors be non-selective [27], on the other hand they have long life, strong sensitivity and rapid recovery; in addition, they are low cost (20-30 Euro on average) and easy to be integrated in the circuitry.

Table 1. MOS-based gas sensors integrated in the Wize Sniffer’s measurement module.

Detected molecule	Sensor	Best detection range
Carbon monoxide	MQ7	20-20 ppm
	TGS2620	50-5000 ppm
Ethanol	TGS2602	1-10 ppm
	TGS2620	50-5000 ppm
Carbon dioxide	TGS4161	0-40000 ppm
Oxygen	MOX20	0-16 %
Hydrogen sulfide	TGS2602	1-10 ppm
Hydrogen	TGS821	10-5000 ppm
	TGS2602	1-10 ppm
	TGS2620	50-5000 ppm
	MQ7	20-200 ppm
Ammonia	TGS2444	1-100 ppm
	TGS2602	1-50 ppm

The aim of developing a device which could be useful as a stand-alone device for user’s health self-monitoring, also in home environment, is evident about software implementation. We implemented a client-server architecture in order to send breath data also to a remote personal computer. It means that, after performing a test and processing the results, the device, thanks to an internet connection and a communication protocol, can send the results to the family doctor, for instance. For this purpose, Arduino is programmed to process sensors’ raw data and to execute a daemon on port 23. By implementing a Telnet server, it waits a command line from the remote personal computer and provides the data.

Finally, in Fig. 2, WS’ operation modes are shown. In the smaller picture, the WS is working as a Wize Mirror’s tool. In the other picture, the WS is working as a stand-alone device.



Fig. 2. The two Wize Sniffer's operation modes: as a Wize Mirror’s tool (on the left) and as a stand-alone device (on the right).

3. Wize Sniffer Functionality Tests and Data Analysis

Breath analysis performed by low-cost technology based gas sensors is a great challenge. If, on one hand, semiconductor-based gas sensors are low cost, robust and very simple to integrate in the circuitry, on the other hand, their behavior is strongly affected by humidity and cross-sensitivity.

Indeed, often each sensor may be not selective for one volatile compound only, but it may be sensitive to a broader set VOCs. As a consequence, the estimation of the breath molecules’ concentration is an arduous challenge.

Moreover, breath gases are something extremely variable: breath composition may vary according to heart rate, breath flow rate [28], posture [29], ambient air [30], lung volume [31], breath sampling mode [32]. Exhaled breath is affected by a strong inter-variability (among different subjects), and also by a marked intra-variability (relative to the same subject).

As summarized in Fig. 3, we have to face first with an uncertainty of measure relative to those factors that affect the gas sensors’ behavior; then, we have also an uncertainty due to all the physiological conditions that influence breath composition. For instance, in our case, also factors such as BMI [33], sex, age may influence ethanol’s concentration in breath.

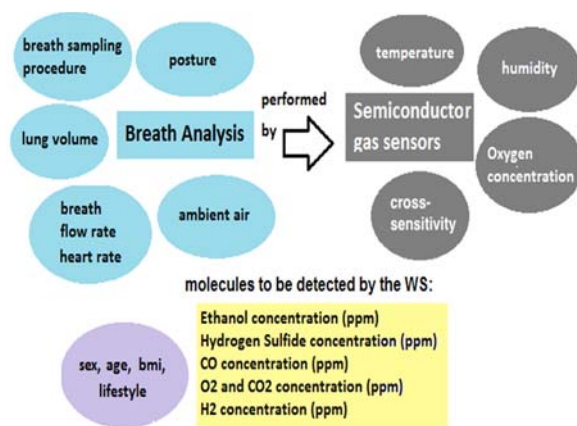


Fig. 3. All the influencing factors (in the circles) related to breath analysis performed by semiconductor-based gas sensors.

3.1. Sensitivity Tests on Gas Sensors

In order to better understand and assess MOS-based gas sensors' behavior we

1) Investigated their response to a variation in humidity;

2) Investigated their sensitivity in precise measurement conditions (3 °C+/-7 %, 70 % RH+/-5 %, that are the ones that occur in the sampling box during a breath test, as shown in Fig. 4);

3) Investigated how the several breath molecules influence each other in the chemical interaction with the sensors' sensing element.

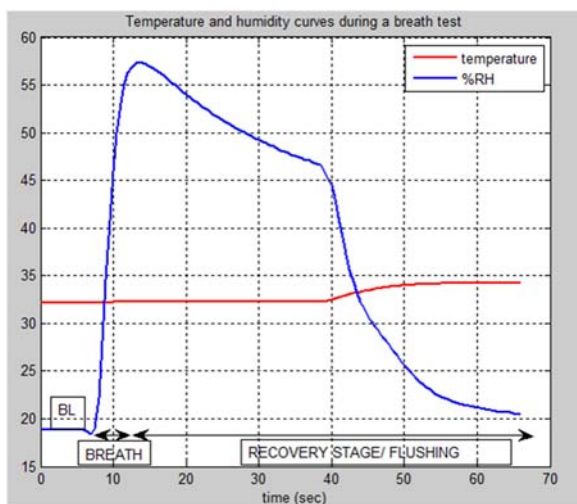


Fig. 4. Temperature and relative humidity in the gas sampling box when a breath test is performed.

Calculating the sensors' humidity drift is useful to potentially compensate it during the data processing. Fig. 5 shows how the humidity strongly affects sensors' output (in this case the one of MQ7 gas sensor). The relationship between humidity and sensors' output generally can be modeled by means of a power law (Eq. (1):

$$V_{out} = f(hum) = a * (hum)^b + c, \quad (1)$$

where a, b and c are the constants. We considered the entire range of humidity variation (for instance, 50 %-55 %RH in the case of MQ7, as shown in Fig. 5) and then we calculated the slope of the curves. Based on the slope, drift coefficients were assessed (see Table 2) as the decrease in sensors' output (Volt) per unit decrease in humidity, as given in Eq. (2):

$$S_d = \Delta V / \Delta hum \quad (2)$$

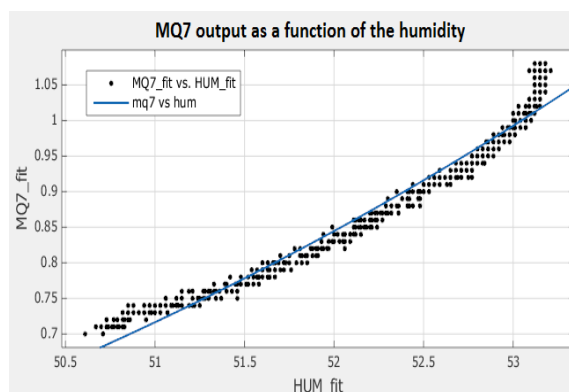


Fig. 5. MQ7 output when a rise in humidity occurs.

Table 2. Sensors' drift due to humidity.

Sensor	$\Delta V / \Delta hum$ (mV)
MQ7	296
TGS2620	60
TGS2602	82
TGS821	120
TGS244	84

By keeping the humidity constant, sensors' output will depend on the gas concentration only. For this purpose, we investigated the sensors' output in response to a well-known gases concentration. The sensors were put into a vial. The humidity into the vial was kept at 70 % RH+/-5 % by means of a saturated solution of NaCl placed on the bottom; then, we injected well-known gases concentration and registered sensors' output. The raw sensors' output were read by an Arduino Mega2560 connected via serial port to a personal computer. The experimental data were displayed in real time on the computer screen and stored as text files for later processing.

Just as example, in Fig. 6, we can see TGS2620 output when well-known concentration of carbon monoxide (CO), ethanol (C₂H₆O) and hydrogen (H₂) were separately injected into the vial. Also in this case, the relationship between sensors' output and gases concentration can be modeled by means of an equation similar to Eq. (1).

Nevertheless, when a breath analysis is performed, a mixture of gases spreads into the gas sampling box

and chemically interacts with the sensors. In this case, the phenomenon known as cross sensitivity makes these sensors non selective. In Fig. 7, we can see TGS2620 response when well-known mixed concentrations of the same three gases (carbon monoxide, ethanol and hydrogen) were injected into the vial at the same time.

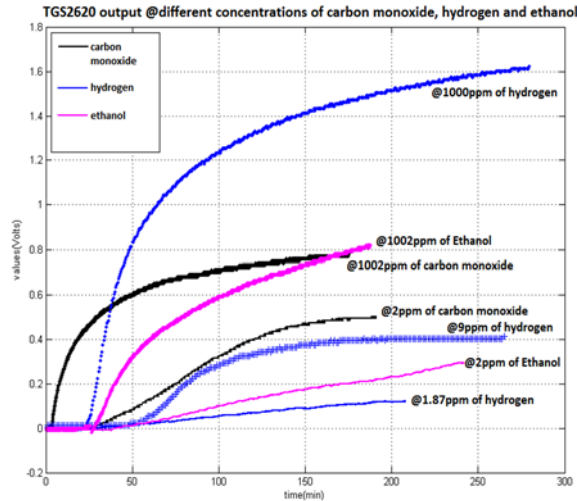


Fig. 6. TGS2620 output when well-known concentrations of CO, H₂ and C₂H₆O were separately injected into the vial.

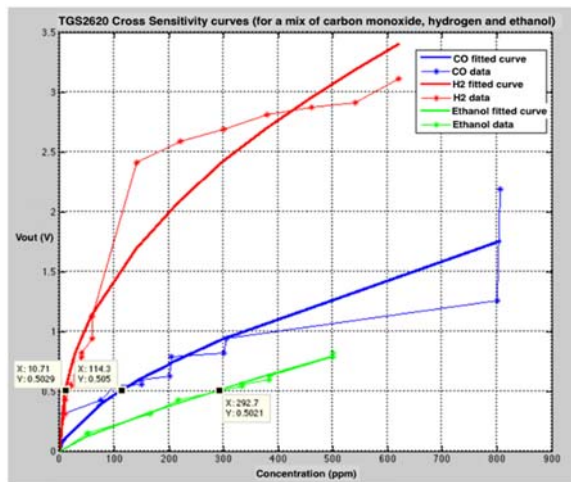


Fig. 7. TGS2620 output when well-known mixed concentrations of CO (blue plot), C₂H₆O (green plot) and H₂ (red plot) were injected into the vial.

In this way, how the different VOCs add together and influence gas sensors' output can be understood. The single gas contribution can be modeled by a power law (Eq. (1)) but each of them has its "weight" on the overall output.

3.2. WS Functionality Test: the Clinical Validation

The aim of the functionality tests was to assess WS' performances, that means, if it was able to

monitor and evaluate the individuals' noxious habits for cardio-metabolic risk (smoke and alcohol intake in particular).

For this purpose, as described in [22], the WS underwent a clinical validation in three research centers: CNR in Pisa and Milan, CRNH (Centre de Recherche en Nutrition Humaine) in Lyon. The campaign involved 77 volunteers overall, male and female, between 30-65 years of age, with different habits and lifestyles. People answered Audit and Fagerstrom tests, which respectively assessed their alcohol and smoke dependence, and other questionnaires about lifestyle in general.

Considering the methodological issues about breath sampling [32], we drafted a protocol which considered the mixed expiratory air sampling, since our interest was focused on both endogenous and exogenous biomarkers. The subjects took a deep breath in, held the breath for 10 s, and then exhaled once into the corrugated tube trying to keep the expiratory flow constant and to completely empty their lungs.

The study was approved by the Ethical Committee of the Azienda Ospedaliera Universitaria Pisana, protocol n.213/2014 approved on September 25th, 2014; all patients provided a signed informed consent before enrollment.

As mentioned before, MOS-based gas sensors are strongly affected by cross-sensitivity. Such characteristic makes the quantitative analysis of the detected VOCs very difficult.

As a consequence, a more classical data analysis approach was used, based on multivariate methods of pattern recognition. Pattern recognition exploits sensors' cross-correlation and helps to extract qualitative information contained in sensors' outputs ensemble. Then, first Principal Component Analysis (PCA) was performed, in order to provide a representation of the data in a space of dimensions lower than the original sensors' space. From an exploratory analysis of the data, the presence of clusters (see Fig. 8) can be observed. Then, a K-nearest neighbor (KNN) classification algorithm, previously trained with the data collected during another acquisition campaign, was adopted to classify the subjects according to their habits: Healthy (that means, not in danger of cardio-metabolic diseases), Light Smoker, Heavy Smoker, Social Drinker, Heavy Drinker, LsSd (Light smoker and Social drinker), LsHd (Light smoker and Heavy drinker), HsSd (Heavy smoker and Social drinker), HsHd (Heavy smoker and Heavy drinker).

The outcomes of the Audit and Fagerstrom questionnaires were our ground truth. The KNN classifier was able to correctly classify in 89.61 % of cases. Errors were probably due to TGS2602 and TGS2620 cross-sensitivity for hydrogen. In fact, for instance, three no-risk subjects were classified as social drinker probably because of high presence of hydrogen in their breath, which caused a rise in these sensors voltage output.

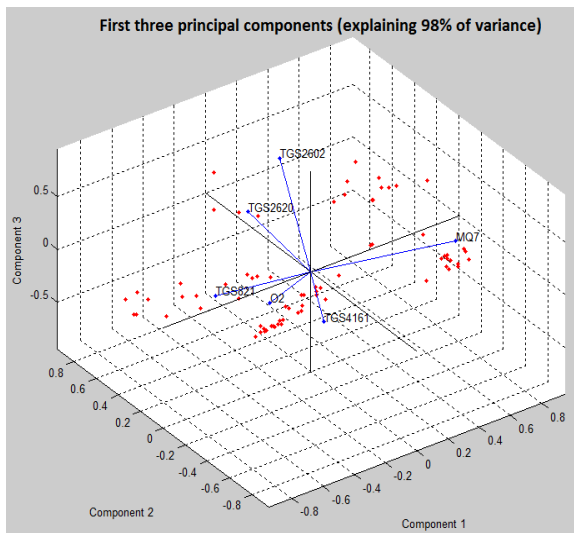


Fig. 8. First three principal components. The presence of several clusters can be observed.

Then, the number of volunteers increased up to 169 subjects. Such subjects were classified by clinicians into “low risk population”, “medium risk population”, “high risk population” and “very high risk population”, basing on the Risk Score (RS), that is, the sum of the scores relative to Audit (AS), Fagerstrom (FS) and lifestyle questionnaires, which were our ground truth also in this case.

Also in this case, mixed expiratory air sampling method was used.

Given the significant number of subjects, we tried to implement a method of data analysis which was able to predict subjects' RS on the base of breath data. First, we extracted the value at the plateau from raw breath curves, which corresponds to the chemical equilibrium between the sensor's sensing element and the volatile compounds. Then, sensors' raw data were zero-centered and normalized, thus putting in evidence their qualitative aspects. Then, also in this case, the principal components were extracted and the PC scores were plotted against the subjects' RS, as shown in Fig. 9.

As can be deduced from the colours (green points derive from no-risk subjects, the blue ones from low-risk subjects, the yellow ones from medium risk subjects, the red ones from high risk subjects, the magenta ones from very high risk subjects), subjects' RS are arranged in ascending order. Except for PC3, from a visual, exploratory analysis, we saw that the PC scores did not have a sharp increasing or decreasing linear trend with respect to RS, thus not having enough information to contribute to any prediction model. Such result matches the one reported in [34]. Being inspired by this study, we also implemented an Independent Component Analysis (ICA) on our data. ICA is a high-order transformation method for data representation which extracts independent component from the data set. If, on one hand, PCA exploits the real sensors' cross-correlation, ICA originates from the assumption that the data has a non-Gaussian

distribution, which often is a property of the gas sensors' array measurement data [35].

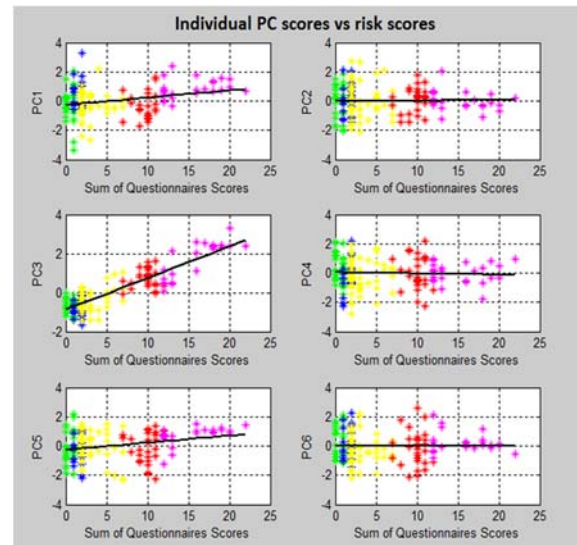


Fig. 9. PC scores against subjects' risk scores arranged in ascending order.

In our case, breath signals and the environmental ones (noise) get mixed with each other before the chemical interaction with the sensor array. As a consequence, each sensor's output is the result of a combination of different gaseous contributions. We applied FastICA algorithm to our data set, and plotted individual independent components (IC) against subjects' RS. As shown in Fig. 10, in this case sharper linear trends emerge.

Then, the data set was split into two data-set (train data set and validation data set) to build the prediction model, which was developed by means of the Matlab LinearModel Tool. Indeed, by using the independent components, a linear regression model was built to establish a relationship between the RS and the breath data pre-processed by ICA. Then, such model was validated by using the validation data set. In Fig. 11 we can see that the correlation coefficient (r) between actual and estimated risk scores is 0.8976.

4. Conclusions

In this paper, we describe how breath analysis could be exploited for a simple self-monitoring by using a portable, low cost, very easy to use device that we developed and called Wise Sniffer. In the presented use case, the WS can provide the user with him/her risk score, thus helping to monitor his/her habits and potentially prevent his/her cardio-metabolic risk.

The safety and the unobtrusiveness of the device allow for a daily monitoring which, even if without a real diagnostic meaning yet, could represent a pre-screening, useful for an optimal selection of more standard medical analysis.

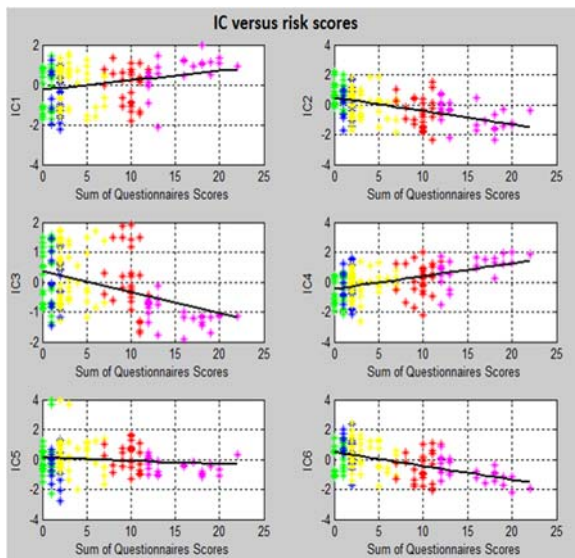


Fig. 10. IC scores against subjects' risk scores arranged in ascending order.

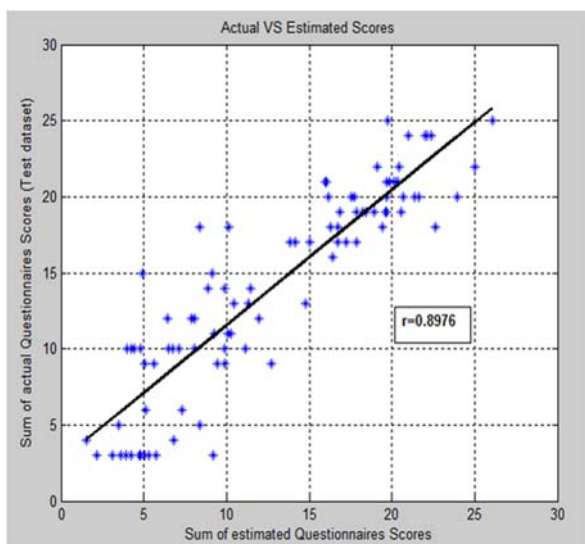


Fig. 11. Actual risk scores versus predicted ones.

The core of our device is the array of MOS-based gas sensors. They are low cost, easy to be integrated in the circuitry, they have long life and rapid recovery time. Nonetheless, their use entails a very robust data processing because of the difficulty of discriminating the molecules' contribution due to sensors' cross sensitivity. Pattern recognition algorithms turn out the best way to overcome such problem.

In addition, the WS modular configuration allows for changing the gas sensors according to the molecules (and then, to the related diseases) to be monitored. Such characteristic allows for using such device in broader applications. For instance, in future we will evaluate WS performances in the case of cirrhotic patients. In particular, we will exploit TGS2444 MOS-based sensor, selective to ammonia,

to discriminate and monitor patients with acute liver diseases.

In conclusion, we highlight the cooperation among scientists (clinicians, engineers, chemists, physicists, etc.) and big effort that should be encouraged in order to introduce breath analysis in clinical practice.

Acknowledgements

This work was funded in the framework of the Collaborative European Project SEMEOTICONS (SEMEiotic Oriented Technology for Individuals CardiOmetabolic risk self-assessment and Self-monitoring), grant No. 611516. Paolo Paradisi, Massimo Martinelli, Massimo Guidi and COSMED s.r.l. are warmly acknowledged for useful support.

References

- [1]. C. Lourenco, C. Turner, Breath analysis in disease diagnosis: methodological considerations and applications, *Metabolites*, Vol. 4, No. 2, 2014, pp. 465–498.
- [2]. F. Di Francesco, R. Fuoco, M. Trivella, A. Ceccarini, Breath analysis: trends in techniques and clinical applications, *Microchemical Journal*, Vol. 79, No. 1-2, 2005, pp. 405–410.
- [3]. W. Miekisch, J. Schubert, G. Noeldge-Schomburg, Diagnostic potential of breath analysis- focus on Volatile organic compounds, *Clinica Chimica Acta*, Vol. 347, No. 1-2, 2004, pp. 25–39.
- [4]. D. Hill, R. Binions, Breath analysis for medical diagnosis, *International Journal on Smart Sensing and Intelligent Systems*, Vol. 5, No. 2, 2012, pp. 465–498.
- [5]. J. Fenske, S. Paulson, Human breath emission of VOCs, *Journal of the Air and Waste Management Association*, Vol. 49, No. 5, 1999, pp. 594–598.
- [6]. M. Phillips, R. Cataneo, J. Greenberg, R. Grodman, M. Salasar, Breath markers in oxidative stress in patients with unstable angina, *Heart Disease*, Vol. 5, No. 2, 2003, pp. 95–99.
- [7]. R. Salerno-Kennedy, D. Cashmark, Potential applications of breath isoprene as a biomarker in modern medicine: a concise overview, *Wienklin Wochenschr*, Vol. 117, No. 5-6, 2005, pp. 180–186.
- [8]. F. Pabst, W. Miekisch, P. Fuchs, S. Kischkel, J. K. Schubert, Monitoring of oxidative and metabolic stress during cardiac surgery by means of breath biomarkers: an observational study, *Journal of Cardiothoracic Surgery*, Vol. 2, 2007, 9pp.
- [9]. D. Guo, a. L. Z. D. Zhang, N. Li, J. Yang, A novel breath analysis system based on electronic olfaction, *IEEE Transaction on Biomedical Engineering*, Vol. 57, Issue 11, 2010, pp. 2753–2763.
- [10]. I. Essiet, Diagnosis of kidney failure by analysis of the concentration of ammonia in exhaled breath, *Journal of Emerging Trends in Engineering and Applied Sciences*, Vol. 4, Issue 6, 2013, pp. 859–862.
- [11]. R. Adrover, *et al.*, Breath-Ammonia Testing of Healthy Subjects and Patients with Cirrhosis, *Digestive Diseases and Sciences*, Vol. 57, Issue 1, 2012, pp. 189–195.

- [12]. A. Wilson, Recent progress in the design and clinical development of electronic-nose technologies, *Nanobiosensors in Disease Diagnosis*, Vol. 5, 2016, pp. 15–27.
- [13]. T. de Meij, *et al.*, Electronic nose can discriminate colorectal carcinoma and advanced adenomas by fecal Volatile biomarker analysis: proof of principle study, *International Journal of Cancer*, Vol. 134, Issue 5, 2014, pp. 1132–1138.
- [14]. N. Yusuf, *et al.*, In-vitro diagnosis of single and poly microbial species targeted for diabetic foot infection using e-nose technology, *BMC Bioinformatics*, Vol. 16, 2015, pp. 158–169.
- [15]. P. Montuschi, N. Mores, A. Trov, C. Mondino, P. Barnes, The electronic nose in respiratory medicine, *Respiration*, Vol. 80, No. 1, 2013, pp. 72–84.
- [16]. URL: <http://www.bedfont.com/>
- [17]. D. Walt, *et al.*, Optical sensor array for odor recognition, *Biosensors and Bioelectronics*, Vol. 13, Issue 6, 1998, pp. 697–699.
- [18]. F. Lai, H. Huang, Fabrication of high frequency and low-cost surface-acoustic wave filters using near field phase shift photolithography, *Microelectronic Engineering*, Vol. 83, Issue 4, 2006, pp. 1407–1409.
- [19]. L. Fan, H. Ge, S. Zhang, H. Zhang, J. Zhu, Optimization of sensitivity induced by surface conductivity and adsorbed mass in surface acoustic wave gas sensors, *Sensor Actuat B-Chem.* 2012, Vol.161, pp.114–123.
- [20]. D. Germanese, *et al.*, A low cost, portable device for breath analysis and self-monitoring, the Wize Sniffer, De Gloria A. (eds.) *Applications in Electronics Pervading Industry, Environment and Society. ApplePies 2016. Lecture Notes in Electrical Engineering*, Vol. 409, 2017, pp. 51–57.
- [21]. M. D’Acunto, *et al.*, Wize sniffer - a new portable device designed for selective olfaction, in *Proceedings of the International Conference on Health Informatics, HEALTHINF’14*, Angers, France, 3-6 March 2014, pp. 577–582.
- [22]. D. Germanese, M. D’Acunto, M. Magrini, M. Righi, O. Salvetti, A Low Cost Technology-based Device for Breath Analysis and Self-monitoring, in *Proceedings of the 2nd International Conference on Advances in Signal, Image and Video Processing, SIGNAL’17*, Barcelona, Spain, 22-25 May 2017, pp. 8-13.
- [23]. URL: <http://www.semeoticons.eu/>
- [24]. S. Colantonio, *et al.*, A smart mirror to promote a healthy lifestyle, *Biosystems Engineering, Special Issue: Innovations in Medicine and Healthcare*, Vol. 138, 2015, pp. 33–43.
- [25]. P. Henriquez, *et al.*, Mirror Mirror on the Wall... An Unobtrusive Intelligent Multisensory Mirror for Well-Being Status Self-Assessment and Visualization, *IEEE Transaction on Multimedia*, Vol. 19, Issue 7, 2017, pp.1467-1481.
- [26]. D. Shier, J. Butler, R. Lewis, *Hole’s Human Anatomy and Physiology*, McGraw-Hill 11th Ed., 2007.
- [27]. P. Clifford, D. Tuma, Characteristics semiconductors gas sensors I. Steady state gas response, *Sensors and Actuators*, Vol. 3, 1983, pp. 233–254.
- [28]. J. Jones, S. Clarke, The Effect of expiratory flow rate on regional lung emptying, *Journal of Applied Physiology*, Vol. 27, 1969, pp. 343–356.
- [29]. N. Anthonisen, P. Robertson, W. Ross, Gravity-dependent sequential emptying of lung regions, *Journal of Applied Physiology*, Vol. 28, 1970, pp. 589–595.
- [30]. F. Di Francesco, *et al.*, Implementation of fowler’s method for end-tidal air sampling, *Journal of Breath Research*, Vol. 2, 3, 2008, pp. 037009.
- [31]. J. Jones, The Effect of Pre-inspiratory Lung Volumes on the Result of the Single Breath O₂ Test, *Respiratory Physiology*, Vol. 2, Issue 3, 1967, pp. 375–385.
- [32]. W. Miekisch, *et al.*, Impact of sampling procedures on the result of breath analysis, *Journal of Breath Research*, Vol. 2, Issue 2, 2008, p. 026007 (7pp).
- [33]. K. E. Maudens, L. Patteet, A. L. N. van Nuijs, C. V. Broekhoven, A. Covaci, H. Neels, The influence of the body mass index (BMI) on the Volume of distribution of ethanol, *Forensic Science International*, Vol. 243, 2014, pp. 74–78.
- [34]. S. Balasubramanian, S. Paniraghi, C. Logue, C. Doetkott, M. Marchello, J. Sherwood, Independent component analysis-processed electronic nose data for predicting salmonella typhimurium populations in contaminated beef, *Food Control*, Vol. 19, 2008, pp. 236-246.
- [35]. M. Kermit, O. Tomic, Independent component analysis applied on gas sensors array measurement data, *IEEE Sensors Journal*, Vol. 3, No. 2, 2003, pp. 218-228.



Automated Indexing and Search of Video Data in Large Collections with *inVideo*

¹ Shuangbao Paul Wang, ² Xialong Cheng, ³ Carolyn Maher, ⁴ William Kelly

¹ Metonymy Corporation, Fairfax, Virginia, 22030, USA

² George Washington University, Washington, DC, 20052, USA

³ Rutgers University, New Brunswick, NJ, 08901, USA

⁴ Metonymy Corporation, Fairfax, Virginia, 22030, USA

¹ Tel.: 703.628.7936

¹ E-mail: paul.wang@computer.org

Received: 1 June 2017 /Accepted: 7 August 2017 /Published: 31 August 2017

Abstract: In this paper, we present a novel system, *inVideo*, for automatically indexing and searching videos based on the keywords spoken in the audio track and the visual content of the video frames. Using the highly efficient video indexing engine we developed, *inVideo* is able to analyze videos using machine learning and pattern recognition without the need for initial viewing by a human. The time-stamped commenting and tagging features refine the accuracy of search results. The cloud-based implementation makes it possible to conduct elastic search, augmented search, and data analytics. Our research shows that *inVideo* presents an efficient tool in processing and analyzing videos and increasing interactions in video-based online learning environment. Data from a cybersecurity program with more than 500 students show that applying *inVideo* to current video material, interactions between student-student and student-faculty increased significantly across 24 sections program-wide.

Keywords: Video processing, Video index, Big data, Learning analytics, Education.

1. Introduction

Big data analytics are used to collect, curate, search, analyze, and visualize large data sets that are generated from sources such as texts (including blogs and chats), images, videos, logs, and sensors [1]. Video data is a major format of unstructured data, and should be an indispensable area of big data analytics. However, most analytics tools are only effective in analyzing structured data. Due to the nature of the special file format, traditional search engines hardly penetrate into videos, and therefore video indexing becomes a problem [2–13].

Videos contain both audio and visual components, and neither of these components is text based. To understand a video, viewers must actually play it and use their eyes and ears to analyze the sounds and

visuals being presented to them. Without watching a video, it is hard to glean information from its content or even know whether there is information to be found within. Existing search engines and data analytics tools such as Google, SAS, SPSS, and Hadoop are effective only in analyzing text and image data. Video data, however, are difficult to index and therefore difficult to analyze.

In education, video presents a large opportunity for both classroom and online education [14]. In addition, video is a great teaching format because it can be both more enjoyable and more memorable than other instruction formats [15]. Furthermore, video instruction allows for students to work at their own pace, for teachers to be able to teach more students, and for more reusable teaching materials to be available when compared to an in-person lecture.

MOOC (Massive Open Online Courses) creators realize the many benefits of video, as evidenced by the prevalence of video in MOOCs. Many MOOCs focus on video files for the bulk of their instructional material so it is clear that the MOOCs of the future must also focus on videos.

inVideo [16], developed under a US Department of Education grant, is able to analyze video content (language and video frames) prior to initial close researcher review of the video. A highly efficient video indexing engine can analyze both language and video frames based on natural language and referent objects. Once a video is indexed, its content becomes searchable, and statistical analysis as well as qualitative analysis are possible. Commenting and tagging add a layer of hyper-information and therefore increase the accuracy of the transcript, which was automatically extracted from the video by the *inVideo* tool. The indexing technology is especially useful in mining video data in large video collections. *inVideo* also has an automatic caption system that can transcribe the words spoken in the video. Instructors can use the tool to construct in-place video quizzes for assessments.

Learning is an integration of interaction. The interaction might exist between learners and instructors or between learners and computers. While the traditional approach would be to analyze grades at the end of the semester, this lacks the benefits that come from interactions that occur during the course [17]. As an increasingly large number of educational resources move online, analyzing interactions between students and online course material is becoming more important. Many learning management systems (LMS) have built-in learning analytics tools to look into the data [18–20]. Due to the limitation of the data gathering and indexing, the built-in tools are generally not sufficient in assessing study outcomes, especially for video content.

2. Related Work

Automatic video index and search have wide applications in education, public security, and many other video-intensive areas.

An airport traffic and security monitoring system constantly indexes videos gathered from surveillance cameras and searches for the suspect based on the graphical and textual information provided by the authority [9].

A video content indexing and retrieval tool indexes digital videos automatically on 34 hours of TV news broadcast. The sampled frames are then used in providing the basis for various analyses [21].

Big data and learning analytics can become part of the solutions integrated into administrative and instructional functions of higher education [22]. Traditional face-to-face instruction supports a traditional data-driven decision-making process. Videos as a form of big data are more extensive, and particularly time-sensitive, learning analytics

application. It is important that instructional transactions are collected as they occur.

Learning analytics can provide powerful tools for teachers in order to support them in the iterative process of improving the effectiveness of their course and to collaterally enhance their students' performance [23]. Dyckhoff developed a toolkit to enable teachers to explore and correlate learning object usage, user behavior, and assessment results based on graphical indicators. This learning analytics system is able to analyze data such as time spent, areas of interest, usage of resources, participation rates, and correlation with grades data, and visualize them using a dashboard. However, the system is unable to analyze the interactions between students and the online learning systems on videos.

In order to analyze videos for various applications, we have developed a video index engine to look at every word spoken in the video and categorize it using our custom index algorithm. In addition, a content-based pattern recognition engine can search individual frames of the video to recognize objects and individuals being displayed. The collaborative commenting, tagging, and in-place quizzes make videos more accessible and also increase the accuracy of the search engine [7-8], [10].

3. Video Indexing and Search Algorithm

Videos are a different data type than text and images, in that they are unstructured data. Traditional search engines are mostly text based, with a few tools that allow for searching of images. In order to index a video, a search engine needs to extract meaningful language from the audio and convert it to text, while simultaneously converting the visual frames into a series of images that can be used to recognize persons and objects in the video. This is an extremely difficult task, given that videos are a compound format. Not only are the audio and visual components integrated, but also within each of these components there is a blend of information being presented in a manner that cannot be distinguished as easily by a computer as by a human brain. For example, the audio of the file may contain speech, music, and background noises that a computer will have a hard time recognizing and analyzing.

3.1. Automatic Indexing Algorithm

The video indexing engine uses the vector space model to represent the document by a set of possible weighted content terms. The weight of the term reflects its importance in relation to the meaning of the document [24].

After calculating the normalized frequency of a term in the document, the weight to measure the relative importance of each concept or single term is obtained. The automatic index algorithm then calculates the final position in n-dimensional space.

The result is to be used for generating search results or visualization.

3.2. Searching Videos by Keywords

Video search involves two steps: analyzing by keywords and analyzing by image references. When a keyword is entered, the system looks through the indexed audio transcript to see if there is a match. An image reference may refer to either a picture or keywords that describe an object in the video using an appropriate semantic space. Video clips whose language contains the keywords will be retrieved. Fig. 1 shows how indexed videos can be searched using keywords in the spoken language.

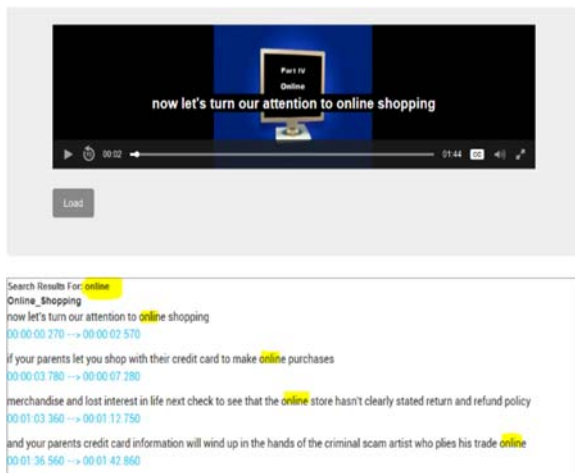


Fig. 1. Analyzing Videos by Keywords.

3.3. Searching Videos by References

Searching videos by references examines the frames of the video to see if the given picture or keyword is found. If the reference is a picture, then the system uses a Content Based Image Retrieval (CBIR) algorithm to find the match frames and return the video clips that contain the reference picture. Fig. 2 shows the image-based CBIR algorithm that retrieves the video frames corresponding to the reference picture (at the bottom).



Fig. 2. Analyzing Videos by Image References using the CBIR Algorithm.

If the reference is a keyword (e.g. credit card) then the system uses a knowledge tree to find matches in the video. If one video frame contains an object matching the features associated with the keyword, the section of the video is returned. Fig. 3 shows how a search for the keyword credit card will retrieve the video frames that contain objects as credit cards.



Fig. 3. Analyzing videos by Keyword References using a Knowledge Tree.

3.4. Searching Videos in Multiple Languages

Sometimes multiple languages may be found in videos. Transcription engines normally only work in one language or in closely related languages. For other languages, a different transcription engine may be required. *inVideo* addresses this problem by allowing videos with different languages to be searched from a single user interface. The *inVideo* system does not translate between languages. It only transcribe based on the language of original videos. For example, a Chinese video will result in a transcript in Chinese. Fig. 4 shows the indexing engine properly analyzing the Chinese language.



Fig. 4. Analyzing Videos with Different Languages.

When entering the word “student” in Chinese, the video search engine will locate that term in the transcript and return the corresponding frames. Currently, there are multiple languages that can be analyzed by the *inVideo* system, with more to be added.

3.5. Elastic Search and Content-Aware Elastic Search

Elastic search makes the *inVideo* application capable of searching video data across distributed environments with HTTP protocol and schema-free JSON documents. Elastic search makes it possible to expand the community by deploying a pluggable cloud architecture, configurable automatic discovery of cluster nodes, persistent connections, and load balancing across all available nodes. Video collections under ACE are no longer restricted to a particular video collection. More importantly, there is no need to move other video collections in a centralized site, which is merely feasible anyway.

Indexed videos can be searched by keywords. When a keyword is entered, the cloud system searches its generated transcript of the audio files to find matches. Video clips whose audio track contains the keywords are retrieved.

The enhanced elastic search partitions videos into individual frames. Thus, users also have the ability to search a video by examining the video frames to see if a given object is found. The enhanced elastic search algorithm matches contents in the frames and returns the video clips that contain the reference objects. This process allows us to combine images and words to create hybrid metadata.

For instance, in mathematics education, there is interest in studying the representations students make. The CBIR algorithm allows us to search the videos for particular representations that a student would make, such as images of rods, blocks, or tree diagrams. Students may construct these models without talking about them, and thus an audio transcript would miss it. By being able to search the frames of the video, a user interested in tracing a student's construction or explanation of a representation can query the database. If a frame of the video contains an object matching the particular representation, this section of the video is returned.

3.6. Machine Learning and Cloud-based Data Analytics

It should be noted that the goal of the software is not to reproduce the word-for-word accuracy of a human-generated transcript of video files. Rather, the goal is to determine the extent to which voice-to-text analysis and image analysis are able to retrieve desired sections of the video for enriched human analysis. The critical task is for the system to identify a sufficient amount of relevant hits that pertain to the search reference terms or images. Search queries have advanced from keywords to natural language. The *inVideo* software uses artificial intelligence and machine learning technologies to analyze videos and use big data analytics tool to explore, index, and visualize videos. *inVideo* also has security features that secure data and communication in the cloud and protect privacy [2-6, 11-12].

3.7. Transcript Time-Stamping

inVideo also includes a Transcript Time-stamping System (TTS), a new software tool built by the research team, which turns traditional video transcripts generated by external transcription methods into time-stamped transcripts, which can be incorporated into the *inVideo* application. The TTS application adds timestamps to existing transcripts and formats them in a way that is amenable to video search through the *inVideo* platform. The application is semi-automated; when a timestamp is keyed to a word, the software calculates the time allotted for all surrounding words, so that all the non-keyed words are aligned between timestamps in a reasonable approximation of their occurrence in the audio track. Subdividing each sentence and introducing additional cycles for the algorithm to run on smaller segments of the transcript can increase the accuracy. Fig. 5 shows the timestamp creation process:

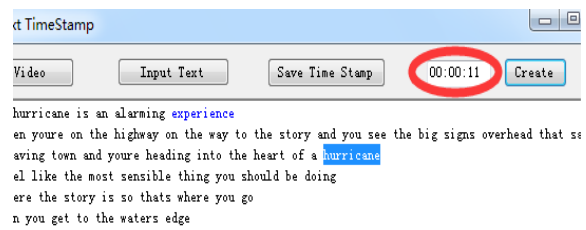


Fig. 5. Automatically calculating timestamps.

4. Collaborative and Interactive Learning

Automatically generated video transcripts may have accuracy problems. Besides, the vast numbers of videos in MOOCs make them impossible to be retrieved correctly with just one or a few simple keywords. To solve these problems, we have implemented a collaborative filtering mechanism that includes commenting, tagging, and in-place quizzes. These features improve accuracy and increase interactions between students and the online learning systems. With collaborative filtering, learning resources retrieval on MOOC systems is greatly improved, and better student achievement is therefore expected.

4.1. Collaborative Filtering

Collaborative filtering is a process of improving accuracy of the automatic indexing algorithm by leveraging user feedback. This is popular on websites that have millions of users and user-generated content. Users are able to create time-stamped comments on videos. These comments can be hidden or made public so that someone else who views the video can see the comment at a specific time. These comments help

increase accuracy of the search tool and transcript and enhance interactions in online learning.

Tagging on videos is another implementation in the *inVideo* system. It is to attach keyword descriptions to identify video frames with categories or topics. Videos with identical tags can then be linked together, allowing students to search for similar or related content. Tags can be created using words, acronyms, or numbers. This is also called social bookmarking.

A search term usually yields many related results, which in many cases are hard to differentiate. Commenting and tagging add additional information, refine the knowledge, and increase the video search accuracy. At a time when information is exponentially growing, these features are extremely helpful for students to obtain the knowledge with the least amount of time.

4.2. In-place Assessment with iQuiz

Internet computing has the advantage of employing powerful CPUs on remote servers to provide applications across the network. *inVideo* comes with an Internet Computing- based video quiz system (iQuiz) to utilize the computational power of remote servers and provide video quiz services to users across the Internet. Currently, videos are mostly non-interactive, and thus there are no interactions between students and the learning content. Students either view videos online or download them to their personal devices. There is no way for educators to know whether a student has understood the content or even to know whether the student has viewed the video or not.

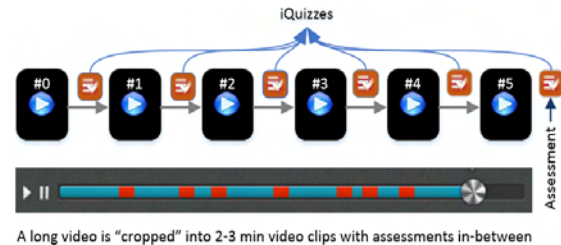
iQuiz can be used to assess learning outcomes associated with video study. Quizzes can be embedded into videos at any place where an instructor wants to assess the outcome of the student's study. iQuiz runs as a service on servers. This enables users to execute this resource-intensive application with personal computers or iPads, which would not be possible otherwise.

Instructors can enter into the authoring mode where they can write quizzes by indicating the start and stop positions on the video and adding questions. Video quizzes are stored in XML format, and are automatically loaded while students are watching the video in the learning mode. Answers to the quizzes, either correct or incorrect, are also stored in the XML database for immediate assessments. Assessment of adaptive learning on videos provides better outcomes for students than the traditional video content study with little or no feedback [25].

4.3. Transform Linear Videos into Interactive Learning Objects

Videos are linear in nature. This structure is hardly interactive, nor does it contain branches. Using the

inVideo tool, classical videos can be transformed into a series of video clips with assessments in between and at the end. Through this process, the video-based learning material becomes interactive. Fig. 6 shows a test that we conducted, which turned a 46-minute video into six selected 2-3 minute video clips. The red segments on the stage bar are the samples, so it is clear that not all video content was used in the samples.



A long video is "cropped" into 2-3 min video clips with assessments in-between

Fig. 6. Transform Linear Videos into Interactive Learning Objects.

5. Experimental Results

5.1. Classroom Interventions

To test the *inVideo* system, we selected the 20 most recent videos from National Science Digital Library (NSDL) in cybersecurity and used the *inVideo* tool to extract keywords that appeared in the transcripts. From this set, we selected the top two ranked keywords: Target (data breach) and encryption (using encryption to secure data). We were confident that those two keywords made good discussion topics that could increase classroom interactions.

As a result, we added two discussion topics to the Masters of Science in Cybersecurity program for Spring 2014 (24 class sections; each section has 25 students on average).

Videos lack interactions between learners and the online learning environment. Even worse, videos above a certain length will likely never be watched at all, because students cannot easily determine what content is within it or how to locate that content. To address this issue, we used the *inVideo* tool to index the content and break the large videos into a series of small video clips. By doing so, we made it possible for students to watch short video clips covering individual key concepts directly, while retaining the ability to view the whole video if necessary. This served to not only increase student interest and engagement in the lesson, but also, more importantly, to improve their ability to comprehend and retain information.

Student responses and interactions can be used as a proxy for their degree of engagement with any particular part of the course. As one example of how the *inVideo* indexing served to increase this measure, consider Week 2 of the class. In our assessment of past offerings (pre-*inVideo*) we discovered that this part of the course is a quiet week, because the individual assignment starting in the week will not be due until

Week 8. This meant that the interactions in the classrooms dropped significantly from Week 1. Based on this assessment, we decided to use the *inVideo* intervention in an attempt to generate more interactions during Week 2 of the course.

Our initial observation of one class was very promising; the total number of responses, defined as each posting after viewing a video clip, for Week 2 reached sixty-eight, as compared to only two for the same week in the previous semester. This initial finding encouraged us to investigate the results for all twenty-four sections program-wide. Fig. 7 shows the number of responses for the 24 sections comparing Fall 2013 to Spring 2014 during Week 2.

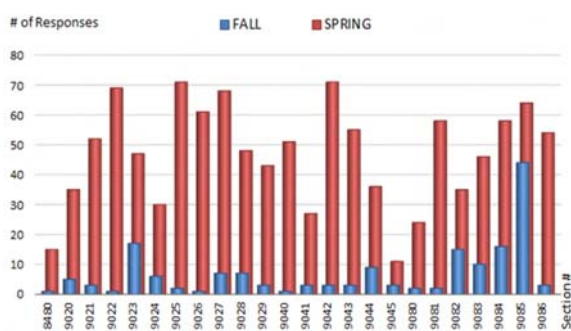


Fig. 7. Number of Responses for 24 Sections – Week 2 Discussions.

For the research we conducted, Week 2 student responses across the 24 sections were almost seven times higher during Spring 2014 (1,129 responses) than during Fall 2013 (164 responses).

For the cybersecurity online/hybrid class, we have five graded discussions, one individual assignment, one team assignment, and two lab assignments. Two more hands-on exercises (labs) have been added since Spring 2014. Data from the team projects, using the same intervention method, show that student-student and student-faculty interactions were 6.5 times greater for the courses with the *inVideo* intervention (104 responses compared to 16 responses). We also measured student performance against desired learning outcomes. The average grades on both team projects and final grades was higher in Spring 2014 than in Fall 2013. Here we see that the index and data analytics tool *inVideo*, in combination with just-in-time assessment and intervention, improved learning outcomes.

Based on our finding, we are in the process of breaking up every large learning module into several learning objects using *inVideo*. The new competency-based learning objects will be used to construct the knowledge cloud. These new learning modules will consist of many competency-based learning objects, and will be more interactive, rational, and accessible.

We will use *inVideo* to expand the scope of this research to other activities in courses within the cybersecurity program. This tool could also be useful to courses in other disciplines. Using the *inVideo* tool,

linear videos are transformed into a series of interactive learning objects. This is vital in an online learning environment where interactions and learning outcomes are valued the most.

5.2. RBDIL Study and Accuracy Factors

The *inVideo* system has also been tested on the Robert B Davis Institute for Learning (RBDIL) mathematics education video collection at Rutgers University. The collection features decades of classroom video tracking a cohort of students as they learn mathematics over the years. This collection has been used extensively throughout the testing and refinement of the *inVideo* system.

One interesting outcome of the RBDIL research has been on the nature of videos and how certain factors impact index accuracy. Through our experiments, we found that some videos have very low accuracy rates (10 %) for transcripts created using *inVideo*, while others had significantly better results ranging from 40-90 % and above. We conducted a study to determine what the main contributing factors were that cause the inaccuracy in certain files. The team consulted with senior engineers at the National Institute of Standards and Technologies (NIST) and other professionals in the area. Using signal-processing technology, we analyzed the video signals and discovered interesting results.

Videos with significant ambient noise or unclear signals are known to have accuracy problems, and one of our key findings in this study has shed light on video attributes that would lead to decreased accuracy in a given sample. By investigating this phenomenon further and identifying possible methods to counteract these mitigating factors now that we are aware of their influence, we have been teaching the *inVideo* software to improve its outcomes with those videos featuring one or more confounding attributes.

To this end, we compared different videos to observe which factors are primarily involved in affecting the accuracy, and have worked to create methods for counteracting these factors. Fig. 8 and Fig. 9 show the frequency and quefrequency distributions for two videos: one with an acceptable level of indexing accuracy and one with one or more mitigating factors that confound accurate indexing.

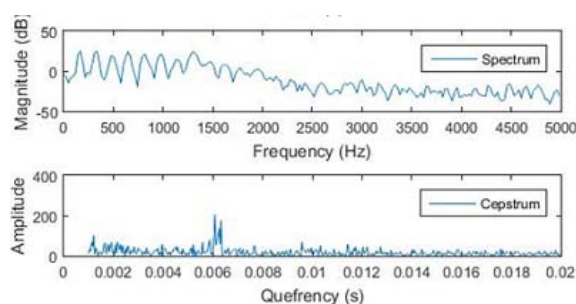


Fig. 8. Signal analysis for video with 90 % accuracy.

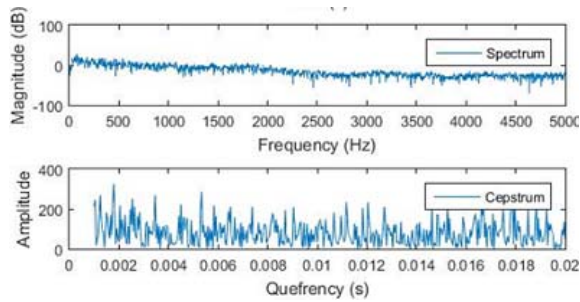


Fig. 9. Signal analysis for video with 10 % accuracy.

Our study shows that ambient noise (reflected through the quefrequency) plays an important role in the accuracy of the transcripts. Ambient noise may come directly from the environment or from the natural distortions that can occur due to recording practices, such as the reverberation that results when the distance between vocal and microphone is not ideal. Acceptable tolerance levels for distance-based reverberation will vary based on the type of microphone used. This supports our conclusion that the type of recording equipment used and the methods by which it is deployed is one of several key factors in determining accuracy.

Based on these results, the team conducted experiments in which the voices were re-recorded on select videos and the resulting audio track was layered back to the original videos. For these tests, the team used a condenser microphone and took steps to ensure that it was directed optimally in relation to the source and within an acceptable distance. As expected, the accuracy improved from less than 20 % to 80 % or above.

It is worth noting as well that there is a distinction between ambience and signal clarity problems when it comes to human and computer comprehension. Many instances of poor signal quality are obvious to the human observer, because the information will be hard to understand. However, the human brain is quite good at inferring meaning in less than ideal signals in ways that computers can't accomplish as easily. There exists a range of issues that may exist in a video file that can create issues for automated indexing and search, despite appearing acceptable to a human viewer. Any researcher or educator creating video content would be wise to consider this.

6. Conclusion and Future Work

This paper discussed a novel video index and analytics tool used to analyze video data. Video indexing engines analyze both audio and visual components of a video, and the results of this analysis provide novel opportunities for search. To improve accuracy, we can either improve the transcription engine, analyze video frames better where there is no audio, or crowd-source accuracy through collaborative filtering. For transcription accuracy, one potential

accuracy improvement can come from using a self-learning artificial intelligence (AI) system that could be taught to recognize certain accents or languages. The process or requirements for instituting such a system and the magnitude of the improvement in accuracy are to be studied in the future.

At present, the *inVideo* tool is limited to only analyze native (non-streaming) videos. We will continue our research on analyzing live videos and streaming videos and make *inVideo* available to broader video collections and applications.

Acknowledgements

This research is funded in part by grants from the US National Science Foundation (NSF) [EAGER-1419055 and DGE-1439570].

References

- [1]. K. Bakshi, Considerations for big data: Architecture and approach, in *Proceedings of the IEEE Aerospace Conference*, 2012, pp. 1–7.
- [2]. S. Wang, Dual-data defense in depth improves SCADA security, *Signal*, 2016, pp. 42–44.
- [3]. S. Wang, W. Kelly, Smart cities architecture and security in cybersecurity education, in *Proceedings of the Colloquium of Information Systems Security Education (CISSE)*, 2017.
- [4]. P. Wang, W. Kelly, A novel threat analysis and risk mitigation approach to prevent cyber intrusions, *The Colloquium for Information System Security Education (CISSE)*, Vol. 3, Issue 1, 2015, pp. 157–174.
- [5]. S. Wang, A. Ali, W. Kelly, Data security and threat modeling for smart city infrastructure, in *Proceedings of the IEEE International Conference on Cyber Security of Smart Cities, Industrial Control System and Communications*, 2015, pp. 1–6.
- [6]. S. P. Wang, R. S. Ledley, *Computer Architecture and Security: fundamentals of designing secure computer systems*, Wiley, 2013.
- [7]. S. Wang, W. Kelly, J. Zhang, Using novel video indexing and data analytics tool to enhance interactions in e-learning, in *Proceedings of the World Conference on E-Learning in Corporate, Government, Healthcare, and Higher Education (E-Learn)*, 2015, pp. 1919-1927.
- [8]. S. Wang, A. Ali, J. Zhang, W. Kelly, *inVideo* - a novel big data analytics tool for video data analytics and its use in enhancing interactions in cybersecurity online education, *WIT Transactions on Information and Communication Technologies*, Vol. 60, 2015, pp. 321-328.
- [9]. S. Wang, J. Zhang, A video data search engine for cyber-physical traffic and security monitoring systems, in *Proceedings of the IEEE/ACM Fourth International Conference on Cyber-Physical Systems*, 2014, pp. 225–226.
- [10]. S. Wang, W. Kelly, *inVideo* - a novel big data analytics tool for video data analytics, in *Proceedings of the IT Professional Conference*, 2014, pp. 1-19.
- [11]. S. Wang, R. Ledley, Modified Neumann architecture with micro-OS for security, in *Proceedings of the*

- China-Ireland International Conference on Information and Communications Technologies (CICT'07), 2007, pp. 303–310.
- [12]. S. Wang, F. Shao, R. S. Ledley, Computer - A framework of intrusion-free secure computer architecture, in *Proceedings of the International Conference on Security & Management (SAM'06)*, Las Vegas, Nevada, USA, June 26-29, 2006, pp. 220–225.
- [13]. A. Serrano-Laguna, J. Torrente, P. Moreno-Ger, B. Fernandez-Manjon, Tracing a little for big improvements: Application of learning analytics and videogames for student assessment, in *of the Fourth International Conference on Games and Virtual Worlds for Serious Applications (VS-GAMES'12)*, Genoa, Italy, October 29-31, 2012, pp. 203–209.
- [14]. V. J. Rideout, U. Foehr, D. Roberts, Generation m2: Media in the lives of 8- to 18-year-olds, 2010. <http://kaiserfamilyfoundation.files.wordpress.com/2013/01/8010.pdf>
- [15]. H. Choi, S. Johnson, The effect of context-based video instruction on learning and motivation in online courses, *The American Journal of Distance Education*, Vol. 19, No. 4, 2005, pp. 215–217.
- [16]. S. Wang, M. Behrmann, Video indexing and automatic transcript creation, in *Proceedings of the 2nd International Conference on Education Research*, New Orleans, LA, 2010.
- [17]. T. Elias, Learning analytics: Definitions, processes and potential, 2011, <http://www.learninganalytics.net/LearningAnalyticsDefinitionsProcessesPotential.pdf>
- [18]. C. E. Hmelo-Silver, C. A. Maher, A. Alston, M. Palius, G. Agnew, R. Sigley, C. M. Mills, Building multimedia artifacts using a cyber-enabled video repository: The VMCAnalytic, in *Proceedings of the 46th Hawaii International Conference on System Sciences, HICSS'13*, Wailea, HI, USA, January 7-10, 2013, pp. 3078–3087.
- [19]. C. E. Hmelo-Silver, C. A. Maher, G. Agnew, M. Palius, S. J. Derry, The video mosaic: design and preliminary research, in *Proceedings of the 9th International Conference of the Learning Sciences (ICLS '10)*, Chicago, IL, USA, Vol. 2, June 29 - July 2, 2010, pp. 425–426. [Online]. Available: <http://dl.acm.org/citation.cfm?id=1854729>
- [20]. G. Agnew, C. M. Mills, C. A. Maher, VMCAnalytic: Developing a collaborative video analysis tool for education faculty and practicing educators, in *Proceedings of the 43rd Hawaii International Conference on Systems Science (HICSS-43 2010)*, Koloa, Kauai, HI, USA, 5-8 January 2010, pp. 1–10.
- [21]. C. A. F. P. Filho, T. A. Buck, C. A. S. Santos, An environment for video content indexing and retrieval based on visual features, in *Proceedings of the XV Brazilian Symposium on Multimedia and the Web (WebMedia'09)*, New York, NY, USA: ACM, 2009, pp. 25:1–25:8.
- [22]. D. M. Norris, L. Baer, Building organizational capacity for analytics: Panel proposal, in *Proceedings of the 2nd International Conference on Learning Analytics and Knowledge (LAK'12)*, New York, NY, USA: ACM, 2012, pp. 18–19.
- [23]. A. L. Dyckhoff, D. Zielke, M. Bultmann, M. A. Chatti, U. Schroeder, Design and implementation of a learning analytics toolkit for teachers, *Educational Technology & Society*, Vol. 15, No. 3, pp. 58–76, 2012, <http://www.ifets.info/downloadpdf.php?jid=56&a id=1257>
- [24]. S. Wang, J. Chen, M. Behrmann, Visualizing search engine results of data-driven web content, 2004, <http://www.w3.org/WAI/RD/2003/12/Visualization/VisSearch/VisualSearchEngine.htm>
- [25]. S. Wang, M. Behrmann, Automatic adaptive assessment in learning, in *Proceedings of the IADIS International Conference on Cognition and Exploratory Learning in Digital Age*, 2009, pp. 435–438.
- [26]. S. Wang, X. Cheng, C. Maher, W. Kelly, InVideo: An Automatic Video Index and Search Engine for Large Video Collections, in *Proceedings of the Second International Conference on Advances in Signal, Image and Video Processing (SIGNAL'17)*, Barcelona, Spain, 21-25 May 2017.



Universal Frequency-to-Digital Converter (UFDC-1)

- 16 measuring modes: frequency, period, its difference and ratio, duty-cycle, duty-off factor, time interval, pulse width and space, phase shift, events counting, rotation speed
- 2 channels
- Programmable accuracy up to 0.001 %
- Wide frequency range: 0.05 Hz ... 7.5 MHz (120 MHz with prescaling)
- Non-redundant conversion time
- RS-232, SPI and I²C interfaces
- Operating temperature range -40 °C ... +85 °C

www.sensorsportal.com info@sensorsportal.com SWP, Inc., Canada



Semi-Implicit Additive Operator Splitting Scheme for Image Segmentation Using the Chan-Vese Model

¹Messaoudi Zahir, Berki Hemza and Younsi Arezki

Ecole Militaire Polytechnique, BP 17, Bordj-El-Bahri Algiers, 16111, Algeria

¹Tel.: +213661241644

¹E-mail: messaoudi_zahir06@yahoo.fr

Received: 1 June 2017 /Accepted: 7 August 2017 /Published: 31 August 2017

Abstract: Active contour models are designed to evolve an initial curve, called level set, to extract the desired object(s) in an image. Most approaches are based on semi-implicit schemes which are stable for all time steps. Various models are used for the global segmentation such as Chan-Vese (CV) model. The CV model has the global segmentation property to segment all objects in an image. The problem with this model is the high time computing. In order to reduce it, our contribution in this work is the association of a semi-implicit Additive Operator Splitting (AOS) technique with the CV model in biphasic and multiphase cases. The basic idea behind AOS schemes is to decompose a multi-dimensional problem into one-dimensional ones that can be solved very efficiently. In this paper, we present the new association in biphasic and multiphase cases with simulations showing the efficiency of the proposed method.

Keywords: Image segmentation, Active contours, Chan Vese, AOS scheme, Level set.

1. Introduction

Image segmentation is the task of partitioning an image into multiple regions. The most known region based method has been proposed by Mumford Shah [1] who have introduced a general optimization framework. To determine desired curves or surfaces, this method uses an energy functional based on regional geometric properties such as the area of the region, its contour length and the variation of individual pixel intensities inside and outside the region. However, the Mumford Shah [2] model cannot be easily implemented. The CV method [2] is a special implementation of Mumford Shah using a level set function for the case of two phases with two piecewise constants. The basic idea of CV model is to minimize energy functional by solving the Euler-Lagrange equation. This minimization takes enough time in image segmentation.

To reduce the time of segmentation, Weickert et al. [3] provide a fast algorithm using the semi-implicit AOS scheme. The basic idea behind the AOS schemes is to decompose a multi-dimensional problem into one-dimensional ones that can be solved very efficiently. Then the final multi-dimensional solution is approximated by averaging the one-dimensional solutions. In [4], the authors present a combination of the semi-implicit AOS scheme and a narrow-band technique which is associated to the geodesic active contours. This association requires re-initialization for each iteration which is the weakness of the method. As solution, Kuhne et al. [5] provide a fast algorithm using a semi-implicit AOS scheme technique which is suitable both for the geometric and the geodesic active contour model. In [6], the authors propose a new selective segmentation model, combining ideas from global segmentation that can be reformulated in a convex way such that a global minimizer can be found

independently of initialization. They present the Convex Distance Selective Segmentation (CDSS) functional (based on CV model) which is associated with the semi-implicit AOS scheme. In our work, we use a level set representation of the CV model with the semi-implicit AOS scheme in order to improve the speed of the segmentation in biphasic and multiphase cases.

This paper is organized as follows. Section 2 contains a review of level set method and the CV model for biphasic and multiphase cases. In Section 3, we present the semi-implicit AOS scheme. Then, we present the CV model with the semi-implicit AOS scheme in biphasic and multiphase cases in Section 4. Experimental results are given in Section 5.

2. Active Contour Models

In this section, we shall first provide an overview of level set theory before we get into the details of the CV model.

2.1. Level Set Method

A level set method is a numerical technique, which helps with tracking moving fronts to interfaces and shapes. This technique was first introduced by Osher et al. in [7], where the boundaries are given by level sets of a function $\varphi(x)$, naming it as the level set method. This method is very successful due to a very easy way of following shapes that change topology. For a given interface $\Gamma = \partial\Omega$ as shown in **Fig. 1**, the level set is independent of the parametrisation of the contour and can be used to represent the interface evolution. The idea of the level set method is to implicitly represent an interface Γ as the level set of a function φ . The level set function φ of the closed front Γ is defined as follows:

$$\begin{cases} \varphi(x) > 0 & \text{inside } \Gamma \\ \varphi(x) < 0 & \text{outside } \Gamma, \\ \varphi(x) = 0 & \text{on } \Gamma. \end{cases}$$

where $x \in R^2$.

The adjusting contour at time t is denoted by $\varphi(x(t); t)$

$$\begin{cases} \varphi(x(t); t) > 0 & \text{inside } \Gamma \\ \varphi(x(t); t) < 0 & \text{outside } \Gamma, \\ \varphi(x(t); t) = 0 & \text{on } \Gamma. \end{cases}$$

The level set value of a point on the contour with motion must always be 0.

$$\varphi(x(t); t) = 0, \quad (1)$$

A derivation of (1) with respect to t and after some manipulation, yields PDE equation:

$$\frac{\partial \varphi}{\partial t} + F |\nabla \varphi| = 0, \quad (2)$$

where F stands for the speed in which the contour propa-gates in normal direction with an initial condition $\varphi(x, t = 0)$ (the initial drawn curve)

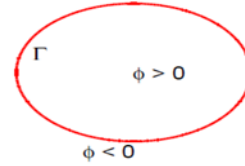


Fig. 1. Representation of the interface Γ .

2.2. The Chan-Vese Model

2.2.1. Biphasic Case

In [2], the authors present a special implementation of the CV method based on the use of the level set method to minimize the piecewise constant two phases Mumford Shah functional [1]. The advantage of this implementation is the possibility to detect objects whose boundaries are not necessarily defined by gradient and overcame the problematic tracking of Γ . For a given image u_0 in domain Ω , the CV model is formulated by minimizing the following energy functional:

$$\begin{aligned} F^{CV} = & \mu \int_{\Omega} \delta(\varphi) |\nabla \varphi| dx dy + \nu \int_{\Omega} H(\varphi) dx dy + \\ & \lambda_1 \int_{\Omega} |u_0(x, y) - c_1|^2 H(\varphi(x, y)) dx dy + \\ & \lambda_2 \int_{\Omega} |u_0(x, y) - c_2|^2 (1 - H(\varphi(x, y))) dx dy \end{aligned} \quad (3)$$

where μ, λ_1 and λ_2 are positive parameters, φ is a level set function, $H(\varphi)$ is the Heaviside function and $\delta(\varphi)$ is the Dirac function. Generally, the regularized versions are selected as follows:

$$\begin{cases} H_{\varepsilon}(\varphi) = \frac{1}{2} \left(1 + \frac{2}{\pi} \arctan \left(\frac{\varphi}{\varepsilon} \right) \right), \\ \delta_{\varepsilon}(\varphi) = \frac{1}{\pi} \frac{\varepsilon}{\varphi^2 + \varepsilon^2} \end{cases}, \quad (4)$$

The two piecewise constants c_1 and c_2 are defined as

$$c_1 = \frac{\int_{\Omega} u_0(x, y) H_{\varepsilon}(\varphi(x, y)) dx dy}{\int_{\Omega} H_{\varepsilon}(\varphi(x, y)) dx dy}, \quad (5)$$

$$c_2 = \frac{\int_{\Omega} u_0(x, y)(1 - H_{\varepsilon}(\varphi(x, y))) dx dy}{\int_{\Omega} (1 - H_{\varepsilon}(\varphi(x, y))) dx dy}, \quad (6)$$

The evolution equation is given by:

$$\frac{\partial \varphi}{\partial t} = \delta_{\varepsilon}(\varphi) \left[\begin{array}{l} \mu \nabla \cdot \left(\frac{\nabla \varphi}{|\nabla \varphi|} \right) - \nu - \lambda_1 (u_0 - c_1)^2 \\ + \lambda_2 (u_0 - c_2)^2 \end{array} \right], \quad (7)$$

2.2.2. Multiphase Case

The CV model for multiphase piece-wise constant (we use two level set functions φ_1 and φ_2) is formulated by minimizing the following energy functional [8]:

$$F = \mu \int_{\Omega} |\nabla H_{\varepsilon}(\varphi_1)| dx dy + \mu \int_{\Omega} |\nabla H_{\varepsilon}(\varphi_2)| dx dy + \int_{\Omega} (u_0 - c_{11})^2 H_{\varepsilon}(\varphi_1) H_{\varepsilon}(\varphi_2) dx dy + \int_{\Omega} (u_0 - c_{10})^2 H_{\varepsilon}(\varphi_1) (1 - H_{\varepsilon}(\varphi_2)) dx dy + \int_{\Omega} (u_0 - c_{01})^2 (1 - H_{\varepsilon}(\varphi_1)) H_{\varepsilon}(\varphi_2) dx dy + \int_{\Omega} (u_0 - c_{00})^2 (1 - H_{\varepsilon}(\varphi_1)) (1 - H_{\varepsilon}(\varphi_2)) dx dy + \quad (8)$$

where

$$c_{11} = \frac{\int_{\Omega} u_0 H_{\varepsilon}(\varphi_1) H_{\varepsilon}(\varphi_2) dx dy}{\int_{\Omega} H_{\varepsilon}(\varphi_1) H_{\varepsilon}(\varphi_2) dx dy}, \quad (9)$$

$$c_{10} = \frac{\int_{\Omega} u_0 H_{\varepsilon}(\varphi_1) (1 - H_{\varepsilon}(\varphi_2)) dx dy}{\int_{\Omega} H_{\varepsilon}(\varphi_1) (1 - H_{\varepsilon}(\varphi_2)) dx dy}, \quad (10)$$

$$c_{01} = \frac{\int_{\Omega} u_0 (1 - H_{\varepsilon}(\varphi_1)) H_{\varepsilon}(\varphi_2) dx dy}{\int_{\Omega} (1 - H_{\varepsilon}(\varphi_1)) H_{\varepsilon}(\varphi_2) dx dy}, \quad (11)$$

$$c_{00} = \frac{\int_{\Omega} u_0 (1 - H_{\varepsilon}(\varphi_1)) (1 - H_{\varepsilon}(\varphi_2)) dx dy}{\int_{\Omega} (1 - H_{\varepsilon}(\varphi_1)) (1 - H_{\varepsilon}(\varphi_2)) dx dy}, \quad (12)$$

Evolution equations of φ_1 and φ_2 are given by:

$$\frac{\partial \varphi_1}{\partial t} = \delta_{\varepsilon}(\varphi_1) \left\{ \begin{array}{l} \mu \operatorname{div} \left(\frac{\nabla \varphi_1}{|\nabla \varphi_1|} \right) - \\ \left[\left((u_0 - c_{11})^2 - (u_0 - c_{01})^2 \right) (H_{\varepsilon}(\varphi_2)) + \right. \\ \left. \left[\left((u_0 - c_{10})^2 - (u_0 - c_{00})^2 \right) (1 - H_{\varepsilon}(\varphi_2)) \right] \right] \end{array} \right\} \quad (13)$$

$$\frac{\partial \varphi_2}{\partial t} = \delta_{\varepsilon}(\varphi_2) \left\{ \begin{array}{l} \mu \operatorname{div} \left(\frac{\nabla \varphi_2}{|\nabla \varphi_2|} \right) - \\ \left[\left((u_0 - c_{11})^2 - (u_0 - c_{10})^2 \right) (H_{\varepsilon}(\varphi_1)) + \right. \\ \left. \left[\left((u_0 - c_{01})^2 - (u_0 - c_{00})^2 \right) (1 - H_{\varepsilon}(\varphi_1)) \right] \right] \end{array} \right\} \quad (14)$$

3. Additive Operator Splitting Scheme

The AOS method is proposed by Tai et al. in [9] and Weickert et al. in [3]. The AOS scheme guarantees equal treatment of all coordinate axes and is stable for big time steps. The scheme presents the semi-implicit algorithm based on a discrete non-linear diffusion scale-space framework. This scheme is applied to the m-dimensional diffusion equation and it is given in the following form:

$$\frac{\partial \varphi}{\partial t} = \operatorname{div}(g \nabla \varphi) + f(x, \varphi), \quad (15)$$

$$\frac{\partial \varphi}{\partial t} = \sum_{j=1}^m \frac{\partial}{\partial x_j} \left(g_j(\varphi) \frac{\partial \varphi}{\partial x_j} \right) + f(x, \varphi), \quad (16)$$

where $[0, T] \times \Omega \subset \mathbb{R}^m$. The initial and boundary conditions are:

$$\varphi(0, \cdot) = \varphi_0 \quad \text{and} \quad \frac{\partial \varphi}{\partial n} = 0 \quad \text{on} \quad \partial \Omega,$$

We consider discrete times $t_k = k \Delta t$, where $k \in N_0$ and Δt a semi-implicit discretization of the diffusion equation.

$$\varphi^{k+1} = \left(I - \Delta t \sum_{l=1}^m A_l(\varphi) \right)^{-1} \hat{\varphi}^k, \quad k = 1, 2, \dots \quad (17)$$

where $\hat{\varphi}^k = \varphi^k + \Delta t f$.

We may consider AOS variant (for $m = 2$)

$$\varphi^{k+1} = \frac{1}{2} \sum_{l=1}^2 \left(I - 2 \Delta t A_l(\varphi^k) \right)^{-1} \hat{\varphi}^k, \quad k = 1, 2, \dots \quad (18)$$

The AOS scheme offers one important advantage [10]: the operators $B_l(u^k) = I - 2 \Delta t A_l(\varphi^k)$ lead to strictly diagonally dominant tridiagonal linear systems, which can be solved very efficiently with Thomas algorithm. This algorithm has a linear complexity and can be implemented very easily.

To implement equation (18), we proceed in three steps [10]:

- 1) Evolution in x direction with step size $2 \Delta t$:
Solve the tridiagonal system $(I - 2 \Delta t A_x(\varphi^k)) v^{k+1} = \hat{\varphi}^k$ for v^{k+1} .

- 2) Evolution in y direction with step size $2\Delta t$:
Solve the tridiagonal system
 $(I - 2\Delta t A_y(\varphi^k))\omega^{k+1} = \hat{\varphi}^k$ for ω^{k+1} .
- 3) Averaging:
Compute $\varphi^{k+1} := 0.5(v^{k+1} + \omega^{k+1})$.

4. The Chan-Vese Model with Semi-Implicit Additive Operator Splitting Scheme

In this section, we present the CV model with the semi-implicit AOS scheme in biphasic and multiphase cases.

4.1. Biphasic Case

From equation (7), we denote:

$$f = \delta_\varepsilon(\varphi) \left\{ - \left[\lambda_1 (u_0 - c_1)^2 - \lambda_2 (u_0 - c_2)^2 \right] - \nu \right\}, \quad (19)$$

To avoid singularities, we replace the term $|\nabla \varphi|$ with $|\nabla \varphi|_\beta = \sqrt{\varphi_x^2 + \varphi_y^2 + \beta}$ and denote $W = 1/|\nabla \varphi|_\beta$. Discretizing (7) by employing the AOS scheme, we get the following equation:

$$\varphi^{n+1} = \frac{1}{2} \sum_{l=1}^2 (I - 2\Delta t A_l(\varphi^n))^{-1} \hat{\varphi}^n, \quad (20)$$

The matrices A_l , for $l=1,2$, are tridiagonal matrices derived using finite differences [11] and $\hat{\varphi}^n = \varphi^n + \Delta t f$.

$$\begin{aligned} (A_1(\varphi^n)\varphi^{n+1})_{i,j} &= \mu \delta_\varepsilon(\varphi^n) \frac{E_{i+1,j}^n + E_{i,j}^n}{2h_x^2} \\ &\quad (\varphi_{i+1,j}^{n+1} - \varphi_{i,j}^{n+1}) \\ &\quad - \mu \delta_\varepsilon(\varphi^n) \frac{E_{i,j}^n + E_{i-1,j}^n}{2h_x^2} \\ &\quad (\varphi_{i,j}^{n+1} - \varphi_{i-1,j}^{n+1}) \end{aligned}$$

$$\begin{aligned} (A_2(\varphi^n)\varphi^{n+1})_{i,j} &= \mu \delta_\varepsilon(\varphi^n) \frac{E_{i,j+1}^n + E_{i,j}^n}{2h_y^2} \\ &\quad (\varphi_{i,j+1}^{n+1} - \varphi_{i,j}^{n+1}) \\ &\quad - \mu \delta_\varepsilon(\varphi^n) \frac{E_{i,j}^n + E_{i,j-1}^n}{2h_y^2} \\ &\quad (\varphi_{i,j}^{n+1} - \varphi_{i,j-1}^{n+1}) \end{aligned}$$

The algorithm of the CV model with the semi-implicit AOS in biphasic case is [12]:

- 1) Initialize φ^0 by φ_0 , $k=0$.
- 2) Compute f from equation (19).
- 3) Compute $c_1(\varphi^k)$ and $c_2(\varphi^k)$ by (5) and (6).
- 4) Compute φ^k using (20).
- 5) Check whether the solution is stationary. If not, repeat 2-5.

4.2. Multiphase Case

From equation (13), we denote:

$$f_1 = \delta_\varepsilon(\varphi_1) \left\{ - \left[\begin{array}{l} ((u_0 - c_{11})^2 - (u_0 - c_{01})^2) \\ (H_\varepsilon(\varphi_2)) + ((u_0 - c_{10})^2 - (u_0 - c_{00})^2) \\ (1 - H_\varepsilon(\varphi_2)) \end{array} \right] \right\} \quad (21)$$

From equation (14), we denote:

$$f_2 = \delta_\varepsilon(\varphi_2) \left\{ - \left[\begin{array}{l} ((u_0 - c_{11})^2 - (u_0 - c_{10})^2) \\ (H_\varepsilon(\varphi_1)) + ((u_0 - c_{01})^2 - (u_0 - c_{00})^2) \\ (1 - H_\varepsilon(\varphi_1)) \end{array} \right] \right\} \quad (22)$$

To avoid singularities, we replace the term $|\nabla \varphi_1|$ with $|\nabla \varphi_1|_\beta = \sqrt{\varphi_{1x}^2 + \varphi_{1y}^2 + \beta}$ and $|\nabla \varphi_2|$ with $|\nabla \varphi_2|_\beta = \sqrt{\varphi_{2x}^2 + \varphi_{2y}^2 + \beta}$.

The algorithm of the CV model with the semi-implicit AOS in multiphase case is:

- 1) Initialize φ_1^0 and φ_2^0 by φ_{10} and φ_{20} , $k=0$
- 2) Compute $c_{11}(\varphi^k)$, $c_{10}(\varphi^k)$, $c_{01}(\varphi^k)$ and $c_{00}(\varphi^k)$
- 3) Compute f_1 and f_2 by equation (21) and (22).
- 4) Compute φ_1^k using (20) and φ_2^k using (20).
- 5) Check whether the solution is stationary. If not, repeat 2-5.

5. Experimental Results

In the biphasic case, the constants are given as follow: $\nu=0$, $\Delta t=1$ and $\lambda_1=\lambda_2=1$.

In Figs. 2 - 5, we illustrate the segmentation by the CV model for boat, MR of knee, MR of brain and CT images. In Figures Figs. 6 - 9, we show the segmentation by the CV model with semi-implicite

AOS scheme for the same images. The segmentation illustrates the two phases and the results are almost similar for the two methods.

For the multiphase case, the constants are given as follow: $\nu = 0$ and $\lambda_1 = \lambda_2 = 1$. In Figs. 10 - 13, we illustrate the segmentation by the CV model for boat, MR of knee, MR of brain and CT images, but in Figs. 14 - 17, we show the segmentation by the CV

model with the semi-implicite AOS scheme for the same images. The two methods give exactly the same segmentation where we can see the four phases.

The comparison study relative to time computing is summarized in Tables 1 - 4; we deduce that the CV model with semi-implicit AOS scheme reduces the time computing of the segmentation by half.

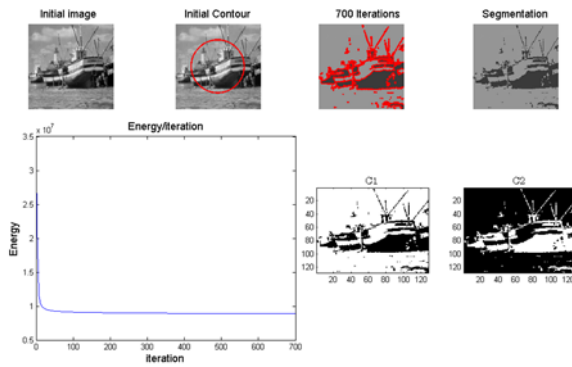


Fig. 2. Segmentation by CV model (biphase case) of boat.

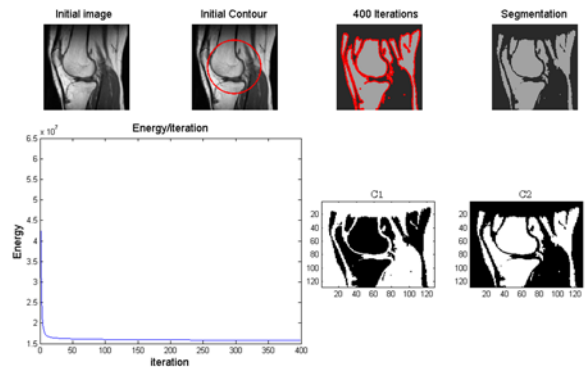


Fig. 3. Segmentation by CV model (biphase case) of MR image of knee.

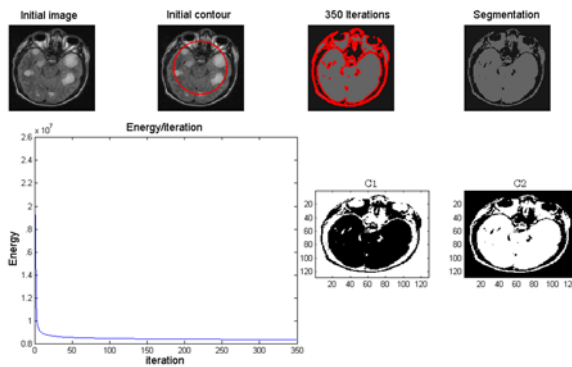


Fig. 4. Segmentation by CV model (biphase case) of MR image of brain.

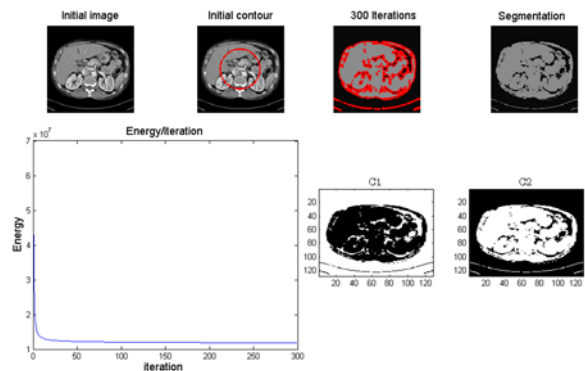


Fig. 5. Segmentation by CV model (biphase case) of CT image.

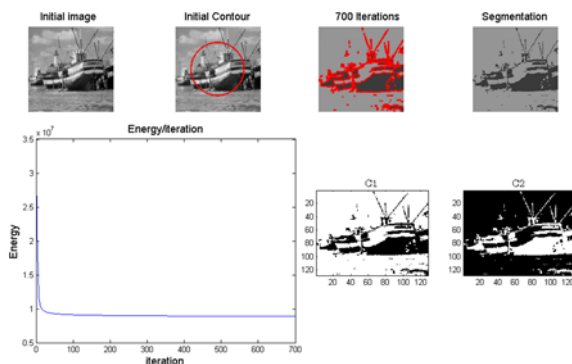


Fig. 6. Segmentation by the CV model with semi-implicite AOS scheme (biphase case) of boat.

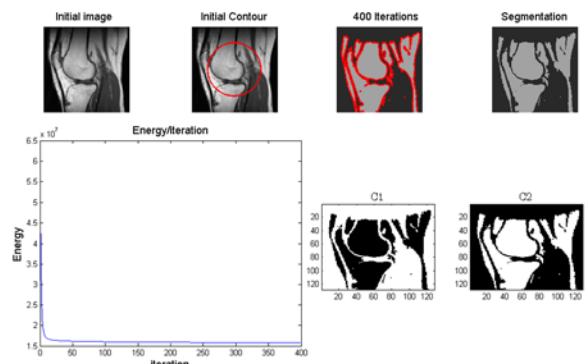


Fig. 7. Segmentation by the CV model with semi-implicite AOS scheme (biphase case) of MR image of knee.

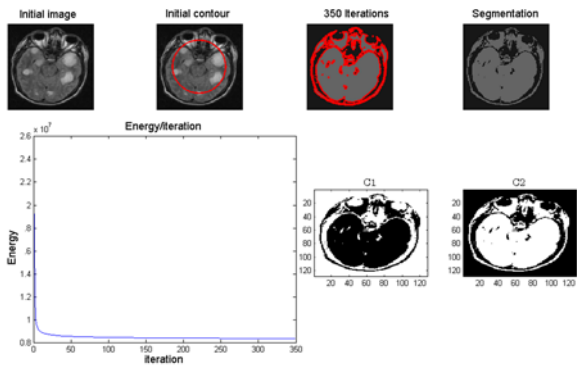


Fig. 8. Segmentation by the CV model with semi-implicit AOS scheme (biphase case) of MR image of brain.

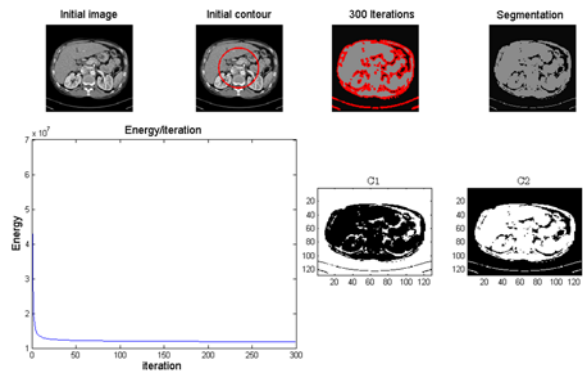


Fig. 9. Segmentation by the CV model with semi-implicit AOS scheme (biphase case) of CT image.

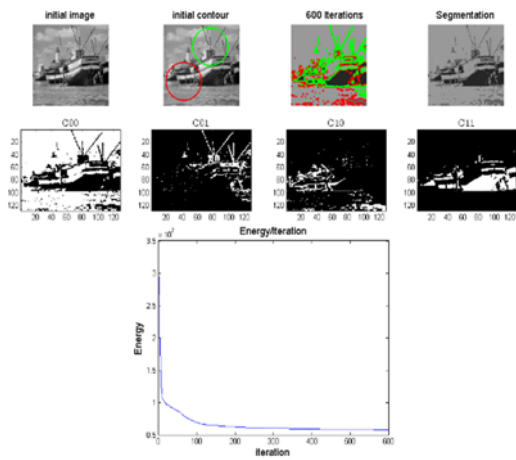


Fig. 10. Segmentation by CV model (multiphase case) of boat.

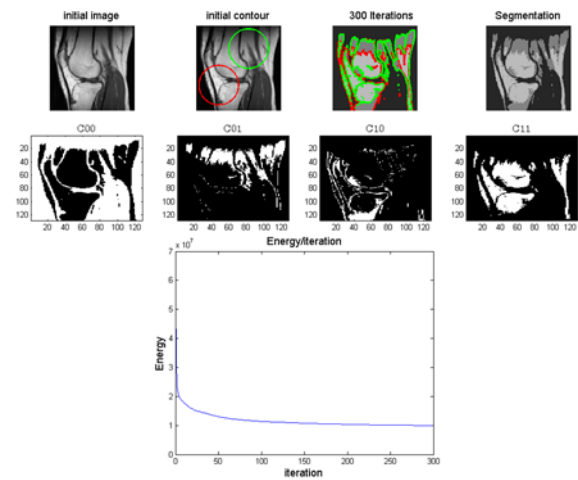


Fig. 11. Segmentation by CV model (multiphase case) of MR image of knee.

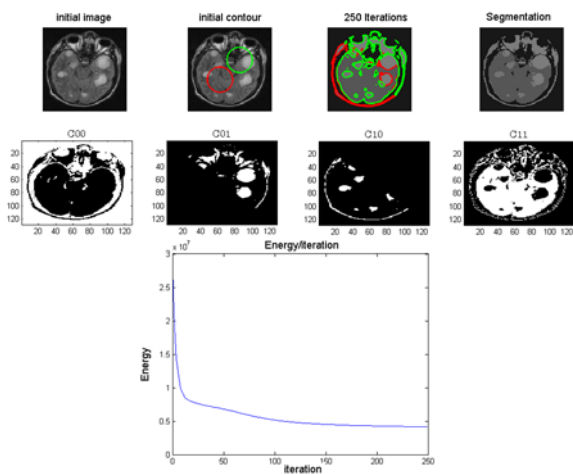


Fig. 12. Segmentation by CV model (multiphase case) of MR image of brain.

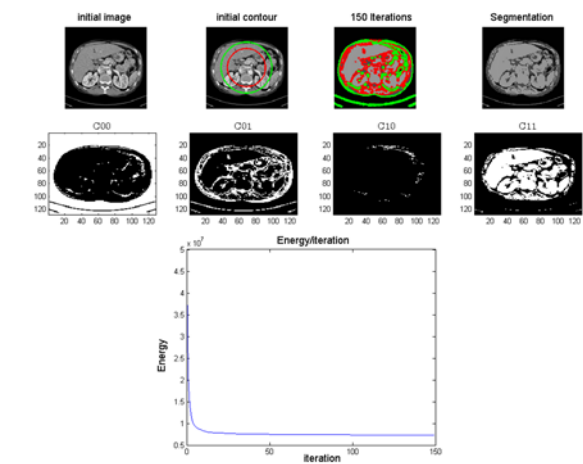


Fig. 13. Segmentation by CV model (multiphase case) of CT image.

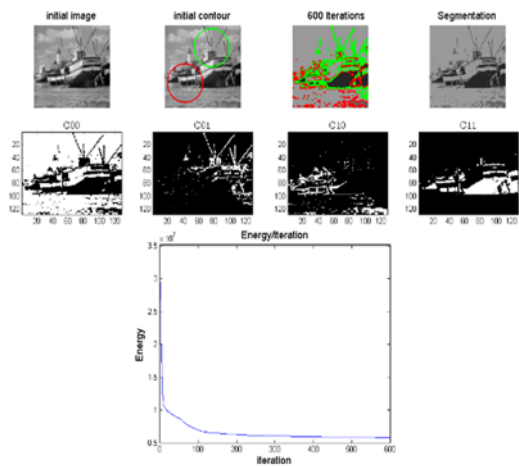


Fig. 14. Segmentation by the CV model with semi-implicit AOS scheme (multiphase case) of boat.

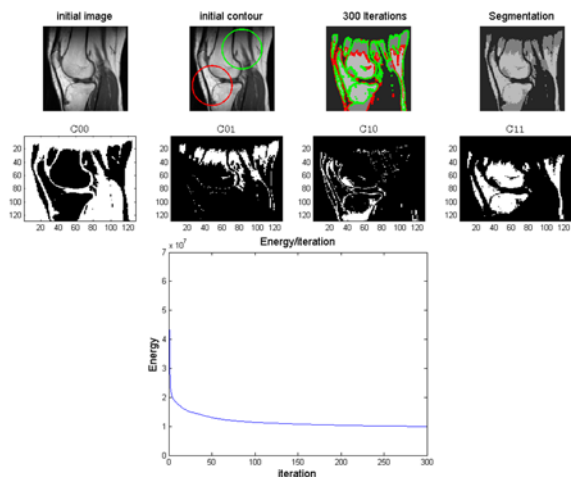


Fig. 15. Segmentation by the CV model with semi-implicit AOS scheme (multiphase case) of MR image of knee.

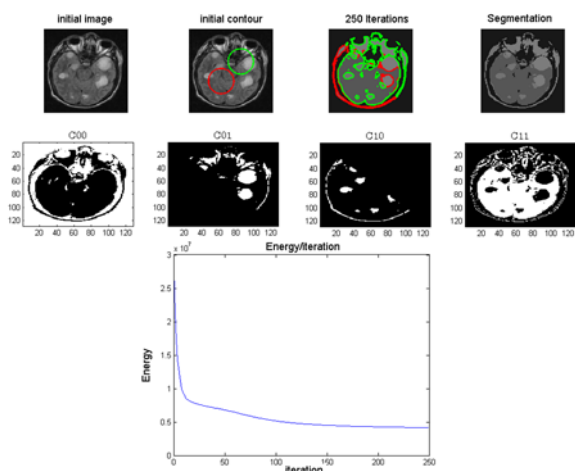


Fig. 16. Segmentation by the CV model with semi-implicit AOS scheme (multiphase case) of MR image of brain.

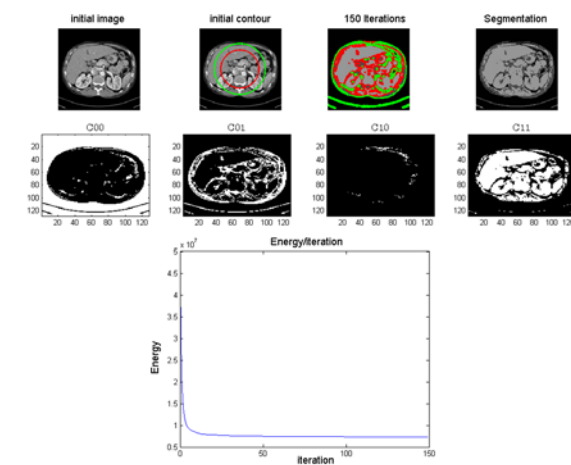


Fig. 17. Segmentation by the CV model with semi-implicit AOS scheme (multiphase case) of CT image.

Table 1. Comparison between the CV model and the CV model with semi-implicit AOS scheme of boat and MR of knee images in biphase case.

Image	boat		MR of knee	
	CV	CV-AOS	CV	CV-AOS
CPU time (s)	110.6671	56.7532	51.9639	22.1521

Table 3. Comparison between the CV model and the CV model with semi-implicit AOS scheme of boat and MR of knee images in multiphase case.

Image	boat		MR of knee	
	CV	CV-AOS	CV	CV-AOS
CPU time (s)	158.2630	71.0429	70.3253	28.1270

Table 2. Comparison between the CV model and the CV model with semi-implicit AOS scheme of MR of brain and CT images in biphase case.

Image	MR of brain		CT	
	CV	CV-AOS	CV	CV-AOS
CPU time (s)	48.8127	20.9665	48.9063	22.7761

Table 4. Comparison between the CV model and the CV model with semi-implicit AOS scheme of MR of brain and CT images in multiphase case.

Image	MR of brain		CT	
	CV	CV-AOS	CV	CV-AOS
CPU time (s)	69.9352	26.3954	39.4527	18.8449

6. Conclusions

In this paper, we have used the advantages of the semi-implicit AOS technique in order to fast the CV model for image segmentation in biphase and multiphase cases. The experimental results show that the segmentation is done in the two cases, with the superiority of the CV model with the semi-implicit scheme compared to the CV model concerning the time computing. As future work, we plan to associate the semi-implicit AOS technique with other active contour.

References

- [1]. D. Mumford and J. Shah, Optimal approximations by piecewise smooth functions and associated variational problems, *Communications on Pure and Applied Mathematics*, Vol. 42, No. 5, 1989, pp. 577–685.
- [2]. T. F. Chan and L. A. Vese, Active contours without edges, *IEEE Transactions on Image Processing*, Vol. 10, No. 2, 2001, pp. 266–277.
- [3]. J. Weickert, B. T. H. Romeny, and M. A. Viergever, Efficient and reliable schemes for nonlinear diffusion filtering, *IEEE Transactions on Image Processing*, Vol. 7, No. 3, 1998, pp. 398–410.
- [4]. E. R. R. Goldenberg, R. Kimmel and M. Rudzsky, Fast geodesic active contours, *IEEE Transactions on Image Processing*, Vol. 10, No. 10, 2001, pp. 1467–1475.
- [5]. M. B. G. Kuhne, J. Weickert and W. Effelsberg, Fast implicit active contour models, *Pattern Recognition, Lecture Notes in Computer Science*, Vol. 2449, 2002, pp. 133-140.
- [6]. J. Spencer and K. Chen, A convex and selective variational model for image segmentation, *Communications in Mathematical Sciences*, Vol. 13, 2015, No. 6.
- [7]. S. Osher and J. A. Sethian, Fronts propagating with curvature-dependent speed: algorithms based on Hamilton-Jacobi formulations, *Journal of Computational Physics*, Vol. 79, No. 1, 1988, pp. 12–49.
- [8]. L. A. Vese and T. F. Chan, A multiphase level set framework for image segmentation using the Mumford and Shah model, *International Journal of Computer Vision*, Vol. 50, No. 3, 2002, pp. 271–293.
- [9]. T. Lu, P. Neittaanmaki, and X.-C. Tai, A parallel splitting-up method for partial differential equations and its applications to Navier-Stokes equations, *RAIRO-Modélisation mathématique et analyse numérique*, Vol. 26, No. 6, 1992, pp. 673–708.
- [10]. J. Weickert and G. Kühne, Fast methods for implicit active contour models, in *Geometric Level Set Methods in Imaging, Vision, and Graphics*, Stanley Osher and Nikos Paragios (Eds.), Springer, 2003, pp. 43–57.
- [11]. L. Rada and K. Chen, Improved selective segmentation model using one level-set, *Journal of Algorithms & Computational Technology*, Vol. 7, No. 4, 2013, pp. 509–540.
- [12]. Messaoudi Zahir, Berki Hemza and Younsi Arezki, Chan-Vese Model with Semi-Implicit AOS Scheme for Images Segmentation: Biphase and Multiphase Cases, in *Proceedings of the 2nd International Conference on Advances in Signal, Image and Video Processing (SIGNAL'17)*, Barcelona, Spain, May 21-25, 2017, pp. 1-5.



Published by International Frequency Sensor Association (IFSA) Publishing, S. L., 2017 (<http://www.sensorsportal.com>).

POWER ELECTRONICS

14th International exhibition
of power electronics
components and systems



Organised by:



+7 (812) 380 6003 / 07 / 00
power@primexpo.ru

Book your stand:
powerelectronics.ru



Color Space Axioms and Fiber Bundles

Edoardo Provenzi

Laboratoire MAP5 (UMR CNRS 8145), Université Paris Descartes
45 rue des Saints Peres, 75006, Paris, France
E-mail: edoardo.provenzi@parisdescartes.fr

Received: 1 June 2017 / Accepted: 7 August 2017 / Published: 31 August 2017

Abstract: In 1974, H. L. Resnikoff published an inspiring paper about the use of differential geometry to study, among others, the intrinsic shape of the space of perceived colors and the Riemannian metrics on it. The mathematical techniques that he used is shared with modern theories of theoretical physics, which are far from being a common background for scientists in color vision and processing. Due to this, Resnikoff's paper remained unnoticed for decades. In this brief contribution, some insights about how to update Resnikoff's ideas will be given and discussed in relationship with a modern theory of color spaces and to the mathematical concept of principal fiber bundle.

Keywords: Geometry of color spaces, Principal fiber bundles, Human perception, Applications to perceived color distances.

1. Resnikoff's Framework for the Space of Perceived Colors

In the 1974 paper [1], H. L. Resnikoff analyzed the geometrical and topological properties of the space of perceived colors \mathcal{P} with a high level mathematical rigor. He decided to start from Schrödinger's axioms [?] for \mathcal{P} : *Axiom 1* (Newton 1704): if $x \in \mathcal{P}$ and $\alpha \in \mathbb{R}^+$, then $\alpha x \in \mathcal{P}$. *Axiom 2*: if $x \in \mathcal{P}$ then it does not exist any $y \in \mathcal{P}$ such that $x + y = 0$. *Axiom 3* (Grassmann 1853, Helmholtz 1866): for every $x, y \in \mathcal{P}$ and for every $\alpha \in [0, 1]$, $\alpha x + (1-\alpha)y \in \mathcal{P}$. *Axiom 4* (Grassmann 1853): every collection of more than three perceived colors is a linear dependent family in the vector space V spanned by the elements of \mathcal{P} . Note, in particular, that Axiom 3 implies that \mathcal{P} is closed under convex linear combinations, i.e., every two colors in \mathcal{P} can be joined by a line segment, i.e., \mathcal{P} is *convex*. References for the quoted axioms are the following: [2], [3] and [4].

Resnikoff added another axiom that of *local homogeneity* of \mathcal{P} with respect to changes of

background illumination of the visual scene. If X is a topological space and G is a group of transformations that acts on X , then X is called a *homogeneous space with respect to G* if, for any two points $x, y \in X$, there exists a transformation $g \in G$ such that $g(x) = y$, i.e., any two points of X can be joined by an opportune transformation g induced by G . X is only *locally homogeneous with respect to G* if this property holds only locally, i.e., if for every $x \in X$ there is an open neighborhood U_x containing it and such that every $x^0 \in U_x$ can be written as $x^0 = g(x)$ for a certain $g \in G$. The reason for introducing this further axiom is that it is possible to modify a color to reach a 'very similar' color with a change of illumination and this means that \mathcal{P} should be locally homogeneous with respect to the group of transformations of illuminations.

Resnikoff claimed that this group can be assumed as the following:

$$GL(\mathcal{P}) := \{g \in GL(V) \mid g(x) \in \mathcal{P} \ \forall x \in \mathcal{P}\}, \quad (1)$$

where $GL(V)$ is the group of orientation-preserving invertible linear operators on V , or, equivalently, the group of real $n \times n$ matrices with determinant greater than zero, where $n = \dim(V) \leq 3$ thanks to Axiom 4. He justifies this choice from the consideration that Axiom 1 implies that P is a cone embedded in V and so a general transformation of illumination must preserve the orientation of the cone and it must also be invertible, since it is possible to turn back to the initial conditions of illuminations. The condition $g(x) \in P$ is perfectly natural because after the change of illumination we can still perceive the colors.

The observation that a change of illumination slightly modifies the perception of colors of a visual scene can thus be stated in this mathematical formalism by saying that P is locally homogeneous with respect to $GL(P)$. But, thanks to Axiom 3, for every couple of perceived colors $x, y \in P$ there exists the line segment that join x to y . This segment is compact, hence it can be covered by a finite partition of open neighborhoods U_1, \dots, U_n and the color x can be moved along this line segment passing from a neighborhood to the next one with the transformations g_1, \dots, g_n . Thus, the global transformation that enables us to pass from x to y is the composition of the single transformations, i.e., $y = g(x)$, $g = g_n \circ \dots \circ g_1$ and so local homogeneity for the convex P implies its global homogeneity.

For this reason, Resnikoff postulates a fifth axiom on the structure of the color space: *Axiom 5* (Resnikoff 1974): P is globally homogeneous with respect to the group of transformations of illumination $GL(P)$.

Starting from the set of axioms 1-5 and by using Lie groups and algebras representation theory [5], Resnikoff managed showed that the only two geometrical structures compatible with these axioms are:

$$\mathcal{P} \simeq \mathbb{R}^+ \times \mathbb{R}^+ \times \mathbb{R}^+,$$

or

$$\mathcal{P} \simeq \mathbb{R}^+ \times SL(2, \mathbb{R})/SO(2),$$

where $SL(2, \mathbb{R})$ is the group of 2×2 matrices with real entries and determinant +1 and $SO(2)$ is the group of matrices that perform rotations in the plane \mathbb{R}^2 .

The first geometrical structure agrees with the usual trichromatic space, such as RGB, XYZ, and so on. The second geometric structure instead is novel: \mathbb{R}^+ can be interpreted as an achromatic coordinate, but no clear explanation of the Poicare-Lobachevsky two-dimensional space of constant' negative curvature $SL(2, \mathbb{R})/SO(2)$ in terms of color features is available yet.

Once determined the only two possible structures of P , Resnikoff used a phenomenological property of human vision, namely *color constancy*, as an invariance principle which allowed him determining the metric on P . In the colorimetric interpretation, a metric on P allows measuring perceptual differences of color in a visual scene.

Color constancy is the name reserved to the robustness of perception of color differences with respect to global illumination changes. If we indicate with d the metric which measures the difference of colors in P , then color constancy implies that d must be $GL(P)$ -invariant, i.e.

$$d(x, y) = d(g(x), g(y)) \quad \forall x, y \in \mathcal{P}, \quad \forall g \in GL(\mathcal{P}). \quad (4)$$

Resnikoff showed that there is only one metric compatible with this invariance for both representations of P . If $\mathcal{P} \simeq \mathbb{R}^+ \times \mathbb{R}^+ \times \mathbb{R}^+$, then

$$ds^2 = \alpha_1 \left(\frac{dx_1}{x_1} \right)^2 + \alpha_2 \left(\frac{dx_2}{x_2} \right)^2 + \alpha_3 \left(\frac{dx_3}{x_3} \right)^2, \quad (5)$$

where $x_j \in \mathbb{R}^+$ and α_j are positive real constants, for $j = 1, 2, 3$. This metric agrees with the Helmholtz-Stiles color distance.

If $\mathcal{P} \simeq \mathbb{R}^+ \times SL(2, \mathbb{R})/SO(2)$, then one must use the following parameterization

$$\mathcal{P} \ni x = \begin{pmatrix} x_1 & x_3 \\ x_3 & x_2 \end{pmatrix},$$

x is a 2×2 positive-definite real symmetric matrix,

$$x = \det(x) \begin{pmatrix} x & \\ & \det(x) \end{pmatrix},$$

$$\det(x) \in \mathbb{R}^+$$

and

$$\frac{x}{\det(x)} \in SL(2, \mathbb{R})/SO(2).$$

With this notation we have:

$$ds^2 = \text{Tr}(x^{-1} dx x^{-1} dx), \quad (6)$$

where Tr is the trace operator, which guarantees invariance thanks to its cyclic property. Again, this is a novel color metric that has never been studied.

Once we have color metrics on P , the perceptual difference among two colors $x, y \in P$ can be calculated with the integral

$$d(x, y) = \int_{\gamma} ds, \quad \gamma(0) = x, \quad \gamma(1) = y, \quad (7)$$

where γ is the geodesic which connects x to y .

In particular, Resnikoff computed $d(x, y)$ in the case $\mathcal{P} \simeq \mathbb{R}^+ \times \mathbb{R}^+ \times \mathbb{R}^+$ and $y_j = \lambda x_j$, $\lambda \in \mathbb{R}^+$, i.e. when x and y differ only in their intensities. In this situation the metric will measure the brightness difference. The calculation of the integral gives

$$d(x, \lambda x) = \sqrt{\alpha_1^2 + \alpha_2^2 + \alpha_3^2} \int_1^\lambda \frac{dt}{t} = \sqrt{\alpha_1^2 + \alpha_2^2 + \alpha_3^2} \log(\lambda) \quad (8)$$

i.e. the difference in brightness is proportional to the logarithm of the intensity difference. This is coherent with what stated by Weber-Fechner's law [6].

2. Updating Resnikoff's Model: Principal Fiber Bundles

Resnikoff's model is one of the most elegant treatises on color perception and it paved the road to the introduction of some advanced mathematical techniques used in theoretical physics, e.g., differential geometry, Lie groups and algebras representation theory and Jordan algebras, to the theory of color perception. In this section, it is discussed the idea that another fundamental mathematical object commonly used in classical and quantum field theory of mathematical physics, the principal fiber bundle, can be a fundamental (missing) piece in the Resnikoff framework.

First of all, note that Axiom 1 fails for $\alpha \simeq 0$ and $\alpha \gg 1$. In fact, as α approaches zero, the retinal cones responsible for color vision do not work anymore and retinal rods are activated, allowing only black and white vision, which can be identified with achromatic colors in P. However, rods sensitivity is finite, so that under a certain threshold $\bar{\alpha}$, vision ceases and with it the geometric structure of P. The same can be said when α overcomes an upper limit, after which retinal cones saturate and sight is lost.

A second issue is that, in Resnikoff's model, only independent light stimuli over a uniform background are considered; however, color vision in real world conditions is much more complex. In fact, color perception of natural scenes is intrinsically local: hue, saturation and brightness of a patch strongly depend on the surrounding patches, a phenomenon called 'induction', see Fig. 1.

This is the reason why one must distinguish between spectral colors of light sources isolated from the rest of the visual field, and *color in context*. Induction analysis is an active research field both in image processing and cognitive psychology, see e.g., [7–15].

When induction phenomena are taken into account, it is clear that if we want to represent color differences a spatially variant Riemannian metric on P must be considered, instead of a global one. This is where the framework of principal fiber bundles [16 - 20] can be helpful.

Without entering in the very complicated matter of field theory, it is nevertheless possible to give an idea of what fiber bundles are by considering a *field* as an entity which assigns to every point x of a manifold M a point f of another manifold F , representing the value taken by the field in x . A *configuration* of a field on an open subset U of M is a map $\varphi: U \subset M \rightarrow F$ completely defined by its graph, i.e., by the set

$$\text{Graph}(\varphi) := \{(x, f) \in U \times F \mid f = \varphi(x)\}.$$

It is quite natural to think at $U \times F$ as the local model of a more complicated geometric structure

obtained by 'gluing together' these Cartesian products (in a suitable way). This structure is precisely what is called a fiber bundle over M with standard fiber F . Hence, naively, a fiber bundle can be seen as a generalization of the concept of a manifold, now modeled on a Cartesian product instead of an Euclidean space. A fiber bundle is a *principal bundle* if the standard fiber is a Lie group G .

The importance of considering Lie groups has been discussed in the previous section, thus it seems necessary to consider, among all fiber bundles, principal fiber bundles as the candidates to provide the rich geometrical structure needed to introduce in Resnikoff's framework the phenomenon of local induction. A formalization of this idea can lead to new, context-dependent, color metrics rigorously obtained from first principles and not by ad-hoc procedures.

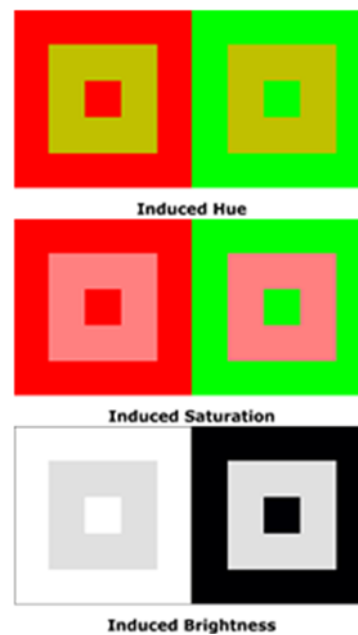


Fig. 1. Top to bottom: the induction phenomena. In all the pictures, the pierced square is the same in both columns, however it is surrounded, inside and outside, by another stimulus, which is different in the two columns. The top row shows that the (fixed) hue (tint) of the pierced square is perceived as greenish or reddish depending on the surrounding. The middle row shows that the (fixed) saturation (color purity) of the pierced square is perceived more or less intense with respect to the neighborhoods. Finally, in the bottom row, we can see that the brightness (perceived luminosity) of the pierced square changes dramatically when the surrounding area changes.

3. Conclusion

The Resnikoff's model of perceived color space has been recalled and some critics about its assumptions have been pointed out. These observations can be the starting point for a new analysis of color spaces, based on the mathematical concept of principal fiber bundles, which it has been motivated to seem the most adequate framework to further develop Resnikoff's analysis.

References

- [1]. H. Resnikoff, Differential geometry and color perception, *Journal of Mathematical Biology*, Vol. 1, 1974, pp. 97–131.
- [2]. I. Newton, Opticks, or, a treatise of the reflections, refractions, inflections & colours of light, *Courier Corporation*, 1979.
- [3]. H. Grassmann, Zur theorie der farbmischung, *Poggendorff's Annalen der Physik*, Vol. 89, 185, pp. 69–84.
- [4]. H. von Helmholtz, Handbuch der physiologischen Optik. Allgemeine Encyclopdie der Physik, IX. Band, *Leopold Voss*, Leipzig, 1867.
- [5]. A. Knapp, Representation Theory of Semisimple Groups: An Overview Based on Examples, *Princeton University Press*, 2016.
- [6]. G. Wyszecky and W. S. Stiles, Color science: Concepts and methods, quantitative data and formulas. *John Wiley & Sons*, 1982.
- [7]. H. Wallach, Brightness constancy and the nature of achromatic colors, *Journal of Experimental Psychology*, Vol. 38, No. 3, 1948, pp. 310–324.
- [8]. A. Parducci, Contextual effects: A range-frequency analysis, in Handbook of Perception, Vol. 2, *Academic Press*, 1974, pp. 127–141.
- [9]. M. Rudd and I. Zemach, Quantitive properties of achromatic color induction: An edge integration analysis, *Vision Research*, Vol. 44, 2004, pp. 971–981.
- [10]. E. Provenzi, L. De Carli, A. Rizzi, and D. Marini, Mathematical definition and analysis of the retinex algorithm, *Journal of the Optical Society of America A*, Vol. 22, No. 12, December 2005, pp. 2613–2621.
- [11]. R. Palma-Amestoy, E. Provenzi, M. Bertalmio, and V. Caselles, A perceptually inspired variational framework for color enhancement, *IEEE Transactions on Pattern Analysis and Machine Intelligence*, Vol. 31, No. 3, 2009, pp. 458–474.
- [12]. E. Provenzi, Achromatic induction: A variational interpretation of rudd-zemach's edge integration model, in *Proceedings of the International IEEE Conference on Signal-Image Technology & Internet-Based Systems (SITIS' 13)*, 2013, pp. 424–429.
- [13]. E. Provenzi and V. Caselles, A wavelet perspective on variational perceptually-inspired color enhancement, *International Journal of Computer Vision*, Vol. 106, January 2014, pp. 153–171.
- [14]. G. Gronchi and E. Provenzi, A variational model for context-driven effects in perception and cognition, *Journal of Mathematical Psychology*, Vol. 77, 2017, pp. 124–141.
- [15]. E. Provenzi, Computational Color Science: Variational Retinex-like Methods, *John Wiley & Sons*, 2017.
- [16]. J. Baez and J. Muniain, Gauge fields, knots and gravity, *World Scientific Publishing Co Inc.*, Vol. 4, 1994.
- [17]. L. Fatibene and M. Francaviglia, Natural and gauge natural formalism for classical field theorie: a geometric perspective including spinors and gauge theories, *Springer Science & Business Media*, 2003.
- [18]. E. Provenzi, A differential geometry model for the perceived colors space, *International Journal of Geometric Methods in Modern Physics*, Vol. 13, No. 08, 2016, p. 1630008.
- [19]. C. Isham, Modern differential geometry for physicists, *World Scientific Publishing Co Inc*, Vol. 61, 1999.
- [20]. E. Provenzi, Principal fiber bundles and geometry of color spaces, in *Proceedings of the SIGNAL'17 Conference*, 2017, p. 13.



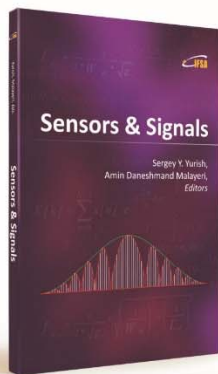
Published by International Frequency Sensor Association (IFSA) Publishing, S. L., 2017 (<http://www.sensorsportal.com>).



International Frequency Sensor Association (IFSA) Publishing

Sensors & Signals

Sergey Y. Yurish, Amin Daneshmand Malayeri, Editors



Formats: printable pdf (Acrobat) and print (hardcover), 208 pages

ISBN: 978-84-608-2320-9,
e-ISBN: 978-84-608-2319-3

Sensors & Signals is the first book from the Book Series of the same name published by IFSA Publishing. The book contains eight chapters written by authors from universities and research centers from 12 countries: Cuba, Czech Republic, Egypt, Malaysia, Morocco, Portugal, Serbia, South Korea, Spain and Turkey. The coverage includes most recent developments in:

- Virtual instrumentation for analysis of ultrasonic signals;
- Humidity sensors (materials and sensor preparation and characteristics);
- Fault tolerance and fault management issues in Wireless Sensor Networks;
- Localization of target nodes in a 3-D Wireless Sensor Network;
- Opto-elastography imaging technique for tumor localization and characterization;
- Nuclear and geophysical sensors for landmines detection;
- Optimal color space for human skin detection at image recognition;
- Design of narrowband substrate integrated waveguide bandpass filters.

Each chapter of the book includes a state-of-the-art review in appropriate topic and well selected appropriate references at the end.

With its distinguished editors and international team of contributors *Sensors & Signals* is suitable for academic and industrial research scientists, engineers as well as PhD students working in the area of sensors and its application.

http://www.sensorsportal.com/HTML/BOOKSTORE/Sensors_and_Signals.htm

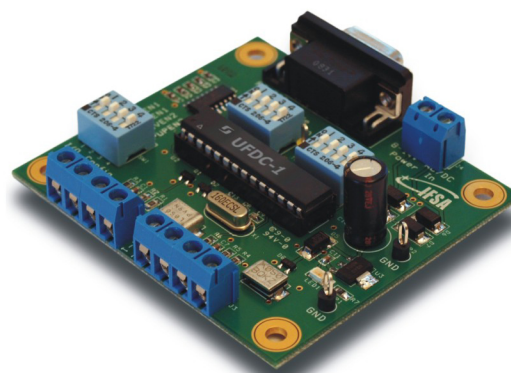
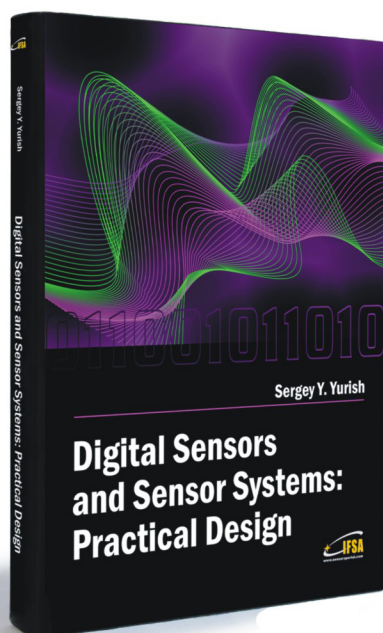
Theory:

Digital Sensors and Sensor Systems: Practical Design

and

Practice:

Development Board EVAL UFDC-1/UFDC-1M-16



Buy book and Evaluation board together. **Save 30.00 EUR**

Development Board EVAL UFDC-1 / UFDC-1M-16

Full-featured development kit for the Universal Frequency-to-Digital Converters UFDC-1 and UFDC-1M-16. 2 channel, 16 measuring modes, high metrological performance, RS232/USB interface, master and slave communication modes. On-board frequency reference (quartz crystal oscillator). Operation from 8 to 14 V AC/DC. Development board software is included.

All existing frequency, period, duty-cycle, time interval, pulse-width modulated, pulse number and phase-shift output sensors and transducers can be directly connected to this 2-channel DAQ system. The user can connect TTL-compatible sensors' outputs to the Development Board, measure any output frequency-time parameters, and test out the sensor systems functions.

Applications:

- Digital sensors and sensor systems
- Smart sensors systems
- Data Acquisition for frequency-time parameters of electric signals
- Frequency counters
- Tachometers and tachometric systems
- Virtual instruments
- Educational process in sensors and measurements
- Remote laboratories and distance education

Order online:

http://www.sensorsportal.com/HTML/BOOKSTORE/Digital_Sensors_and_Board.htm



International Frequency Sensor Association Publishing



www.sensorsportal.com

ISSN 1726- 5479



9 771726 547001